HYDROCHEMICAL CHARACTERISATION OF NORTHERN KWAZULU-NATAL HISTORIC COAL MINING DISTRICTS, NORTHEASTERN SOUTH AFRICA

by

HLUMELA MDUDUMA

Submitted in fulfilment of the academic requirements for the degree of

Master of Science

School of Agricultural, Earth and Environmental Sciences,

Discipline of Geological Science,

University of KwaZulu-Natal

Durban

South Africa

December 2018

PREFACE

The research reported in this dissertation was completed by the candidate while based in the Discipline of Geological Science, School of Agriculture, Earth and Environmental Sciences of the Collage of Agriculture, Engineering and science, University of KwaZulu-Natal, Westville Campus, South Africa. The research was financially supported by the school through Dr Molla Demlie.

The contents of this work have not been submitted in any form to another University. Except where the work of others is acknowledged in the text, the results reported are due to investigations by the candidate.

_____ _____

Signed: Date:

DECLARATION OF PLAGIARISM

I, Hlumela Mduduma, declare that:

i. The research reported in this dissertation, except where otherwise indicated or acknowledged, is my own original work;

ii. This dissertation has not been submitted in full or in part for any degree or examination to any other university;

iii. This dissertation does not contain other persons' data, pictures, graphs or other information, unless specifically acknowledged as being sourced from other persons;

iv. This dissertation does not contain other persons' writing, unless specifically acknowledged as being sourced from other researchers. Where other written sources have been quoted, then:

    a. Their words have been re-written but the general information attributed to them has been referenced;
    b. Where their exact words have been used, their writing has been placed inside quotation marks, and referenced;

v. Where I have used material for which publications followed, I have indicated in detail my role in the work;

vi. This dissertation is primarily a collection of material, prepared by myself, published as journal articles or presented as a poster and oral presentations at conferences. In some cases, additional material has been included;

vii. This dissertation does not contain text, graphics or tables copied and pasted from the Internet, unless specifically acknowledged, and the source being detailed in the dissertation and in the References sections.

_____

Signed: Hlumela Mduduma
Date: December 2018

ABSTRACT

This M.Sc. dissertation reports the results of a hydrogeochemical study undertaken on historical coal mining districts of northern KwaZulu-Natal (KZN) Province, South Africa. The research catchment covers an area of about 12945 km^2, located in the head waters of the Tugela River Basin or the uThukela Water Management Area (WMA). The main aim of the study was to assess the effectiveness of the rehabilitation undertaken by the South African Government on the various defunct/abandoned historical coal mines in northern KZN in improving surface water and groundwater quality in the region. Characterisation of surface water and groundwater water in terms of their interconnection, flow and hydrochemistry were undertaken. Primary (original data) and secondary data and information were collected, collated and analysed to understand the hydrogeochemical conditions of the region. The original data collected through a series of field campaigns within the study area, were complimented with secondary data from the Department of Water Affairs and Sanitation (DWS) monitoring programme, the KZN Groundwater Recourse Information Project (GRIP), the National Groundwater Archives (NGA) and borehole logs, hydrochemical and borehole yield data from various reports. The results of the study reveal that since the beginning of groundwater monitoring in 2010, the groundwater has been characterised by circumneutral waters. Time series EC, SO_4^{2-} and Fe^{2+} data reveal no incongruities apart from a few episodes of elevated concentrations. Surface water hydrochemical analyses revealed peaks in EC coupled with low pH at varied sampling points which are presumed to be impacts from Acid Mine Drainage (AMD). Time series saturation states of groundwater with respect to calcite and dolomite indicate that groundwater remains oversaturated with respect to these minerals but under saturated with respect to gypsum as a result of carbonate AMD neutralization reactions. Trace metal data reveal no anomalous concentrations both in surface water and groundwater samples as a result of the circumneutral hydrogeochemical conditions. Major ion hydrochemical data show two main groundwater hydrochemical facies in the study area, namely most upstream boreholes are characterized by Na-Ca-HCO_3-SO_4 and most downstream boreholes are characterised by Ca-Mg-HCO_3-SO_4 hydrochemical water types. All surface water and groundwater samples have δD and $\delta^{18}O$ isotopic values that plot on or below the Local and Global Meteoric Water Lines, indicating recharge from meteoric source with some evaporation mainly within the rehabilitated mine dumps. The detectible tritium signal in the shallow aquifers reflect recent active recharge taking place.

Key words/Phrases: Circumneutral waters; AMD neutralization; Environmental Isotopes; Hydrochemistry; Northern KZN Coal mining District; South Africa

ACKNOWLEDGEMENTS

Firstly, I wish to express my sincere gratitude to my supervisor Dr Molla Demlie for this opportunity and his constant encouragement, patience and supervision throughout the research.

I wish to thank Environmental Resource Management (Pty) Ltd. for awarding me a student grant in order to fund my studies, this project could not have been completed without it.

I wish to thank Mr. Maluleke from the Department of Water and Sanitation for his assistance in this project and for freely making data available whenever it was requested. The South African Weather Service for supplying me with all the necessary weather data, I thank you. I wish to thank Siphesihle Ndlovu, my fellow college, it has been a pleasure sharing an office with you and for all your assistance given wholeheartedly. Thank you for all our time spent sharing knowledge and venting, it has been a pleasure knowing you. To my friends Nkule, Palesa, KG, Sibusiso and Xolani, you have been my greatest support system , my shoulders to cry on, I would have never made it through this degree without you all, thank you does not even begin to express how grateful I am to you.

I wish to thank my parents Vuyolwethu and Thozamile Mduduma, words can never express how grateful I am for your undying prayers, support and encouragement throughout the years. I would also like to thank my son Kwezilomso for giving me a reason to push forward even when times were tough.

TABLE OF CONTENTS

LIST OF TABLES

LIST OF FIGURES

LIST OF ACRONYMS

AMD	Acid Mine Drainage
amsl	Above mean sea level
DEM	Digital elevation model
DWAF	Department of water and forestry
DWS	Department of water and sanitation
EC	Specific electrical conductivity
GMWL	Global Meteoric Water Line
KZN	KwaZulu-Natal
LMWL	Local Meteoric Water Line
µS/cm	microsiemens per centimetre
MAP	Mean annual precipitation
Mt	Million ton
NCE	Natal Coal Exploration
NNC	Northern Natal Coal
P	Precipitation
PC	Principal Component
PCA	Principal component analysis
SAWS	South African Weather Service
SI	Saturation Index
SPSS	Statistical Package for the Social Science
TDS	Total Dissolved Solids
TU	Tritium Unit

CHAPTER 1: INTRODUCTION

1.1. Background and Research Rationale

Coal in South Africa was first mined on a commercial basis in 1857 (Gotz et al., 2014). It is currently the 6th largest coal producer in the world and it remains the primary energy source for power generation in the country (Gotz et al., 2014). Coal mining in South Africa takes place both using open pit and underground methods and approximately equal tonnages come from each. Similarly, coal has been extracted via open pit as well as underground mining in northern KZN province.

Coal mining in northern KwaZulu-Natal commenced in the late 19th century and continues until today as an important economic activity, although most mines have become abandoned (Nel et al., 2003). KwaZulu-Natal's coal is situated within five coalfields, namely, the Klip River, Utrecht, Vryheid, Nongoma and Somkele coal fields. The seams are developed mainly within the Ecca Group of the Karoo Sequence, apart from, Somkele and eastern Nongoma coalfields, which are located in the Beaufort Group. Since 1979, a total of 66 coal mines have operated in the KZN province, among which only 10 are currently operational. Mine closure is a major challenge that has affected both the developed and developing world. Abandoned coal mines are a major source of water pollution in South Africa. These abandoned mines and tailing piles can be sources for AMD and represent risk to human health and the ecosystems (Moncur et al., 2005 in Cravotta, 2008). The impact of mine abandonment becomes more extreme in developing countries, especially when efficient mitigating actions against acidity are not applied. Possible mitigation actions include the neutralization of acid drainage by means of application of lime, hydrated lime, ammonia and fly ash (Akcil and Koldas, 2006 in Campaner et al., 2013).

Today, mine closure requires the rehabilitation of land to a viable post-mining use such as agriculture. Historically, when an ore body was exhausted and mining ceased, mines were boarded up and abandoned. Mining legislation did not address the protection of the environment or water resources (Nel et al., 2003; Limpitlaw, 2004). The Minerals Act of South Africa (Act 50 of 1991) introduced specific requirements for the environmental management on mines in the form of Environmental Management Programme Reports (EMPRs). The three main environmental protection legislations in South Africa are the following:

- The National Water Act (NWA) (Act 36 of 1998),

- The Minerals and Petroleum Resource Development Act (MPRDA) (Act 28 of 2002),
- The National Environmental Management Act (NEMA) (Act 8 of 2004).

While South Africa has made the necessary shift in addressing mine closures and mine water management through legislation and regulatory changes, vulnerabilities in the current system remain.

Groundwater is an important resource that can be used solely or in conjunction with surface water supplies. However, human activities such as mining, has been impacting on groundwater in terms of quality degradation and quantity depletion (DWAF, 1998). Groundwater quality is intrinsically linked to chemical properties of the aquifers geology through which it flows. The oxidation of iron sulphides present within the discard dumps and stockpiles from coal mining may further influence the hydrochemistry. This happens due to the generation of a common problem associated with abandoned coal mines known as AMD. Problems arise due to the reactive nature of coal when exposed to atmospheric conditions. Iron sulphide minerals, which associate with coal deposits, when exposed to atmospheric oxygen and water during mining as well as post mining activities oxidize and release sulphate (SO_4^{2-}), ferrous iron (Fe^{2+}), and hydrogen (H^+), which increases the acidity of the mine water (Alhamed and Wisotzky, 2015). In the Northern KZN region, the nature of the pollution is such that pyrites from the various abandoned mines when brought into contact with air and water oxidise thereby polluting runoff and groundwater in and around the mine sites (DWAF, 1998). The solubility of mineral compounds is also increased as a result of the acidic conditions, releasing undesirable elements which deteriorate the quality of surface water and groundwater resources. Kempster (1982) reported serious pollution of rivers in northern KZN as a result of AMD from coal mining operations in the region.

The safety, environmental and social risks which arise from badly conducted mine closure can result in significant liabilities for mining companies and communities. These threats are related to low pH, the higher total dissolved solids (TDS), the high concentrations of heavy metals as well as total suspended solids. Therefore, it is important that the water quality monitoring and the rehabilitation measures are assessed against the success and failures of rehabilitation strategies taken by national and local governments.

The strategy followed by the South African Government during the rehabilitation programme of Northern KZN abandoned mine are among other, collection of all coal waste of a mine into a well-defined dump, which was then covered with a layer of clay followed by topsoil to give

a total cover thickness of 1m. This is followed by a suitable vegetation cover, for example grass was established on the topsoil. As part of the abandoned mine rehabilitation and water resources protection strategy, surface water and groundwater quality monitoring stations have been established around the rehabilitated abandoned mine.

This M.Sc. research envisages to understand the effectiveness of mine rehabilitation operation in northern KZN coal mining districts in improving surface water and groundwater quality. To that effect, the surface water and groundwater quality monitoring data was collated and interpreted to understand the processes that control the evolution of rehabilitated mine water quality and inform future planning and application of post-mining remedial measures. The former mainly comprises the identification and description of hydrogeochemical processes controlling the evolution of groundwater chemistry and their influence on groundwater quality, which is the focus of this research.

1.2. Research Question

Have government's rehabilitation efforts in northern KZN abandoned mine districts led to the protection of surface water and groundwater resources in the region?

1.3. Hypothesis

The rehabilitation of abandoned mining areas in northern KZN have substantially neutralized AMD threat that would deteriorate surface water and groundwater quality in the region.

1.4. Aims and Objectives

This research aims to characterise the hydrochemistry of the northern KZN coal mining districts by collecting, integrating and analysing relevant hydrogeological and hydrochemical data so as to assess the degree of success of the Government's rehabilitation efforts of the abandoned historic coal mining sites.

The main objectives of the research are:

a) To characterise surface water and groundwater in terms of their interconnection, flow and hydrochemistry.
b) To investigate the effectiveness of the rehabilitation of abandoned coal mines in northern KZN in improving surface water and groundwater quality in the region.
c) To develop a conceptual hydrochemical model for northern KZN historic coal mining districts that will explain the prevailing hydrogeochemical processes in the area.

1.5. Structure of the Dissertation

Chapter 1: this chapter introduces the research and provides a brief background of mining in northern KZN as well as in South Africa as a whole. The research question, hypothesis and the aims and objectives of the study are included in this chapter.

Chapter 2: this chapter encapsulates descriptions of the study area in terms of location, climate, topography, drainage, geological as well as hydrogeological settings of the study area, which are important input in understanding and characterisation of the region.

Chapter 3: literature review on the history of coal mining in South Africa as well as the various coalfields in KZN including the types of coal which they produce are presented in this chapter. The chapter provides an account of the history of mine abandonment and the legislative framework in the country. Additionally, the literature review includes hydrogeochemical characterisation of abandoned mines, including water-rock interactions as well as hydrochemical parameters for determining water quality.

Chapter 4: the chapter encompasses the research methodology and approaches used in this research. Statistical analysis approaches including data reduction tools and detailed descriptions of software used and what they are used for are presented. The distribution of sampling points for collecting primary research data are presented as well.

Chapter 5: the research results including detailed analysis, interpretation and discussion of the primary and secondary data collected are presented in this chapter. These include hydrochemical processes, saturation index calculations are presented on time series graphs. Environmental isotope data are interpreted and included to understand the hydrogeological processes within the study area.

Chapter 6: the conclusions drawn from the study based on the research findings are presented in this chapter. It summarizes the results of the project including some recommendation for future work.

CHAPTER 2: GENERAL OVERVIEW OF STUDY AREA

The following section of this chapter describes the salient features of the study including location, climate, topography, geology and hydrogeological aspects.

2.1. Location of Study Area

The study area is located approximately 340 km North of Durban, in northern KZN Province of South Africa (Figure 2.1). The study area commonly called "Northern KwaZulu-Natal Coalfields" and include important historical and active coal mining towns such as Dannhauser, Dundee, Glencoe and Newcastle in the region. The area comprises three main coalfields namely, Klip River, Utrecht and Vryheid, all of which are located in the Main Karoo Foreland Basin.

2. 2. Climate, Topography and Drainage

The climate of northern KZN is temperate with warm summers especially around the Newcastle (averaged mean maximum temperature in January 25.8^{o}C) and moderately cold winters (average mean minimum temperature in June 15.1^{o}C) as shown in figure 2.2 below. The study area can be characterised by summer rainfall region, where the rainfall pattern is controlled by topography (orographic), with higher lying areas receiving higher precipitation. Most of the region's rainfall occurs between September and April (Figure 2.2), with Newcastle having Mean Annual Precipitation (MAP) of 569 mm/a, Vryheid 484 mm/a and Glencoe at 840 mm/a. Rainfall intensity is high and sporadic with thunderstorms and torrential downpours being typical of the summer rainfall pattern. While winter rainfall is less intense (SAWS, 2017).

Run-off is expected to be high due to the steep gradients and poor soil and vegetation cover in many areas. Extensive drainage channel erosion (dongas) can be seen in the shale and siltstone Karoo formations (DWAF, 1994).

The topography of the study area can be defined in terms of the Drakensberg escarpment along the western margin which attains the highest elevation of 2173m above mean sea level (amsl) (Figure 2.3). Elevations vary from around 300 m amsl in the east and rise westward to 1711m amsl north of Vryheid. This classifies the topography as rolling with some mountainous areas. The river valleys are erosional rather than depositional zones. This is supported by the frequent occurrence of rock outcrops and a general lack of alluvium, along river courses. In the high lying areas and where Karoo rocks predominate, extensive dolerite sills are common.

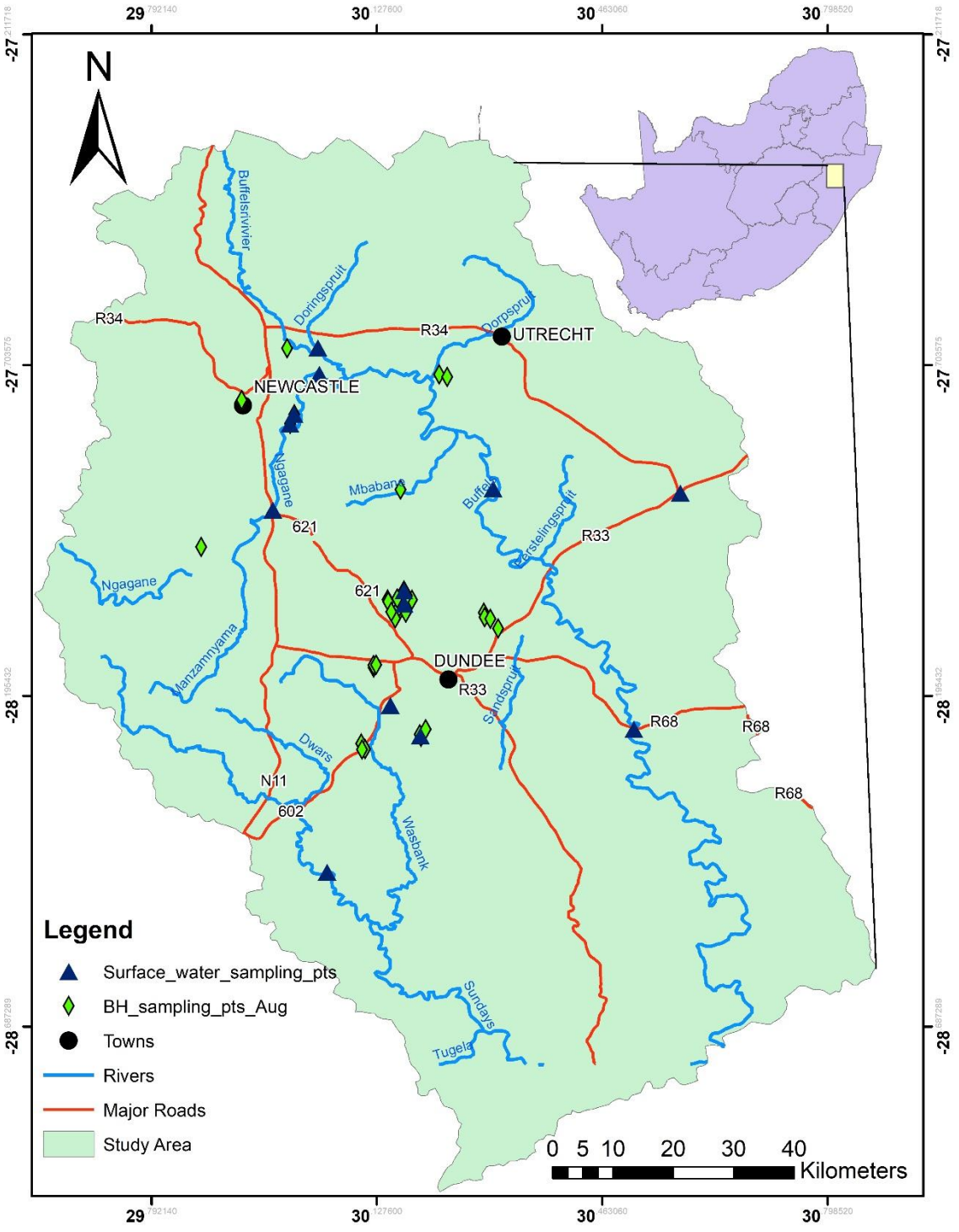

Figure 2. 1. Location of Study Area with sampling points

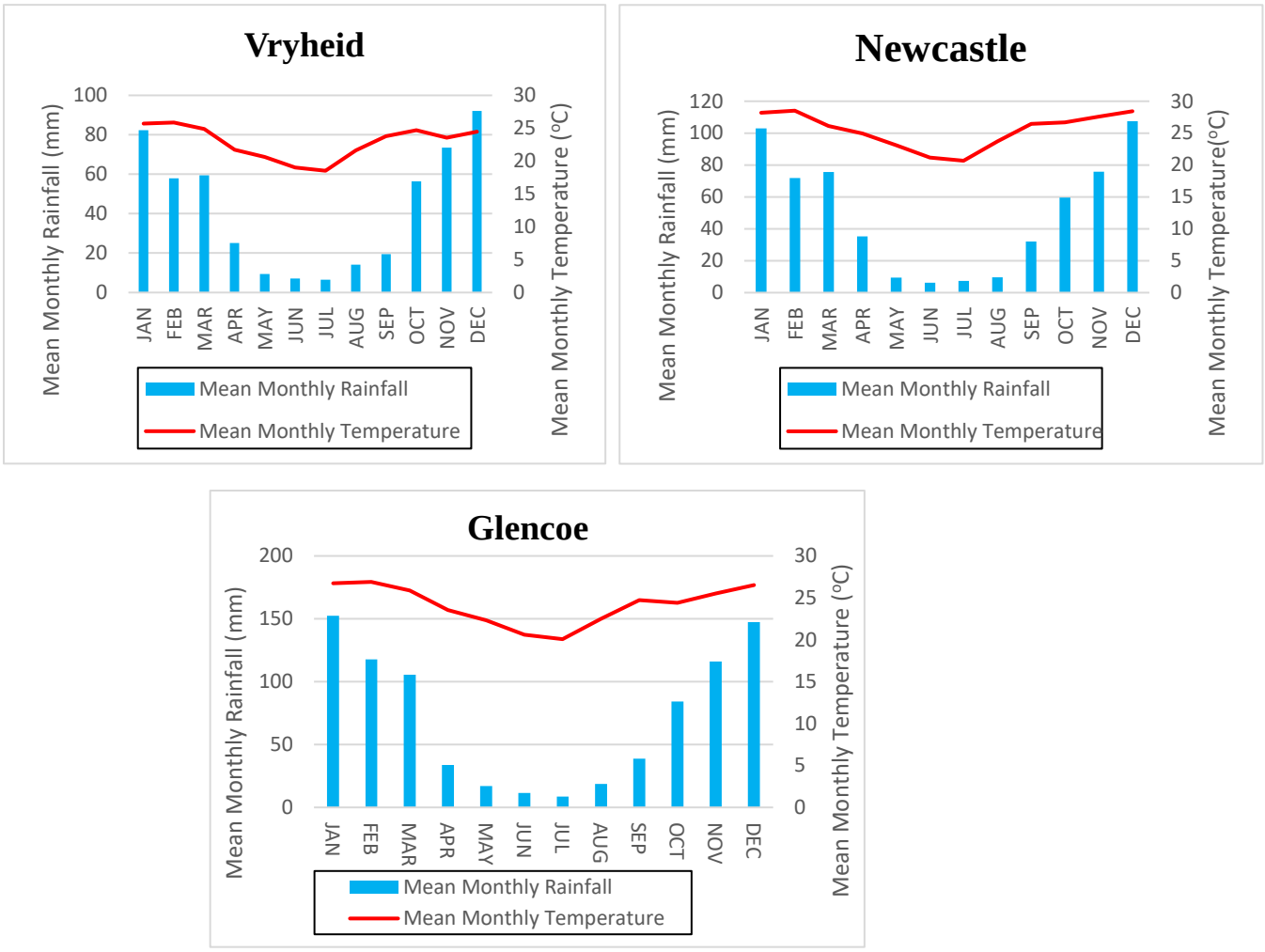

Figure 2. 2. Mean monthly rainfall and temperature for Vryheid, Newcastle and Glencoe metrological stations (Data from SAWS, 217).

The study area is drained by the Tugela River system and the area falls under the uThukela Water WMA. Perennial streams such as Wasbank, Buffels and Ngangane streams drain the study area and eventually join the Tugela River downstream of the study area making it the head waters of the Tugela River Basin. These streams and their tributaries draining the study area make up first and second order streams of the headwaters of the Tugela River. They flow in a south-easterly direction, where they join the main Tugela River near the town of Tugela Ferrry in central KZN. The Tugela River is the largest river in KZN province and has its source in the study area.

Most of the larger town and settlements in the study area rely on surface water resources for their supply. The use of springs for water supply is common, especially in the upland areas where rainfall is high. Vryheid is supplied by the Bloemveld and Grootgewaag dams and in

times of shortages rely on the large Klipfontein dam. Ulundi extracts water from the White Mfolozi River but in times of drought has had to use groundwater supply.

2.3. Geological and hydrogeological setting of the study area

2.3.1. Geological setting

The Karoo Sequence in South Africa records late Palaeozoic to early Mesozoic deposition within the Intracratonic basin (Table 2.1). Granite as well as gneiss form the basement rocks in eastern South Africa. These basement rocks are overlain unconformably by the Palaeozoic rocks of the Natal Group, which in turn is overlain unconformably by the late Carboniferous to Early Permian Dwyka Group and the Permian Ecca Group rocks of the Karoo Supergroup. The general tectonic setting of the Ecca Group is that of a stable shelf slowly subsiding (Hancox and Gotz, 2014).

In northern KZN, some of the main coal resources are contained within the Permian Vryheid Formation of the Ecca Group. The Ecca Group sediments in the study area represent a time span from late Carboniferous to the Permian and fall into the Northern Ecca facies (Mackay, 1988). The sediments are divided into a series of lithostratigraphic subdivisions.

The Vryheid Formation is the most extensive Formation in northern KZN. The basal beds comprise shales, siltstones and sandstone, overlain by coarse-grained, cross-bedded sandstone and grits (Table 2.1). Sediments were transported from the east and northeast and deposited in the river systems as well as related deltas during several regressive cycles (Hancox and Gotz, 2014). Accumulation of rotting vegetation in swampy environments gave rise to coal deposits, which encompasses thick coarse-grained sandstone beds and carbonaceous shale with thin coal seams in the Colenso area. Coal deposits occur in the Klip River, Utrecht and Vryheid coal fields.

The Klip River coalfield includes the whole coal-bearing area between Ladysmith and Newcastle in northern KZN (Hancox and Gotz, 2014). This area is bounded in the east by the Buffalo River and west by the foothills of the Drakensburg. The Vryheid Formation is exposed by the deeply incised Thukela River valley east of Colenso where it is intruded by numerous dolerite sills {Hancox, 2014, South Africas coalfields- A 2014 perspective}. Based on petrological and chronological data, nine types of dolerite sill have been distinguished in northern KZN, the four major ones from oldest to youngest being the Zuinguin, Utrecht, Ingogo, and Talana dolerites (Hancox and Gotz, 2014).

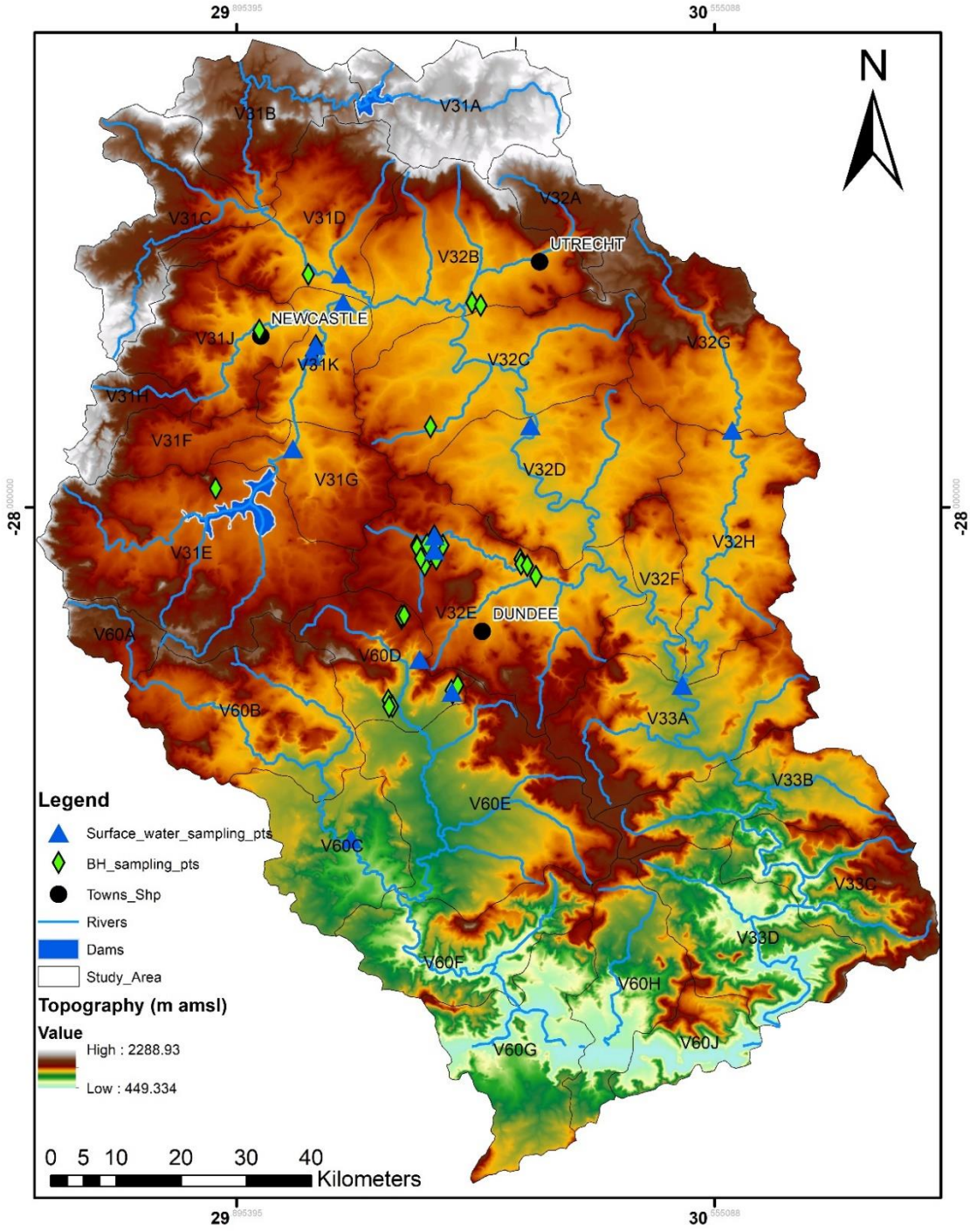

Figure 2. 3. Topographic and drainage map of the study area.

The Kilp River coal seams dip gently to the south, usually less than 3^{o}. Large scale displacements are common, where most of the faulting is related to the intrusion of dolerite dikes and sills (Hancox and Gotz, 2014). The maximum displacement in the Klip River Coalfield as reported by Hancox and Gotz (2014) is 137m, with an uplift of 229 m. According

to Hancox and Gotz (2014), the Utrecht Coalfield consists of five major dolerite intrusions which are recognized.

Table 2. 1 .Stratigraphic subdivision of the Ecca Group in the North-eastern Karoo Basin, with emphasis on the Vryheid Formation (Modified from {Mackay, 1988, Sedimentary Models for Coal Formation In The Klip River Coalfield}.

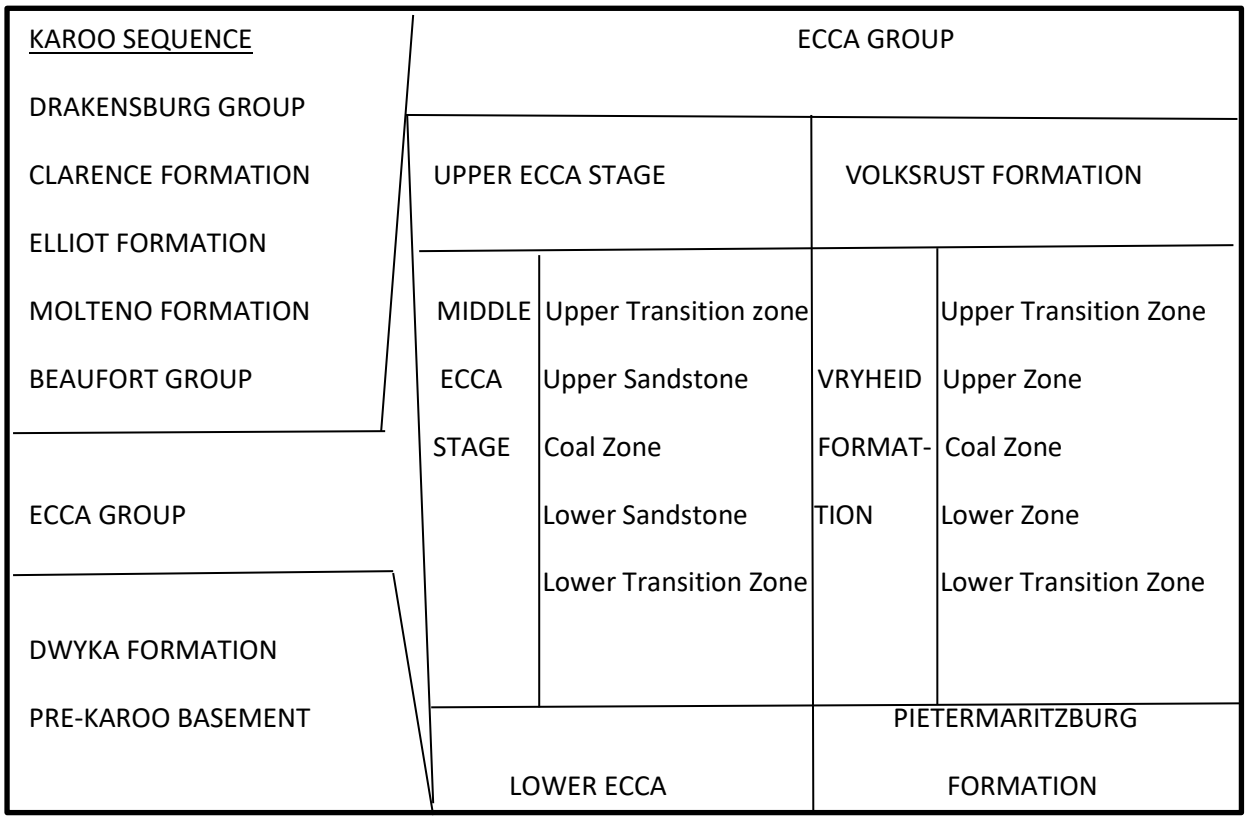

These dolerite intrusions significantly affect the rank and quality of the coals in the coalfield. They are also the main cause of any structural discontinuities along with faults. Sills that occur below the coal zone are said to have a greater metamorphic effect on the coals than sills that occur above the coal zone. The Vryheid Coalfield is intruded by numerous dykes and sills more than the Klip River and Utrecht Coalfield, which renders the surface geology to appear a mixture of dolerite exposures and sedimentary rocks of the Vryheid Formation (Figure 2.4). Displacements of up to 150 m are associated with these intrusions. Thus, dolerite dykes may negatively affect the coal qualities and preferentially intrude into coal seams at other places {Hancox, 2014, South Africas coalfields- A 2014 perspective}.

The uppermost unit of the Ecca Group is the Volksrust Formation (Table 2.1) which rests comfortably on the Vryheid Formation and was probably deposited in an extensive, shallow body of water. It comprises blue-grey or black siltstone and shale which is exposed at the base

of the Normandien Formation along the Drakensberg escarpment foothills, in the Klip River catchment northwest of Ladysmith {Hancox, 2014, South Africas coalfields- A 2014 perspective}. Thin phosphate and carbonate beds are common. Towards the west, these rocks form the low-lying parts of the Sand River catchment. These rocks have been up-thrown against the Adelaide rocks by the Tugela Fault which runs east-west along the river valley through Colenso {Hancox, 2014, South Africas coalfields- A 2014 perspective}. The variation between detrital material and coal seams indicates a fluctuation in the balance between rates of sedimentation and subsidence (Cadle et al., 1993).

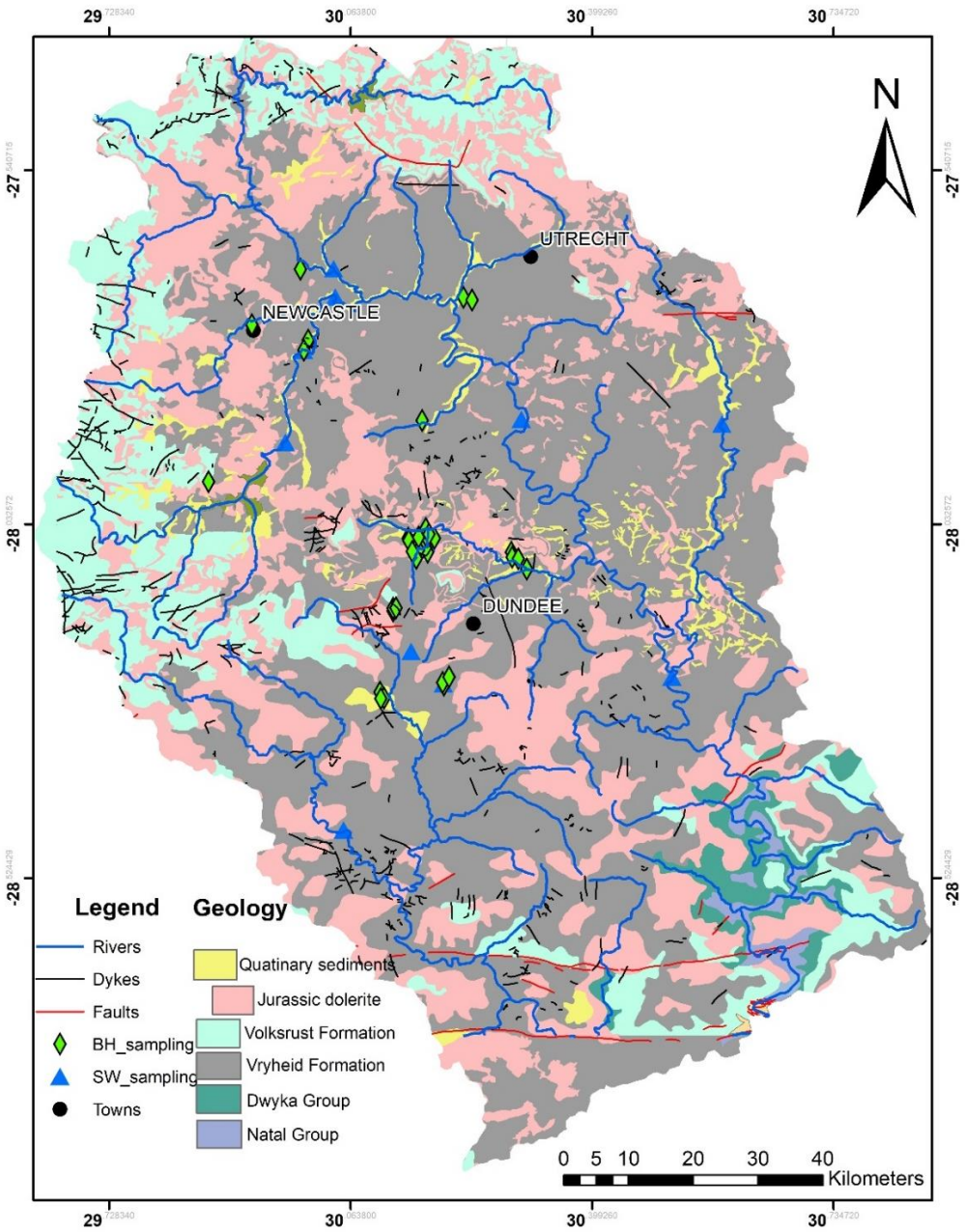

Figure 2. 4. Simplified geological map of the study Area (modified from Council for Geosciences, CGS, 1988).

2.3.2. Regional Hydrogeological Setting

The occurrence of groundwater in the study area is controlled, to a great extent, by the secondary water-bearing properties of various rock units than by their primary porosities (Van Wyk, 1963). The principal processes giving rise to the development of secondary permeability are weathering and fracturing as a result of dolerite intrusions. Karoo dolerite dykes represent thin, linear zones, along which higher permeability which act as conduits for groundwater flow within the country rock forming an aquifer system (DWAF, 1995).

There are two distinct and superimposed groundwater systems in the geological formations of the coalfields of the study area. These are the upper weathered aquifer and the fractured aquifer system below. In the weathered groundwater system, the top 5-15 m normally consists of soil and weathered rock where the principal groundwater occurrence intergranular and fractured aquifer type, with median borehole yields in the range of 0.5 to 2.0 litres per second (l/s) (Figure 2.5) (DWAF, 1994; DWAF, 1995). The upper weathered aquifer zone is recharged from rainfall. This weathered zone is generally low-yielding because of its insignificant thickness. The quality of groundwater in the Vryheid fractured aquifer is normally excellent, attributed to many years of dynamic groundwater flow through the weathered sediment (Vermeulen, 2009).

The range of borehole yields in the Vryheid Formation is presented in Table 2.2. The median borehole yield is 0.6 l/s (DWAF, 1995). Water strikes are mostly encountered in fractured rock, however zones of weathering between sandstone and shale contacts can also yield water. Fractured zones are commonly associated with the intrusion of dolerite in the host rock. The Vryheid Formation in the Newcastle region has a transmissivity ranging between 10 and 30 m^2/d with areas having transmissivity up to 50 m^2/d (DWAF, 1995; DWA, 2011).

The Dwyka Formation is generally a moderate aquifer (Table 2.2) with 51% of boreholes having yields from 0.5 to 3.0 l/s (DWAF, 1994). However, 41% of boreholes have yields in the marginal to poor class (< 0.5 l/s) and 15% in the marginal class with yields < 0.1 l/s. This relatively poor to marginal yields is probably due to the massive, dense matrix behaving as an aquitard, particularly in areas where a clayey impermeable topsoil is developed. Yields are higher in the north, with a median yield of 1 l/s south of Vryheid, compared to 0.5 - 0.7 l/s further south in the Nondweni/ Nhlazatshe areas. This may be, in part, due to the more arenaceous nature of the formation further north and the higher rainfall compared to south of the area. Many successful boreholes which have been drilled in the Dwyka tillite have in fact struck water in underlying hydrogeological units (e.g., the Natal Group). The potential of

drilling a dry borehole in the Dwyka Formation is higher than in any of the other hydrogeological units (DWAF, 1995).

Table 2. 2. Borehole yields for various hydrogeological units around the study area (Adapted from Sherman, 1998).

Regional Hydrogeological Units	Range of Estimated Borehole Yields (l/s)	No. of Records	Median Yield (l/s)
Intrusive rocks, Dolerite sheets and Dykes	0.0-10.0	886	0.46
Basement Rocks	0.01-25.6	197	0.5
Pietermaritzburg and Volksrust Formation shales (and Beaufort Group mudstone and sandstone)	0.01-23.2	428	0.5
Vryheid Formation Sandstone	0.01-26.0	330	0.5
Dwyka Formation tillite	0.01-3.8	36	0.3
Natal Group Sandstone and conglomerate	0.02-5.0	82	0.8

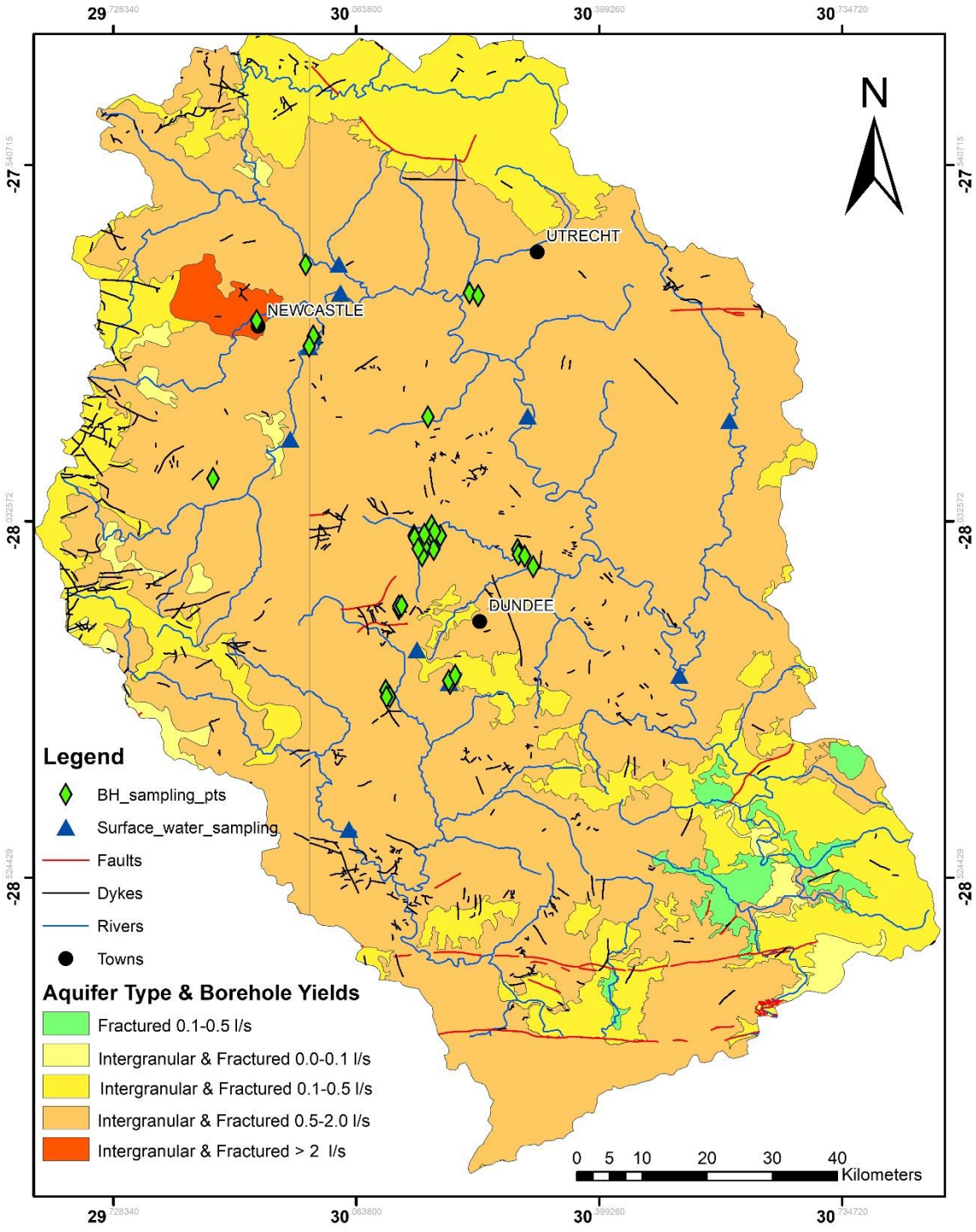

Figure 2. 5. Hydrogeological map of the study area (Modified from DWAF, 1998).

CHAPTER 3: LITERATURE REVIEW

This chapter presents the literature review on the history of coal mining in South Africa. It reviews the different coalfields in KZN and the types of coal produced in the area. The history of mine abandonment in the region, current legislative framework governing the mining industry, water-rock interactions processes controlling the hydrochemical composition of groundwater are briefly described

3.1. Coal Mining in South Africa

Coal is the main source of energy in Southern Africa. In 1997, 68% of the regions energy consumption was coal-based, while the rest of Africa depended primarily on oil for its energy needs (Cairncross, 2001; Jeffrey, 2005). Coal consumption in South Africa currently accounts for 74% of the country's energy usage, the remaining southern African countries mine and use considerably less coal.

With very few exceptions, all the Southern African sub-continent's coal seams are hosted in Permian-age rocks of the Karoo Supergroup. One exception is the Triassic Molteno coalfield in South Africa {Cairncross, 2001, An overview of the Permian (Karoo) coal deposits of southern Africa }. Coal is exploited with varying degrees of sophistication. Cairncross (2001) reports that South Africa is well endowed with coal resources, this is partly due to the Karoo basin within the country. South Africa leads the southern African countries with respect to volumes of coal mined and exported, having produced 224.3 million tons and exported 67 million tons during 1998 (Cairncross, 2001; DMR, 2014). South Africa's coal reserves are estimated to be 66.7 billion tones, which is 5th in the world in 2012.

The Karoo basin in South Africa is regarded as the type-locality for southern African coals (Cairncross, 2001). This is somewhat misleading because although the Karoo basin contains the most complete succession of sedimentary strata and the largest coal resources, the tectonic setting and some of the sedimentary facies in other southern African Karoo coal basins exhibit different traits to those of the main Karoo Basin. The distribution of the Permian Karoo strata is relatively widespread in southern Africa, but the distribution of coal within these strata is less common. Therefore, not all potential Early Permian Karoo lithologies contain coal (Cairncross, 2001). The coal deposits of southern Africa occur in three tectonic basin:

- Foreland (e.g. Karoo basin, South Africa)
- Intercratonic rifts (e.g. Livingstonia, Malawi)

- Intracratonic rifts (e.g. Waterberg basin, South Africa)

Apart from the Karoo basin in South Africa which is a retroarc foreland basin, all of the remaining Southern African coal bearing basins are extensional rift related basins either intra and intercratonic grabens or half grabens. The Permian coal deposits in the Karoo basin define an arc extending from west to east in the northern section of the depository. The depth below surface of the coal seams in this area is relatively shallow with most coal being less than 200 m below surface. This depth increases from south to south-west and west in the Free State area where younger Triassic cover rocks overly the coal bearing Ecca Group strata. In the main coal mining regions of the Witbank, Highveld and KZN coalfields, opencast operations are utilized to extract the shallow coals while underground operations exploit deeper coal (Cairncross, 2001; Jeffrey, 2005).

3.2. History of Coal Mining in Northern KwaZulu-Natal

Large scale commercial exploitation of northern KZN's coal deposits was initiated by the formation of the Dundee coal company in January 1889 under the leadership of Benjamin Greenacre (Guest, 1988; Munnik, 2010). For half a century following the arrival of Voortrekker in the late 1830's, numerous outcrops of coal had been haphazardly exploited for domestic consumption by the white farming community of the region. Starting from the 1840's, small consignments had been transported for sale as far as Pietermaritzburg. Deposits had been found on several properties in the Newcastle vicinity, along the Biggarsberg, near Ladysmith as well as limited quantities in the Msinga district, on the Mvoti and Thukela river, and at Compensation on the coastline north of Durban (Guest, 1988).

By the 1880's, the Klip River had emerged as that part of KZN with the most obvious mining potential. Talana Hill in Dundee where Peter Smith had initiated mining activity, had already been recognised as the coal capital (Guest, 1988; Munnik, 2010). Talana Hill being geographically central to the Klip River coalfield in which prior to 1930's was where most of KZN's mining took place. Two events facilitated the development of commercial mining operations in the region. Firstly, in September 1881 Frederick W. North, a British Geological expert investigated KZN's coal resources. This attracted much attention to the region by the report that Klip River was endowed with a workable coalfield no less than 3496 km^2 and contained 2073 million tons of coal. Secondly, the discovery in 1886 of the main Witwatersrand Gold reef (Guest,1988; Munnik, 2010) and a determination to ensure for Natal a reasonable share in the trade

While the Dundee and Elandslaagte Companies proved to be two of KZN's more enduring mining enterprises, over half of the 60-odd collieries that were opened during the colonial era had closed by 1910. A decade later, a similar pattern of economic devastation played itself out in what was once South Africa's primary coal belts, the northern KZN coalfields, now known as the "Coal-Rim Cluster" (Townsend, 1983). This is one of the country's worst affected mining areas, having the near-total collapse of one of the core economic mainstays of the region.

3.3. History of Mine Abandonment

South Africa's history includes more than a century of mining. From as early as 1903 until 1990s, there were no adequate legislation that addresses environmental and social responsibilities of mining and mining closure (Swart, 2003). Mine owners were fully responsible for mining impacts until they had obtained a certificate of closure, but instead many owners abandoned mines due to bankruptcy, death or to avoid responsibility. To address this, the 'Fanie Botha Accord' was signed in 1975 whereby the Department of Water Affairs and Chamber of Mines took joint responsibility of mines, abandoned mines in the period from 1976 to 1986 {Mutwiri, 2016, Corprate Social Responsibility And its Role In the Realization of the Right To a Clean And Healthy Environment In the Mining Sector: A Case Study of Coal Mining in Kitui County-Mui Basin}, making mine owners partially responsible. After 1986, all mining related responsibility was placed back on mine owners (Swart, 2003; Mutwiri, 2016).

Following the major changes in legislation in the 1990s, a mine is only regarded as closed, once a closure certificate has been issued in terms of section 43 of the Minerals and Petroleum Resources Development Act (MPRDA) (No.28 of 2002). Until then, the owner remains responsible and according to Sections 41 and 43 of the MPRD Act, the owner should financially provide for all the environmental liabilities that are related to the mine (Aken et al., 2005). According to Section 46 of the MPRDA, a mine is proclaimed abandoned if no closure certificate has been issued and no responsible owner can be traced. The abandoned mine becomes the responsibility of Department of Mineral Resources (DMR) to rehabilitate. By 2008, a total of 5906 mines were considered ownerless and dilapidated, becoming the full responsibility of the government (Aken et al., 2005). Most of them had gained that status prior to 2002 when the MPRDA came into force. Auditing of these mines determined a total of 1730 out of the 5906 mines were classified as high-risk. This ranking was founded on levels of air pollution from wind-blown dust or combustion, on contamination of surrounding water

resources by AMD and on physical hazards presented by open shafts and unstable slopes. The audit found that the DMR had exclusively focused on asbestos mines, rehabilitating five of the 5906 mines (Aken et al., 2005).

In a research report conducted by the World Wildlife Foundation (Colvin et al., 2011), land-based activities such as agriculture, industries, mining, and human settlements were found to pollute and alter the biological, chemical and physical characteristics of water, often rendering it unfit for use and/or consumption. Pollution also compromises the health of riverine biota which are indicators of the condition of the river. The research further reported that defunct mines discharge acid water into the environment which might end up in the river. It is therefore important that water resources quantity, quality and use are monitored to ensure protection for sustainable use (Colvin et al., 2011).

One of the main water quality problems experienced in South Africa are that of AMD (Colvin et al., 2011). Significant strides have been taken by the Department of Water Affairs in dealing with the problem of AMD. However, there are still serious cases of localized pollution in some parts of the country, especially in the vicinity of mining and industrial activities. This is evident in the Thukela, Usuthu to Mhlathuze and Olifants WMAs, where historical coal mining resulted in AMD generation in areas such as Vryheid, Dundee, Newcastle and others.

3.4. KwaZulu-Natal's Coal Fields

KZN's coal reserves are situated within five coal fields, namely from west to east, Klip River, Utrecht, Vryheid, Nongoma and Somkele (Figure 3.1 and 3.2). The reserves are small compared to the national reserve, and seams are characteristically thin with numerous geological related obstructions. Faulting is often present which may cause mining problems. Seams are mainly developed within the Ecca Group of the Karoo Sequence apart from Somkele and eastern Nongoma, which are hosted in the Beaufort Group. Faults are frequently associated with various Jurassic dolerite intrusions. Post-Ecca dolerite intrusions impact the coal either by burning the seams or enhancing overall coal rank and quality, therefore the coal in the fields is generally of high quality, ranking largely as anthracite (MINTEK, 2007).

The metamorphic effects of dolerite sills on coals are controlled by intrusion thickness, temperature of intrusion and position of the sill relative to the coal (Jeffrey, 2005). Intrusions may also sometimes cause displacement of the relatively flat lying sediments and seams. The sill phases generally precede dyke emplacement. Earlier dykes are similar and persistent, while

younger intrusions tend to be inconsistent and have winding form. The oldest prominent and persistent sill in the area is the Zuinguin Sill (Jeffrey, 2005). The coalfields can be divided into two groups: Group 1:- The Klip River, Utrecht and Vryheid Coalfields that are situated within deeply-incised topography within the main Karoo basin. Group 2:- The Nongoma and Somkele Coalfields that are located in the eastern sector and are different in character and do not correlate with first group as they lack isolated seams (Jeffrey, 2005).

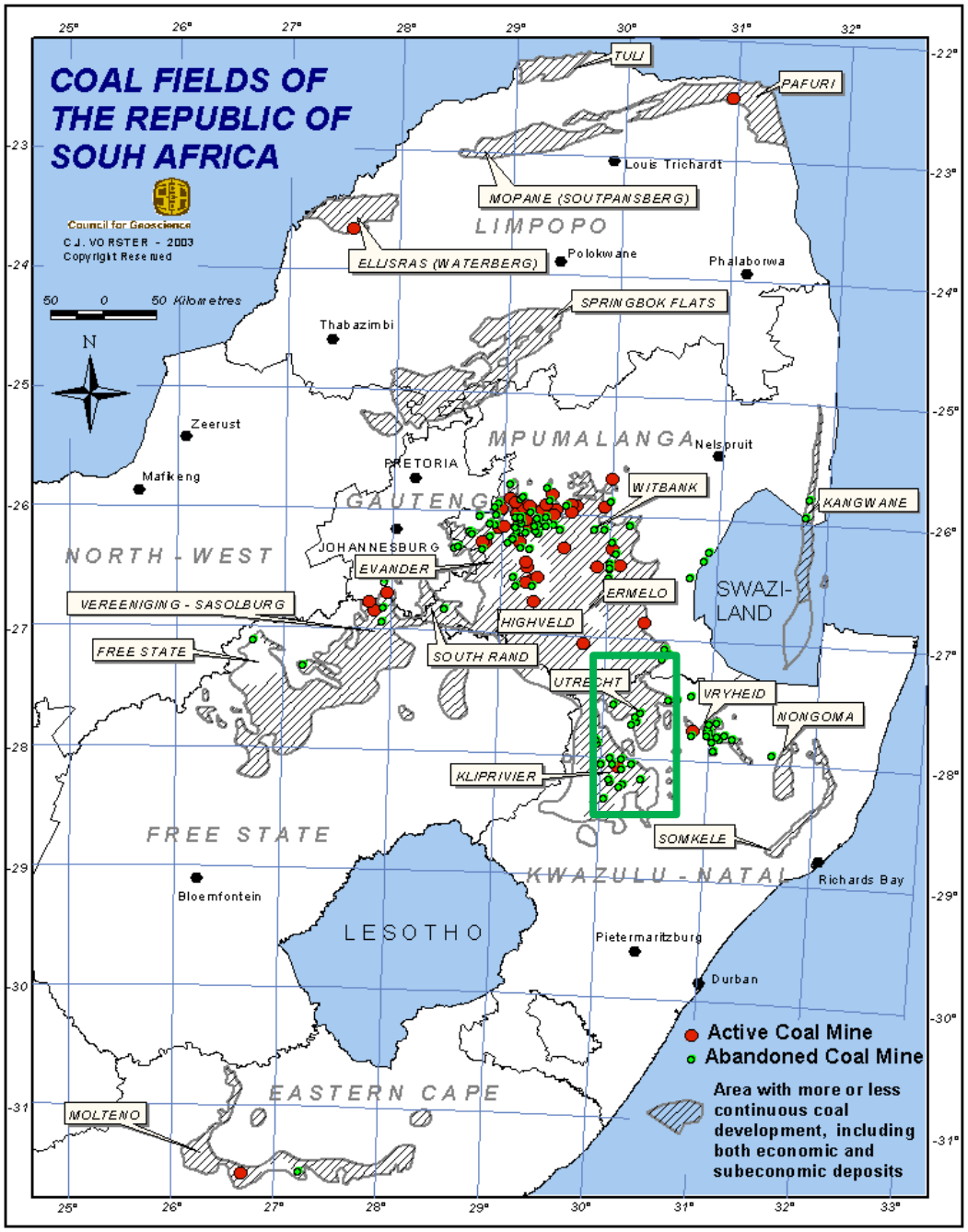

Figure 3. 1. Coalfields of South Africa (Adapted from Vorster, 2003).

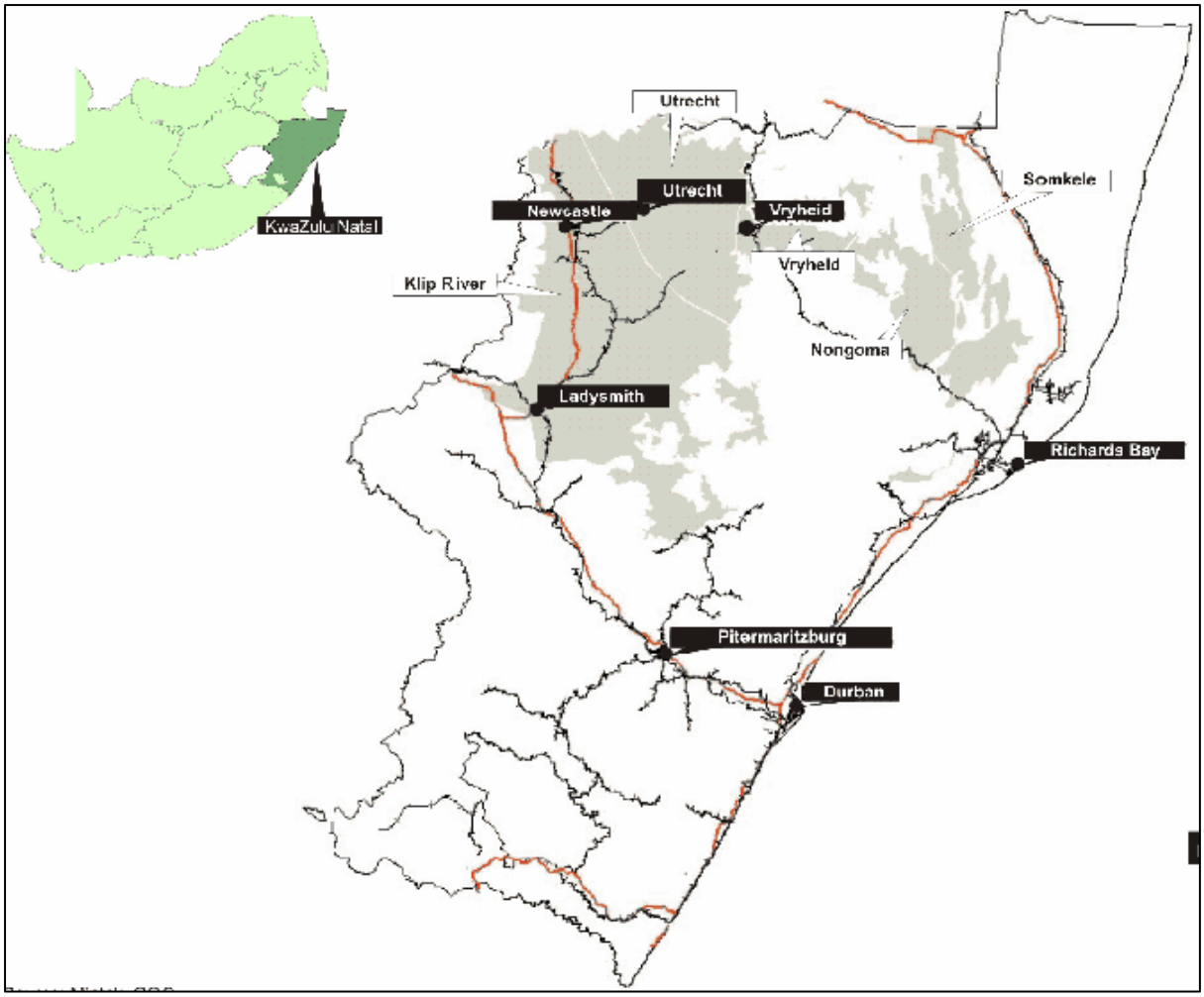

Figure 3. 2. Map showing various coalfields in northern KZN (MINTEK, 2007)

I. Klip River Coalfield

The Klip River Coalfield is the most economically important and largest of the coalfields in KZN. It has an area of 6 000 km^2, 50% of which bears economically extractable coal. The Klip River Coalfiled is inclusive of Dundee, Dannhauser as well as Glencoe areas (Figure 3.1 and 3.2). Faulting in the area is known to have disturbed the coal horizons by over 137 m. The two economic seams present are the Top seam (0.5 - 3.3 m thick) of bright coal and the Bottom Seam (0.5 - 1.3 m thick) with comparatively less coal. Although the quality varies across the seams, they both yield a generally high-grade product with ranks from bituminous coal to anthracite. The best quality coals are produced in the central parts of the field with qualities decreasing and seams thinning to the north and south. Devolatilization of the coal by dolerite intrusion has caused the formation of lean coal and anthracite for domestic use. Methane gas trapped within fissures associated with dyke intrusion can be hazardous (Mintek, 2007). The Top seam is often correlated with the Alfred Seam within the Utrecht and Vryheid Coalfields. Similarly, the bottom seam is considered to be the equivalent of the Gus Seam.

The roof and floor of the Seams are variable in condition across their extent, consisting of sandstone and shale. The seams are separated by coarse grained cross-bedded sandstone that fines up to carbonaceous shale. This forms a competent roof to the bottom seam while the roof of the Top seam is considerably weaker and composed of micaceous sandy shale (MINTEK, 2007; Gotz & Hancox, 2014).

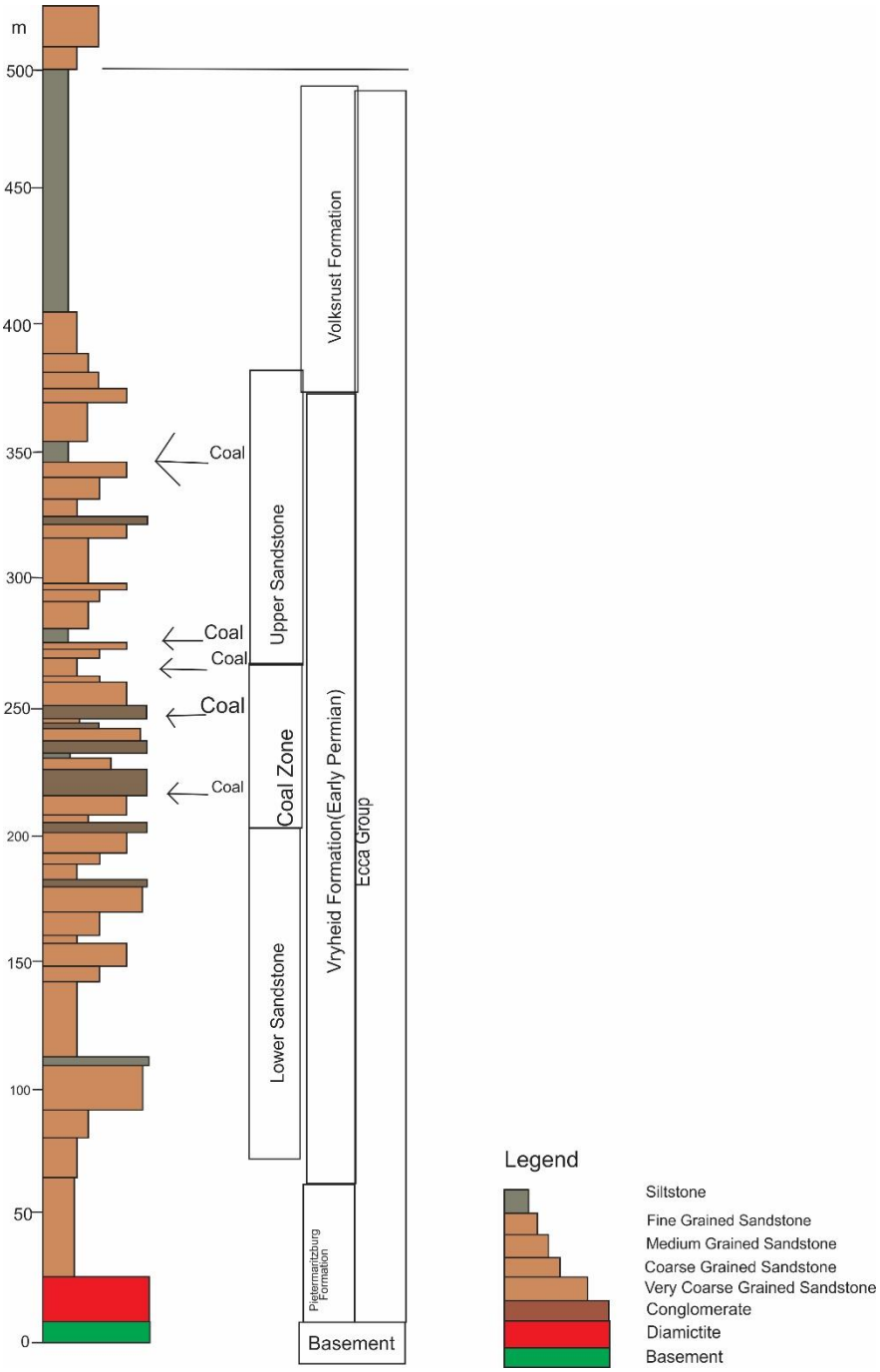

Figure 3. 3. Stratigraphic column of the Klip River Coalfield (Modified from Hancox and Gotz, 2014).

The coal zone in the Dundee coalfields comprises a complex succession of sandstone and siltstone delta-plain deposits and varies in thickness from 30 to 80 m (Figure 3.3). Although this unit is traceable over the entire area, it displays prominent lateral variations in lithology. Correlation of the strata is aided by closely spaced boreholes (Hampson et al., 1999). Both upper-and lower delta-plain environments are identifiable and comprise interdistributary, embayment and distributary-channel sediments (MINTEK, 2007). Lower-delta-plain-sedimentary environments are to be seen primarily near the base of the coal zone and the existence of transitional and upper-delta-plain conditions is indicated by an upward decrease in bioturbation. The economic coal seams are associated with transitional lower- to upper-delta-plain deposits (MINTEK, 2007).

A maximum of four significant coal seams are present in the Coal zone of Dundee and their nomenclature varies from one mine to another. The base of the productive zone has been set by geologists in the MINTEK (2007) report as what they refer to as the Extra Bottom seam. The same coal was called the No.3 seam by Anglo American geologists at Indumeni Colliery which is now closed.

II. Utrecht Coalfield

The Utrecht Coalfield, as described in a report written by MINTEK, (2007) has an area of 5000 km^2 lying in areas which are capped by dolerite. The quality of the coal is described as one which varies from high rank, low volatile anthracite to coking coal, to having four economic seams which are present in the Vryheid Formation of the Ecca Group, namely the Coking, Dundas, Gus and Alfred Seams. These are underlain by the dolerite-intruded lower portions of the Karoo sequence. The relative position of the seam is dependent on the elevation and thickness of sills.

The Coking Seam, generally less than 1m thick, has a maximum thickness of 1.5m. It is comprised of bright, thinly-banded coal and includes sandy or silty lenses where it thickens. The overall quality is good, yielding moderately good coking coal. The Dundas Seam which lies 15m above the coking Seam, has a maximum thickness of 2.6 m. It yields bituminous coal and export-quality anthracite. It consists of dull and bright coal in the upper portion, bright coal in the central region and a mixed coal and shale zone at the bottom {MINTEK, 2007, Assessment of KwaZulu-Natal Provinces coal mining and coal resources}. The Gus Seam lies 17 m above the Dundas Seam and is the most economically important seam. It has a maximum thickness of 3.3 m of bright coal. In the north it splits into an upper, better developed seam and

a lower seam from which it is separated by sandstone. The Gus Seam is divided into three distinct quality zones separated by consistent shale partings. Finally, the Alfred Seam which lies 14 m above the Gus Seam. With average and maximum thickness of 1.9 m and 3.8 m respectively, this seam consists of dull-lustrous coal interbedded with bright coal. The poorer quality predominates but high-quality coal can be found in the area 25 km east of Utrecht. The seam is best developed in a down-faulted block to the south of Utrecht {MINTEK, 2007, Assessment of KwaZulu-Natal Provinces coal mining and coal resources}.

III. Vryheid Coalfields

The Vryheid coalfields were described to have been separated from the Utrecht Coalfields by an area barren of coal (MINTEK, 2007). This coal was removed by erosion. It has a surface area 2500 km^2 of which 15% is coal bearing. Dolerite sills have had a striking effect on the topography of the area. The main coal zone is found within the Vryheid Formation which is situated in the middle of the Ecca Group of the Karoo Sequence, lying above the glacial Dwyka Formation. Sedimentary facies are characterized by a series of coal-capped, upward-finning cycles (Figure 3.4). The rank of coal varies from moderate to high quality. Historically Vryheid has locally been a consistent producer of high-quality metallurgical coal and anthracite. Seams have been affected by displacement and devolatilization due to the presence of dolerite intrusions (Cadle, 1993; Christie et al., 1998; MINTEK, 2007). The 1 m thick Coking Seam is generally thin but of a high grade as it is found in the Utrecht Coal field. The sediments forming the parting between this seam and the overlying Dundas Seam are fine to medium-grained sandstone and exist as an excellent marker bed {MINTEK, 2007, Assessment of KwaZulu-Natal Provinces coal mining and coal resources}. The Dundas Seam in this contain two splits, the lower seam reaches a maximum thickness of 2.5 m of interbedded bright and dull coal that often has a thin shale and sandstone parting on the top portion report by MINTEK (2007). The highest quality anthracite produced in South Africa is found in the Vryheid Coalfields. The Alfred Seam is reported to be of poorer quality than the other seams.

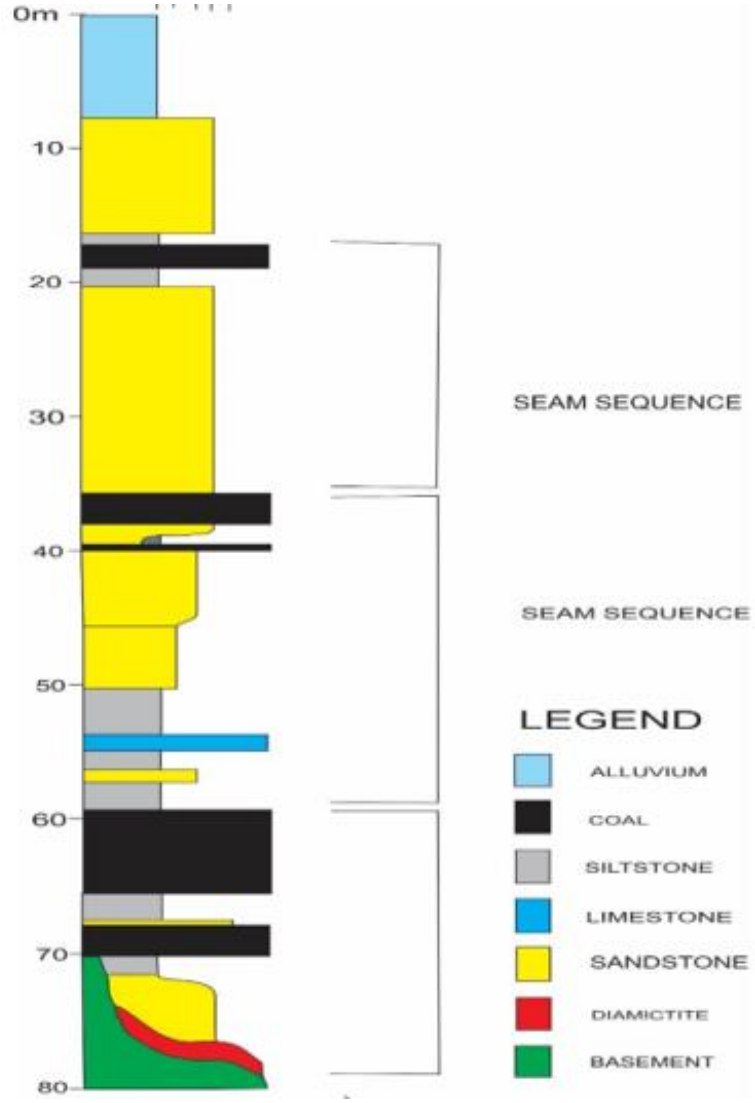

Figure 3. 4. Lithostratigraphy of the Vryheid Coalfields (Adapted fromHancox and Gotz, 2014)

3.5. Current Environmental Legislative Framework

I. National Environmental Management Act (Act No. 107 of 1998)

This Act provides the framework and principles for sustainable development and sets national norms and standards for Integrated Environmental Management (section 24), where all spheres of Government and all organs of state must co-operate, consult and support one another. Section 28 of the Act also imposes a Duty of Care and remediation of environmental damage on any person who causes, has caused or may cause significant pollution or degradation of the environment. Furthermore, sections 32 and 33 of the Act provides for legal standing to enforce environmental laws and private prosecution respectively (Swart, 2003).

II. Minerals Act (Act No.50 of 1991)

The most important requirement concerning the environment and rehabilitation, is that an Environmental Management Programme (EMP) (Swart, 2003), based on environmental impact assessment, must be submitted and officially approved. Section 38 of the 1991 Minerals Act requires that the rehabilitation of land concerned in any prospecting or mining shall be carried out by the holder of the prospecting permit or mining authorization concerned. Government and the mining industry have accepted the principle that the polluter must pay for pollution or the damage that prospecting or mining actions incur on the environment. Regulations have been declared in terms of the 1991 Minerals Act, to ensure that financial provision is made by a mine in the form of guarantees for the execution of its EMP.

III. National Water Act (Act 36 of 1998)

The National water act sets out the fundamental principles and the Act sets out the protection of water resources. Chapter 1 of the Act states that sustainability and equity are identified as central guiding principles in the protection, use, development, conservation, management and control of water resources. These guiding principles recognise the basic human needs of present and future generations, the need to protect water resources, the need to share some water resources with other countries, the need to promote social and economic development through the use of water and need to establish suitable institutions in order to achieve the purpose of the Act. While Chapter 3 of the Act lays down a series of measures which are together intended to ensure the comprehensive protection of all water resources and deals with pollution prevention, and the situation where pollution of a water resource occurs or might occur as a result of activities on land. The person who owns, controls, occupies or uses the land in question is responsible for taking measures to prevent pollution of water resources. If these measures are not taken, the catchment management agency concerned may itself do whatever is necessary to prevent the pollution or to remedy its effects, and to recover all reasonable costs from the person responsible for the pollution (Swart, 2003).

3. 6. Impacts of mining on groundwater resources

One of the most common occurrences of acidic conditions in the environment is associated with the mining of coal and base metals. Pyrite occurs with the ore material because the environment in which the coal or metals were deposited is reducing and is conductive to the formation of pyrite and other sulphide minerals along with the ore (Egboka et al., 2013). Mining operations expose sulphide minerals in the host rock to atmospheric oxygen either in the underground workings or in surface spoils. In the case of coal deposits, pyrite is a minor

component of organic ore material. Strip mining of coal also has the potential for producing acidic conditions if the coal contains sulphide minerals and has a low-neutralizing capacity. This means that water moving through the aquifer will react to varying degrees with the surrounding minerals and other components, and it is these rock-water interactions that give the water its characteristic chemistry (Utom et al., 2012; Okiongbo and Douglas, 2015). The regional geology plays a very significant role in determining the hydrogeochemistry of groundwater system as the mineralogy of the geological units control, to a large extent, the chemical quality of water permeating through the system (Utom et al., 2012; Okiongbo and Douglas, 2015).

AMD has been recognised as a major environmental pollution problem over the past decades. AMD produced as a result of oxidation of minerals containing reduced forms of sulphur (pyrite or its polymorph, marcasite (FeS_2), pyrrhotite (FeS), galena (PbS), sphalerite (ZnS), chalcopyrite ($FeCuS_2$) which commonly occurs when sulphide bearing minerals in rocks, are exposed to air and water, transforming sulphides into sulphuric acid. This means that the more the surface area of rock is exposed, the greater the amount of acid (Younger, 1994). During the mining process, hundreds of tons of rock are dug up and crushed each day. Oxidation of sulphide mine waste can lead to the discharge of high levels of total dissolved solids, particularly metals, SO_4^{2-}, and low pH waters which can be hazardous to the environment and may pollute groundwater resources. Certain bacteria, frequently present in these environments can significantly increase the rate of this reaction. The acid generated leaches and releases heavy metals such as lead, zinc, copper, arsenic, selenium, mercury and cadmium. High concentrations of Fe and Al are also typical in acid sulphate waters. Under typical soil conditions, Al activity appears to be controlled by the solubility of gibbsite or kaolinite, while Fe activity is controlled by goethite or amorphous $Fe(OH)_3$ (Younger, 1994 & Arnesen, 1997). However, in areas of sulphide oxidation, high concentrations of sulphate modify the aqueous geochemistry of Al and Fe. In acid sulphate drainage waters and leachate solutions from mine waste tailings and soils, solubility appears to be controlled by a variety of basic Al/Fe oxides, oxyhydroxides and sulphate phases (Younger, 1994 & Arnesen, 1997).

Many coal and base metal mines have been closed for economical or political reasons during the past decade. Such closures can lead to a variety of environmental impacts, some of the most common being the effects on the hydrogeological environment due to terminantion of dewatering pumping. These negative hydrogeological impacts include the flooding of low-lying areas, particularly areas affected by subsidence which may be regional and up to several

meteres in magnitude, contaminant mobilization and transport via rapid groundwater flow pathways, minning fractures and openings, subsidence of shallow workigs and elevated mine gas emissions (Younger, 1994 in Arnesen, 1997).

3. 7. Acid Mine drainage (AMD)

AMD is one of the major sources of water pollution in and around active and abandoned coal mines, and hence it is regarded as a worldwide issue. AMD causes environmental pollution that affects many countries including South Africa. It is mainly caused by the oxidation of sulphides such as pyrite, marcasite and pyrrhotite (Equeenuddin et al., 2010). Pyrite occurs with the ore mineral because the environment in which the coal was deposited is reducing and is conducive to the formation of pyrite and other sulphide minerals along with the ore (Deutsch, 1997). Due to mining activities, sulphide minerals are exposed to atmospheric oxygen and water which leads to the generation of H_2SO_4. AMD is characterised by low pH, high SO_4^{2-}, Fe, Al, and various toxic metals. The geochemical behaviour of Fe and Al mainly controls the mobility of metals through adsorption and co-precipitation in the acidic sulphate rich water (Equeenuddin et al., 2010). The variation in sulphur content is associated with depositional and diagenetic conditions throughout peat and coal development. Acid mine drainage that has had the opportunity to come into contact with neutralizing minerals such as carbonates along the groundwater flow paths in aquifers is not likely to remain acidic as are surface waters (Deutsch, 1997).

3.7.1. Occurrence of Naturally Acidic Conditions

Acidification is primarily caused by the generation of ferrous iron bearing and minerlized surface water and groundwater (Figure 3.5), transport through the groundwater-surface water interface, as well as iron oxidation and precipitation. The rates of acid generation in mine tailings and dumps, and surface water are often similar (1 to > 10 mol/ m^2yr^{-1}). Weathering processes often tend to buffer groundwaters to only moderately acidic or neutral pH, depending on the type of minerals present. In some mine lakes, the acidity balance is affected by proton release from transformation of metastable iron hydrosulphate minerals to geothite, and ferrous iron sequences by burial of iron sulphides and carbonates in sediments (Blodau, 2006).

The natural occurrence of highly acidic conditions due to, for example, pyrite oxidation is somewhat rare because the rate of acid generation which can be balanced by neutralization reactions. Water and oxygen in the unsaturated zone will oxidize pyrite, but the solution may in turn be neutralized as it flows through the unsaturated and saturated zones on its path to a

discharge point. If the neutralizing capacity of the material along the flow path has been consumed or the rate of neutralization is too slow for the residence time of the groundwater, then the discharge water may remain acidic, but this is likely only for a very short flow path in highly weathered material. The rate of exposure of fresh pyrite and other sulphide minerals to near earth surface oxidizing conditions, hence the rate of acid generation, will be governed by the weathering rate (Figure 3.5). The chemical weathering processes is generally very slow. This will provide time for neutralizing reactions to occur as the landscape naturally weathers and slowly exposes new sulphide minerals to oxidizing conditions. Mechanical weathering such as mass wasting, which is primarily important in areas of high relief, may rapidly expose acid - producing minerals to earth surface conditions. In these cases, localized zones of acidity may be created, and surface waters may be acidic because of the limited opportunities for neutralization by water/rock interactions (Blodau, 2006).

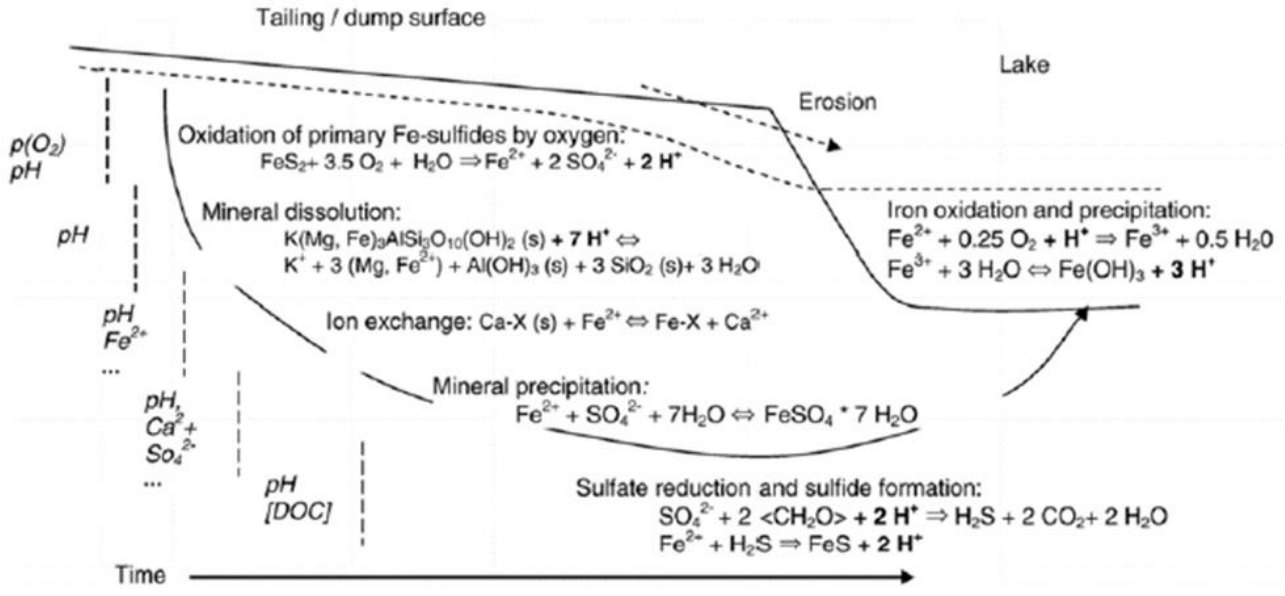

Figure 3. 5. A schematic diagram of processes partaining to acid generation in mine dumps (Blodau, 2006).

3.7.2. Pyrite oxidation

Mining allows for the introduction of oxygen to the deep geological environment and therefore the oxidation of minerals which are in a reduced state. The same occurs when reduced minerals are brought to the surface and deposited in spill tips. The most common of these minerals are the sulphides, some sulphide reduction and formation reactions are shown in Figure 3.5 and Table 3.1. Unlike most geochemical weathering processes, the oxidation of some sulphides leads to the production, rather than the consumption of the protons. Pyrite is present in most

metal sulphide and coal deposits and may exist in potential association with other chalcophile elements such as AS, Bi, Cd, Co, Cu, Ga, In, Hg, Mo, Pb, Re, Sb, Se, Sn, Te and Zn. Pyrite undergoes a complex cycle of reactions during oxidation as shown from equation 1 to 5 {Banks, 1997, Mine-Water chemistry: The good`, the bad and the ugly}:

$2FeS_2 + 2H_2O + 7O_2 \leftrightarrow 2Fe^{2+} + 4SO_4^{2-} + 4H^+_{(aq)}$……(1)

Pyrite + water + oxygen $\leftrightarrow$ ferrous iron + sulphate + acid

Further partial oxidation of ferrous to ferric iron consumes some protons:

$4Fe^{2+} + 4H^+_{(aq)} + O_2 \leftrightarrow 4Fe^{3+} + 2H_2O$……..……..(2)

Ferric iron may act as an electron acceptor for further pyrite oxidation, or hydrolysis may occur, both processes releasing further protons:

$FeS_2 + 14Fe^{3+} + 8H_2O \leftrightarrow 15Fe^{2+} + 2SO_4^{2-} + 16H^+_{(aq)}$……..(3)

Where Fe^{3+} regenerated from Fe^{2+} by iron-oxidizing bacteria and archaea such as acidithiobacillus Ferrooxidans, which oxidises both the Fe^{2+} and reduced sulfur species (thiosulfate and sulfur), and Leptospirillum ferroxidans, which oxidises only Fe^{2+}. Without Fe-oxidising bacteria, pyrite oxidation would stop because the abiotic oxidation of Fe^{2+} at low pH is slow (Nordstrom, 2011).

$Fe^{3+} + 3H_2O \leftrightarrow Fe(OH)_3 + 3H^+_{(aq)}$…….(4)

The overall sequence of reactions is acid-producing:

$4FeS_2 + 14H_2O + 15O_2 \leftrightarrow 4Fe(OH)_3 + 8SO_4^{2-} + 16H^+_{(aq)}$……..……(5)

Table 3. 1. Some selected processes causing changes in acidity of mine waters {Sherman, 1998, The Assessemnt of Groundwater Quality in Rural Communities: Two Case studies from KwaZulu-Natal}.

Processes involved in acidity generation	
Redox Reactions	Stoichiometry
Pyrite Oxidation	$FeS_2 + 3.5O_2 + 3H_2O \rightarrow Fe^{2+} + 2SO_4^{2-} + 2H^+$
Pyrite Oxidation	$FeS_2 + 14Fe^{3+} + 8H_2O \rightarrow 15Fe^{2+} + 2SO_4^{2-} + 16H^+$
Ferrous iron oxidation	$Fe^{2+} + 0.25O_2 + H^+ \rightarrow Fe^{3+} + 0.5H_2O$
Pyrrhotite oxidation	$FeS + 2O_2 \rightarrow Fe^{2+} + SO_4^{2-}$

Sulphur oxidation	$S\ (0) + 1.5O_2 + H_2O \longrightarrow 2H^+ + SO_4^{2-}$
Chalcopyrite oxidation	$CuFeS_2 + 4O_2 \rightarrow Cu^{2+} + Fe^{2+} + 2SO_4^{2-}$
Sphalerite oxidation	$ZnS + 2O_2 \rightarrow Zn^{2+} + SO_4^{2-}$

3.8. Remediation and Rehabilitation of mine sites

If surface water and groundwater monitoring information reveal contamination of the environment, the remediation of an acid-contaminated aquifer is initiated by first eliminating or neutralizing the source. In many coal mines, limestone dust is commonly spread over the mine surfaces to hinder the mobilization of explosive coal dust and to act as a flame barrier in the case of an explosion. This limestone dust may also serve to neutralize mine water (Arnesen., 1997; Blodau, 2006). The addition of limestone or other carbonate mineral to an acid generating source is a common practice. The carbonate serves to neutralize any acid produced and keep the pH high, thereby slowing acid generation. A further possible benefit of using a rapid neutralizer such as carbonate minerals was reported by Nicholson et al., (1990) in Deutsh (1997), who states that ferrihydrite may precipitate on the pyrite during neutralisation, protecting it from further oxidation. On the other hand, if ferrihydrite precipitates on the carbonate minerals, it will impede neutralization. The exact amount of lime required would depend on the balance between neutralization and pyrite oxidation rates, as they occur in the mine. This assumes that no other external influences such as acidity or alkalinity from varied sources in the area. Carbonate dissolution rates have proven to be significantly faster in circumneutral hydrochemical conditions as compared to that of non-carbonates.

Remediation was carried out on all abandoned, liquidated or decommissioned mine workings in northern KZN following the White Paper WP E-87 release in 1987. On site waste rock was converted into discard dumps and strategically placed near the mine site on suitable ground. Powdered $CaCO_3$ was applied and interlayered within the discard dumps, covering a larger surface area with the piles (DWAF, 1998). This mechanism relies on rainfall to mix with the limestone slurry and leach into the pile, reacting with sulphide-bearing mine tailings in order to neutralize it. Once the leachate reaches the groundwater, neutralization reactions would have occurred. Subsequently spoil heaps were levelled and the acidity of the soil reduced, a cover of soil and fertilizers was then applied (Figure 3.6). In order to increase the growth rates, different types of fertilizers were used (DWAF, 1998). The monitoring of 14 surface water points around the rehabilitated mines in northern KZN began in 2003. Major ions including pH and EC were measured to assess the quality of water in streams around rehabilitated mine sites.

Not more than a decade later, new boreholes were drilled by DWAF to monitor groundwater around the mine sites.

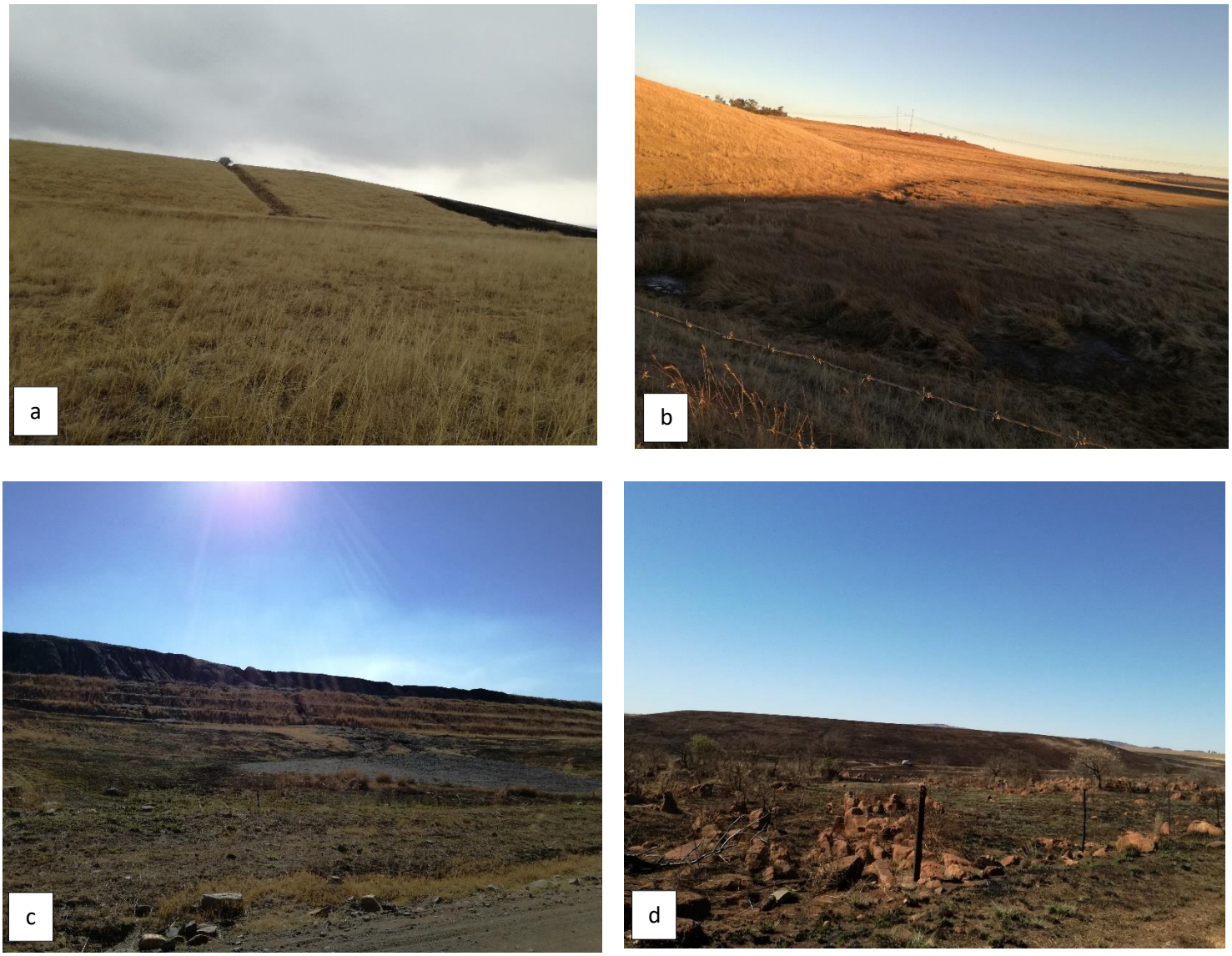

Figure 3. 6. Rehabilitated discard dumps at (a) Newcastle Star (b) Northern Natal Coal (NNC3) (c) St Georges and (d) Northern Natal Coal (NNC1).

3.9. Surface water and Groundwater Monitoring Networks around the Historical mining Districts

Surface water and groundwater monitoring wells and sites have been established in the northern KZN historical mining districts for collecting representative ground-water samples. The location of the different groundwater monitoring wells and surface water monitoring sites around each of the historical mining sites is shown in Figure 3.6. These monitoring sites were established with the aim of monitoring the water quality response of the rehabilitation of

defunct mines in the region's water resources. A total of 65 monitoring wells and 14 surface water monitoring stations have been established by DWAF. Surface water points have been monitored monthly from 2003 – 2013 in most sites, while biannual groundwater samples have been taken from 2010 to present. These monitored data and new data generated in the course of this research for these motoring sites are investigated as part of the hydrogeochemical characterization of the region.

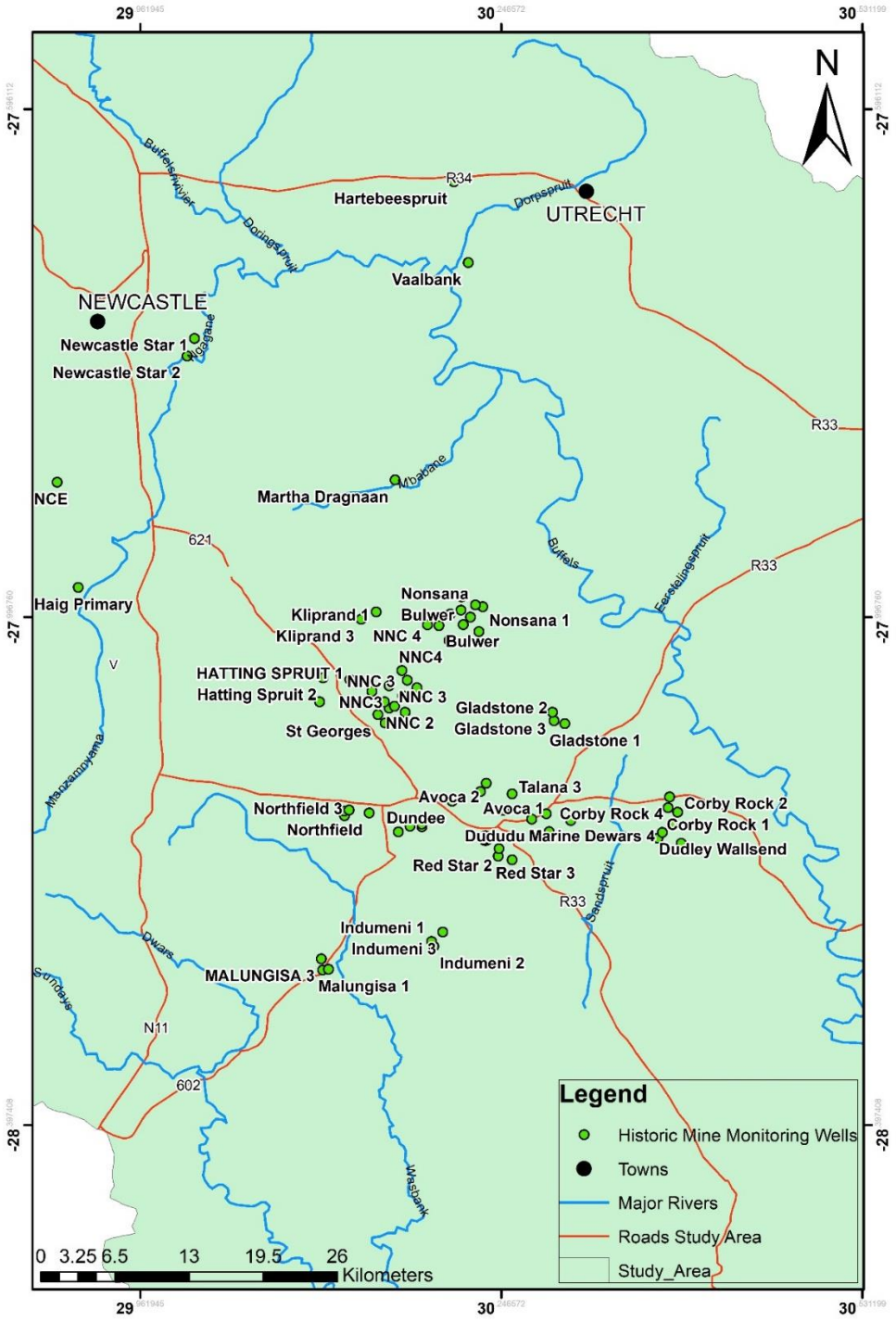

Figure 3. 7. Location of Groundwater monitoring wells around the study area.

CHAPTER 4: RESEARCH METHODOLOGY AND APPROACHES

The methodology, approach and techniques applied in the coarse of the research is presented in the following sections which includes detailed descriptions of the research process of primary data collection, through a well-planned field campaign, laboratory analysis and interpretation.

4.1. Desktop Studies

In order to start any investigation, there needs to be a clearly mapped out plan of action which will act as a guide. This research was started by reviewing existing data and literature on the northern KZN abandoned coal mining districts. Journal articles as well as official reports and Government documents pertaining to the study area were reviewed. Hydrometeorological data were obtained from South African Weather Service (SAWS, 2017). Hydrochemical data monitored from 2010 to 2015 was acquired from Department of Water and Sanitation. All data collected during the desktop study is used to compliment the original data generated throughout the duration of the research project.

4.3. Fieldwork

Primary field data was collected from thirty (30) monitoring boreholes and eleven (11) surface water sampling sites (Figure 4.1 & 4.2) Onsite hydrochemical parameters such as electrical conductivity (EC), pH, and temperature, Dissolved Oxygen (DO), Salinity and oxidation-reduction potential (ORP) were measured in situ using a Hanna HI 9828 multi-parameter water quality meter, which was calibrated after each measurement date. Inactive boreholes were purged of stagnant water to allow for the fresh formation water to be sampled. Total alkalinity, HCO_3^- and CO_3^{2-} concentrations were determined onsite by titration of water using 0.02M hydrochloric acid (HCl). Groundwater levels were measured using a Solinst TLC dip meter.

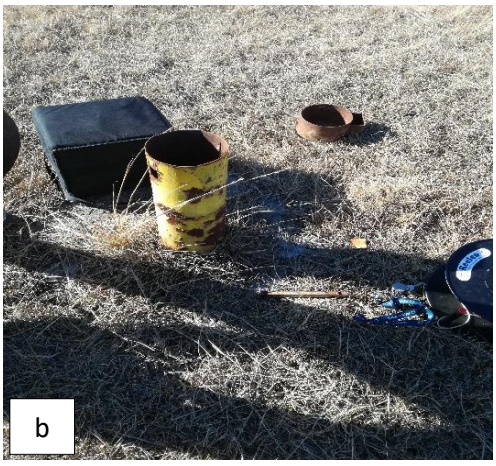

Figure 4. 1. Surface and borehole samples taken in August 2018: (a) Martha Dragnaan (b) NNC 2 (c) Buffels River upstream and (d) Ngangane River downstream

4.3.1. Water sampling procedure

Field sampling and testing equipment were cleaned thoroughly and calibrated before use. The depth to groundwater in boreholes were measured using a Solinist TLC dip meter following which after purging of inactive boreholes, in situ hydrochemical parameters were measured. Anion, cation and trace metal samples were filtered using a 0.45 micrometre filter and collected into 50 ml polyethylene sampling bottles. The cation and trace element samples were acidified immediately after sampling to a pH of < 2 using ultrapure nitric acid (30% HNO_3). Environmental isotope samples were collected unfiltered and untreated. All samples were kept in a cooler box below 4^{o}C. Collected samples were analysed for respective parameters.

The total alkalinity (TAL), carbonate and bicarbonate concentration were calculated from field titration data using the following equation:

$$\text{TAL (mg/l } CaCO_3) = \frac{\text{Total volume of HCl used (ml)} \times 0.02 \times 50\,000}{100} \ldots\ldots\ldots\ldots\ldots\ldots\ldots\ldots\ldots\ldots\ldots \ (6)$$

$$HCO_3 \text{ (mg/l)} = \frac{\text{Volume of acid used} \times 6.102 \times 10\,000}{100} \ldots\ldots\ldots\ldots\ldots\ldots\ldots\ldots\ldots\ldots\ldots\ldots\ldots\ldots\ldots\ldots\ldots \ (7)$$

$$CO_3 \text{ (mg/l)} = \frac{\text{Volume of acid used} \times 3.005}{100} \ldots\ldots\ldots\ldots\ldots\ldots\ldots\ldots\ldots\ldots\ldots\ldots\ldots\ldots\ldots\ldots\ldots\ldots\ldots\ldots. \ (8)$$

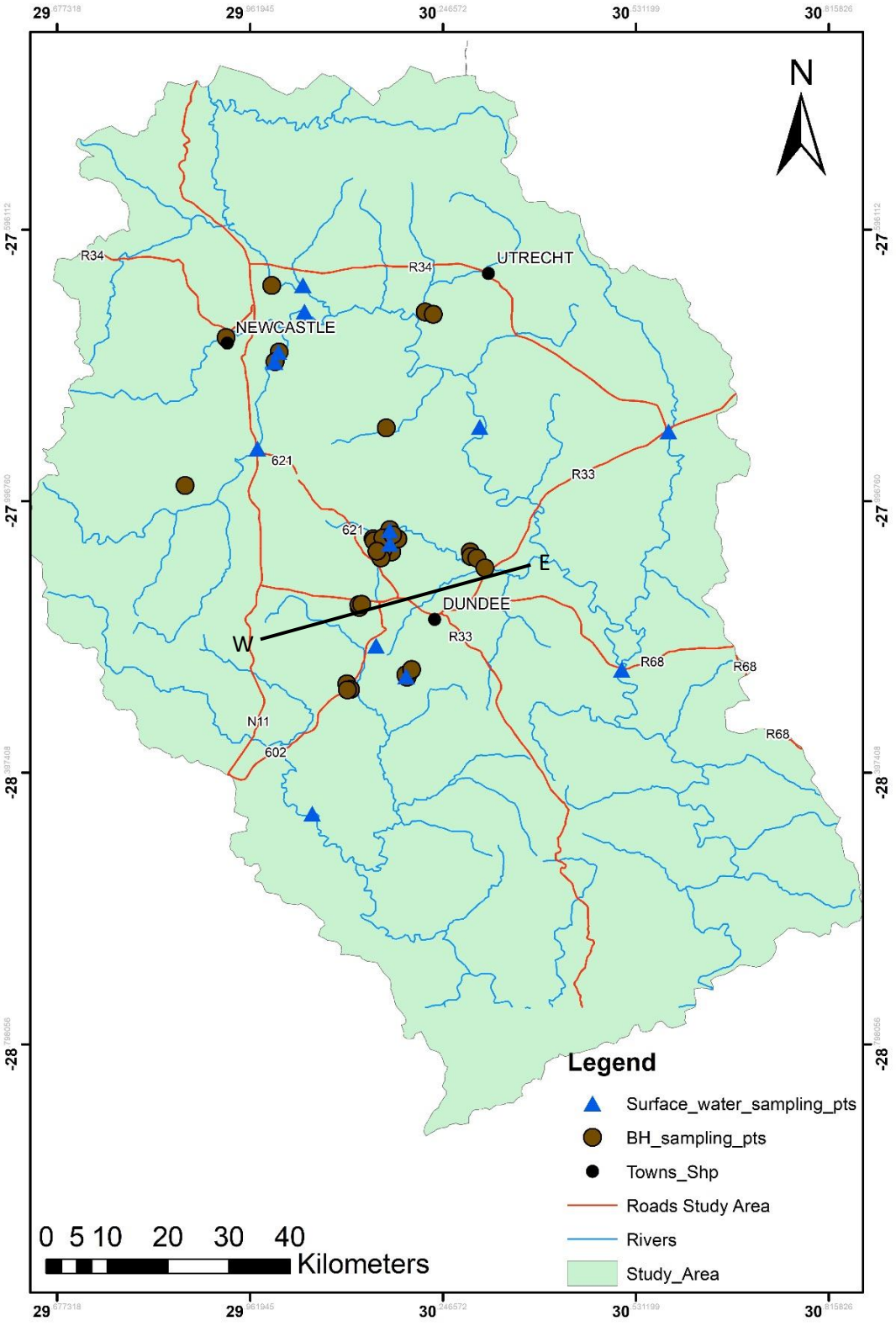

Figure 4. 2. Map showing the location of sampling points within the study area (W-E line in the figure indicates the cross section line of figure 5.24) .

4.4. Laboratory Analysis

Hydrochemical laboratory analyses were undertaken on the samples collected. Major cation and trace metal samples were analysed using Inductively Coupled Plasma Atomic emission spectrometer (ICP-AES) and Mass Spectrometer (ICP-MS), respectively at the University of Stellenbosch analytical laboratory. Major anions were analysed using a Dionex® Ion Chromatography (IC) within the Department of Geological Sciences, University of KwaZulu-Natal. Environmental isotopes (δ^2H and $\delta^{18}O$ and tritium) were analysed at the laboratory of the Environmental Isotope Group (EIG) of iThemba Labs, in Johannesburg, South Africa.

4.5. Data Interpretation Tools

Microsoft Excel was used to organise both surface water and groundwater data into coherent time series which would be easy for analysis and interpretation by exporting into various software. Time series plots for rainfall, pH, EC as well as hydrochemical plots were made possible using Excel. ArcGIS is a mapping software which is used extensively to map the study area, delineating the catchment boundaries as well as to outline the surface of the conceptual model X-section from a digital elevation model. Thereafter Choral Draw was used to for editing in order to better present the model. Aquachem™ was used to plot Trilinear plots (piper and ternary), Correlation plots, Thematic Map Plots (Pie, stiff plots) as well as Schoeller plots which helped in the presentation of the analysed primary and secondary data for interpretation. Piper plots are a very useful interpretative tool in groundwater chemistry and have been used extensively in this research as they are most useful for representing and comparing water quality revealing the similarities and dissimilarities among water samples as those with similar qualities will tend to plot together as groups {Dauda, 2015, Graphical Techniques Presentation of Hydro-Chemical Data}. Statistical Package for Social Science (SPSS) has been used for bivariate and multivariate statistical analysis of primary as well as secondary hydrochemical data. The software is important in finding the degree of association between hydrochemical parameters as field and laboratory data can be too large, random and complicated due to the complex of hydrogeological processes. Which is where multivariate statistical analysis techniques serve an important purpose as a tool to evaluate large hydro-geochemical dataset into manageable classifications with similar characteristics in order to reveal hidden similarities within the dataset. The technique mathematically reduces the parameter space dimensionally, thus simplifying the representation of the data and interpretation (Suk and Lee, 1999). The software has been used to produce Linear Correlation, Principal Component Analysis (PCA), Factor Analysis (FA), Cluster analysis as well as PCA Scatter plots. These plots have been

applied in the present study to understand the variation in major and minor elements in order to identify the processes responsible for the variations.

4.6. Groundwater Recharge

As part of conceptualizing the hydrogeological condition of the study area, mean annual groundwater recharge was estimated using the chloride mass balance method (Eriksson and Khunankasem, 1969). The CMB method uses both wet and dry chloride deposition at the surface and compares it with the chloride concentration in groundwater. The CMB method has been used to evaluate recharge processes in a wide range of environments, including the current study in northern KZN historic mining districts with fractured rock aquifers by comparing chloride concentrations in rainfall as well as in groundwater. The following assumptions are made when applying the method (Allison et al., 1984; Bean, 2003):

- The chloride behaves conservatively, i.e. it is not taken up by or leached from vegetation, unsaturated zone sediments or aquifer Formations.
- Atmospheric input of chloride consisting of wet and dry depositions are normally constant with time over longer periods, therefore long term and continuous monitoring are advisable for long term averages.
- A piston flow regime is assumed but can be nullified by complex transport of moisture vertically as well as horizontally. This may occur in the unsaturated zone as a result of the variability of rainfall and evapotranspiration or uneven topography.
- Preferential flow paths need to be attended to, as the soil moisture and solutes may be transported through the unsaturated zone by means of these pathways.

In this research, the CMB method was applied to estimate recharge using groundwater chloride measurements generated and using the GRAII precipitation chloride concentration (DWAF, 2006). The application of the CMB method is based on the comparison of the chloride concentration in precipitation with the concentration in groundwater (Demlie, 2015). It is worth noting that the CMB method is more effective when used along with other methods.

Therefore, the proportion of rainfall (R) that enters the aquifer as recharge is:

$$R = (Cl_p/Cl_{gw})\ x\ P \qquad (9)$$

Where P is mean annual precipitation (mm), and Cl_p and Cl_{gw} represent the chloride concentration in (mg/l) of precipitation and groundwater, respectively.

CHAPTER 5: RESULTS AND DISCUSSION

This chapter presents the research results including a detailed analysis, interpretation and discussion of the primary and secondary data collected. These include hydrochemical processes, saturation index calculations which are presented on time series graphs. Environmental isotope data are interpreted and included to understand the hydrogeological process within the study area.

5.1. Aquifer framework and groundwater occurrence

The study area lies within the Karoo basin which extends over much of South Africa. The geology of the study area is predominantly characterised by the Vryheid and Volksrust formations of the Ecca Group (Figure 2.4). The Vryheid Formation is the most extensive formation in northern Kwa-Zulu Natal area, where basal beds comprise shales, siltstones and sandstone, overlain by coarse-grained, cross-bedded sandstone and grits (Table 2.1). These are representative of sediments which were transported from the east and north-east and deposited in the river systems as well as related deltas during several regressive cycles (Hancox and Gotz, 2014). The accumulation of rotting vegetation in swampy environments instigated by the irregular pre-Karoo landscape along the north-western edge of the Karoo Basin gave rise to coal deposits, which encompasses thick coarse-grained sandstone beds and carbonaceous shale with thin coal seams (Hancox and Gotz, 2014).

During the Jurassic era, the Karoo sediments were intruded by dolerite dykes and sills. Dykes and sills have comparable geographical distribution and to a great extent control the geomorphology of the present-day landscape (Chevallier et.al., 2001). The aquifer framework is characteristic of intergranular and fractured aquifers of the Karoo basin. Dykes and sills are important for the occurrence of groundwater in the sandstones of the study area due to enhanced fracturing as a result of the intrusions. The average mean aquifer yields in the area are smaller than 1.0 l/s with average transmissivity of 0.84 m^2/d. However, pockets of high yield and transmissivity are reported where there is intense fracturing giving rise to yields and transmissivity as high as 5.0 l/s and 11.86 m^2/d, respectively. Particular interest to the study area is the Vryheid Formation which is the dominant Formation and has a mean borehole yield of 0.6 l/s and transmissivity up to 50 m^2/d (DWAF, 1993).

5.2. Groundwater recharge and groundwater flow in the Study Area

5.2.1. Groundwater Recharge Rate

The CMB method was used to estimate the groundwater recharge at each borehole based on groundwater chloride concentrations measured at each monitoring well during the course of this research and based on the average precipitation chloride deposition reported in the GRAII report (DWAF, 2006). The mean annual groundwater recharge from 30 monitoring wells was estimated at 29.3 mm or 4.1% of the mean annual areal precipitation for the study area. The detailed results of the groundwater chloride concentration along with groundwater recharge estimated using the CMB method are presented in Table 5.1 below.

Table 5. 1. Results of groundwater recharge estimated through saturated zone chloride mass balance (CMB)

Sample ID	Lat	Long	Groundwater Cl(mg/l)	Areal Rainfall (mm)	Runoff (mm)	Effective rainfall (mm)	Average rainfall Cl (mg/l)	Cl_p / Cl_{gw}	Total Recharge (mm)
NC1	-27.6785	29.99413	18	569	262	307	0.6	0.03	10.25
NC4	-27.7769	30.00476	3.5	569	262	307	0.6	0.17	53.36
NC5	-27.791	29.99891	35.9	569	262	307	0.6	0.02	5.13
NC8	-27.7212	30.23239	26.4	569	262	307	0.6	0.02	6.98
NC11	-27.9739	29.86627	1.3	569	262	307	0.6	0.45	139.44
NC13	-28.0589	30.16883	11.1	840	386	454	0.6	0.05	24.55
NC14	-28.0671	30.1625	17.7	840	386	454	0.6	0.03	15.42
NC15	-28.0718	30.17086	18.4	840	386	454	0.6	0.03	14.78
NC16	-27.8888	30.16297	717.6	840	386	454	0.6	0	0.38
NC17	-28.0685	30.15814	11.1	840	386	454	0.6	0.05	24.55
NC18	-28.0804	30.15498	9.8	840	386	454	0.6	0.06	27.86
NC19	-28.0523	30.14371	6.4	940	386	554	0.6	0.09	52
NC20	-28.0554	30.1446	14.6	840	386	454	0.6	0.04	18.62
NC21	-28.0389	30.16813	129.7	840	386	454	0.6	0	2.1
NC22	-28.0509	30.15819	4.5	840	386	454	0.6	0.13	60.78
NC23	-28.0525	30.1801	12.7	840	386	454	0.6	0.05	21.5
NC24	-28.0466	30.17241	3.4	840	386	454	0.6	0.18	80.28
NC25	-28.1534	30.12294	42.2	840	386	454	0.6	0.01	6.45
NC26	-28.1497	30.1227	9.3	840	386	454	0.6	0.06	29.28
NC27	-28.149	30.1267	13.5	840	386	454	0.6	0.04	20.13
NC28	-28.0706	30.14939	8	840	386	454	0.6	0.07	34.01
NC29	-28.0718	30.2869	23.2	840	386	454	0.6	0.03	11.74

NC30	-28.0785	30.28806	12.2	840	386	454	0.6	0.05	22.29
NC31	-28.0808	30.29663	4.6	840	386	454	0.6	0.13	59.28
NC33	-28.2565	30.1935	552.3	840	386	454	0.6	0	0.49
NC34	-28.2528	30.19171	5.9	840	386	454	0.6	0.1	46.54
NC35	-28.2452	30.20051	59.2	840	386	454	0.6	0.01	4.6
NC39	-28.2663	30.10462	7.6	840	386	454	0.6	0.08	35.73
NC40	-28.2747	30.11029	75.6	840	386	454	0.6	0.01	3.6
NC41	-28.2751	30.10575	5.8	840	386	454	0.6	0.1	47.01
Average Values			62	798.2	365.3	432.8	0.6	0.1	29.3

5.2.2. Groundwater levels and Groundwater flow directions

Depth to groundwater measurements undertaken in 2018 and data obtained from the Groundwater Resource Information Project (GRIP, 2010) were used to construct depth to groundwater and groundwater level contour maps (Figure 5.1 and 5.3). Water levels in the study area vary greatly with a flowing artesian well occurring at NNC2 mine site near the Mzinyashana River to deeper water tables occurring near the centre of the study area. The Indumeni (KZN 110006) and Corby Rock (KZN070027) mine monitoring boreholes located few kilometres from the town of Dundee have depths to groundwater levels of 22.2 and 38.24 m bgl respectively. The depth to groundwater level appears to be controlled by topography (Figure 5.1), where topographically higher areas have deeper water levels and vice versa. Groundwater level time series data (Figure 5.2) shows that there is a general decreasing trend in groundwater level monitored from 2011 to 2018. The groundwater level contour map (Figure 5.3) indicates that the regional groundwater flow direction is from the southwest towards the low-lying areas southeast of the study area. However, the local flow vectors show complex flow pattern as a result of local geological, topographic and anthropogenic factors including mining. But, the predominant flow directions of groundwater in the study area is towards the southeast away from the northern elevated regions.

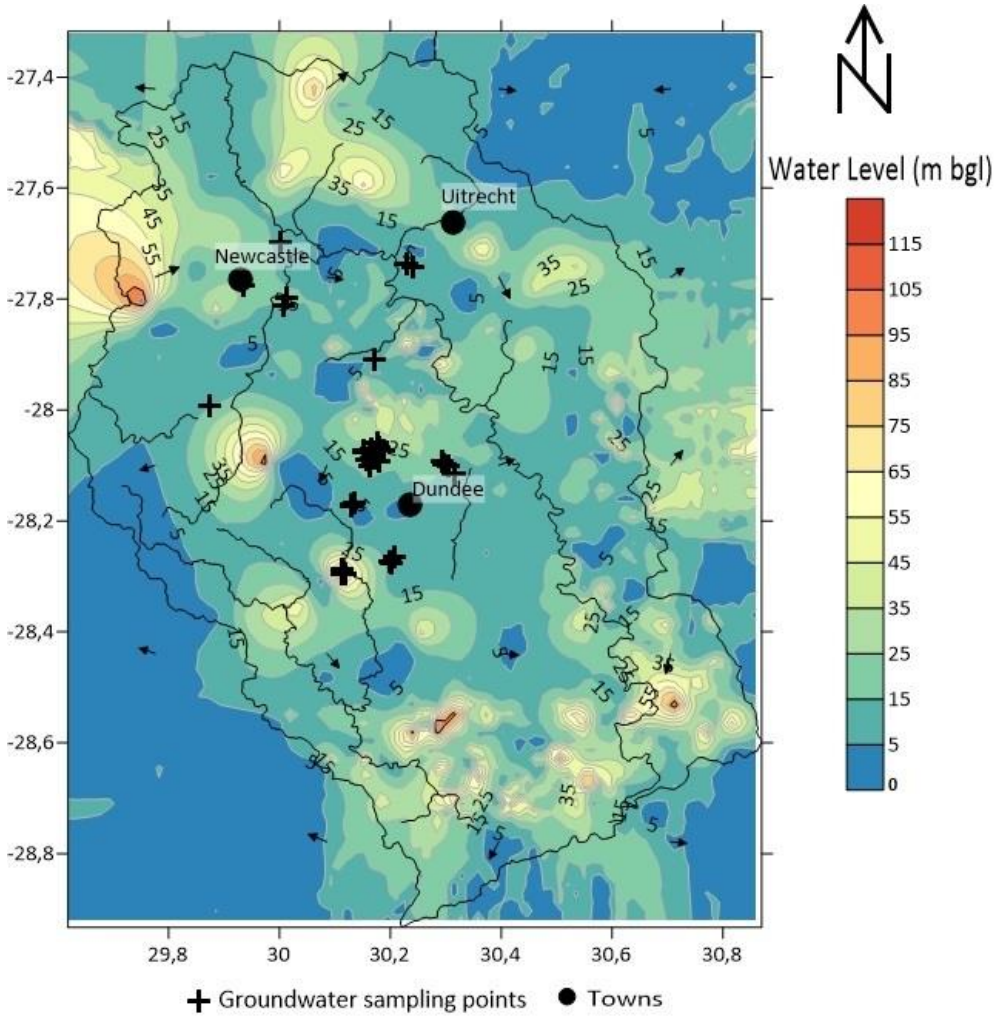

Figure 5. 1. Depth to groundwater level distribution map for the study area.

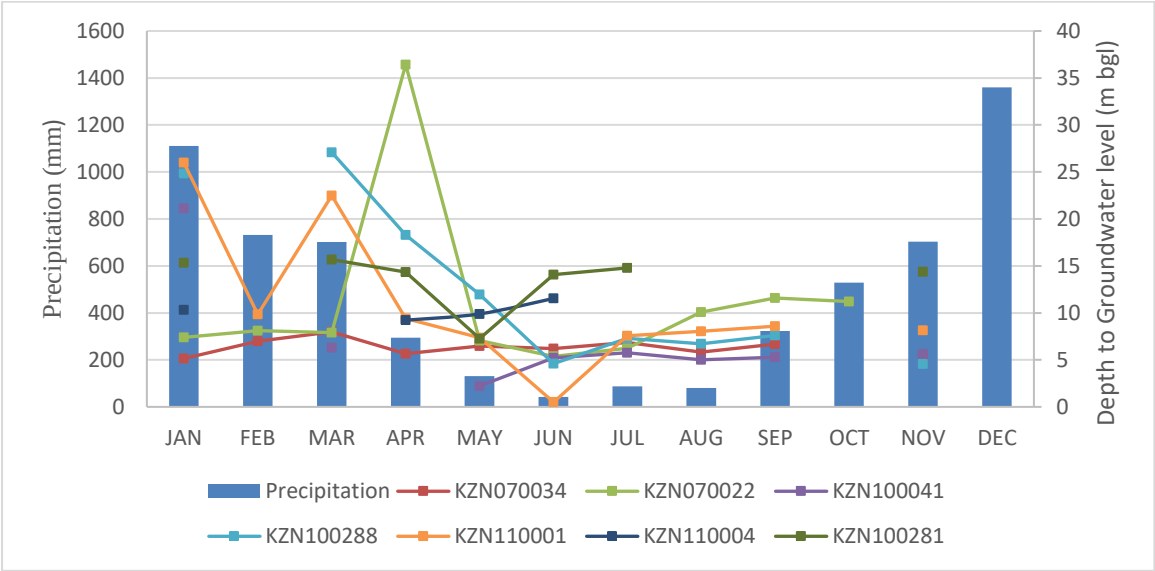

Figure 5. 2. Groundwater level fluctuations along with mean monthly precipitation from 2011 to 2018.

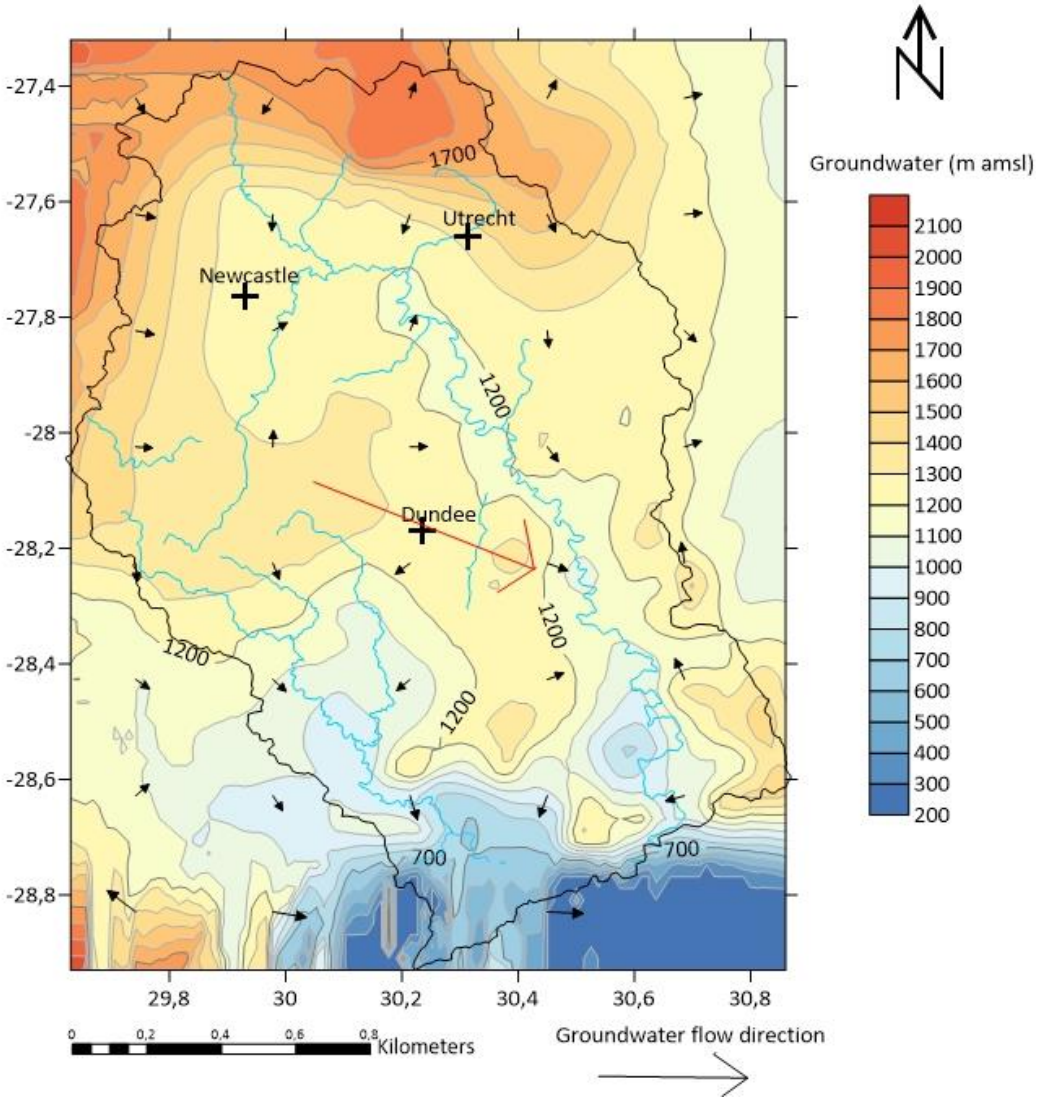

Figure 5. 3. Groundwater level contour and groundwater flow distribution map of the study area

5. 3. Groundwater hydrochemical characteristics

5. 3.1. Groundwater pH Characteristics

Groundwater pH is a property which describes the acidity as well as the alkalinity of the groundwater, and largely controls the amount of dissolved organic and inorganic substances in groundwater. The measured pH of the groundwater samples indicates that the system is almost characterized by circumneutral hydrogeochemical conditions (Figure 5.4a). Circumneutral waters in mines have been generally observed to occur due to one or more of the following hydrogeochemical processes: neutralization of AMD through carbonate mineral dissolution or feldspar dissolution, or mafic-silicate dissolution, or zeolite dissolution and/or through mixing with neutral or higher pH waters (Gomo and Masemola, 2016). Gomo and Vermeulen (2014)

showed the existence of circumneutral waters that had evolved from the dolomite and calcite AMD buffering hydrogeochemical process. The circumneutral hydrogeochemical conditions are key evidence to show the absence of AMD which effectively means there is sufficient neutralizing capacity in the spoils of the rehabilitated mines in most of the study area. Figure 5.4a displays groundwaters which are alkaline in nature, with pH ranging from 7.3-8.5 for the 2010 groundwater samples. The 2011 groundwater samples resemble the same trend and are alkaline in nature, with pH ranging from 6.6-8.9 apart from Northfield1 mine site KZN110001 exhibiting the lowest pH of 5.8 during the March sampling (Figure 5.4b), this mine has since recorded circumneutral pH conditions. Indumeni (KZN10007) showed some acidic condition in 2012 where pH was 2.3 but due to inconsistent time series data a trend could not be followed.

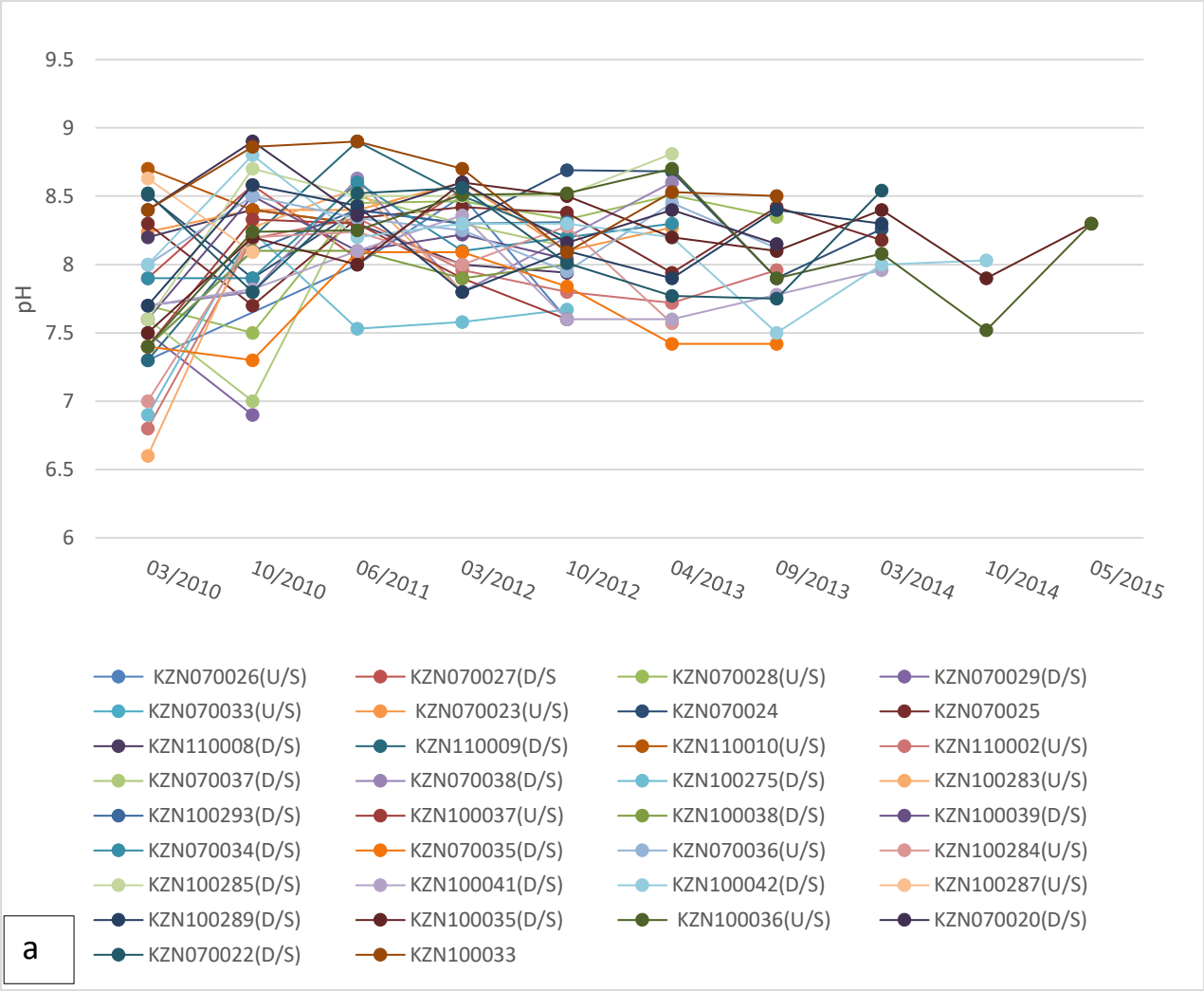

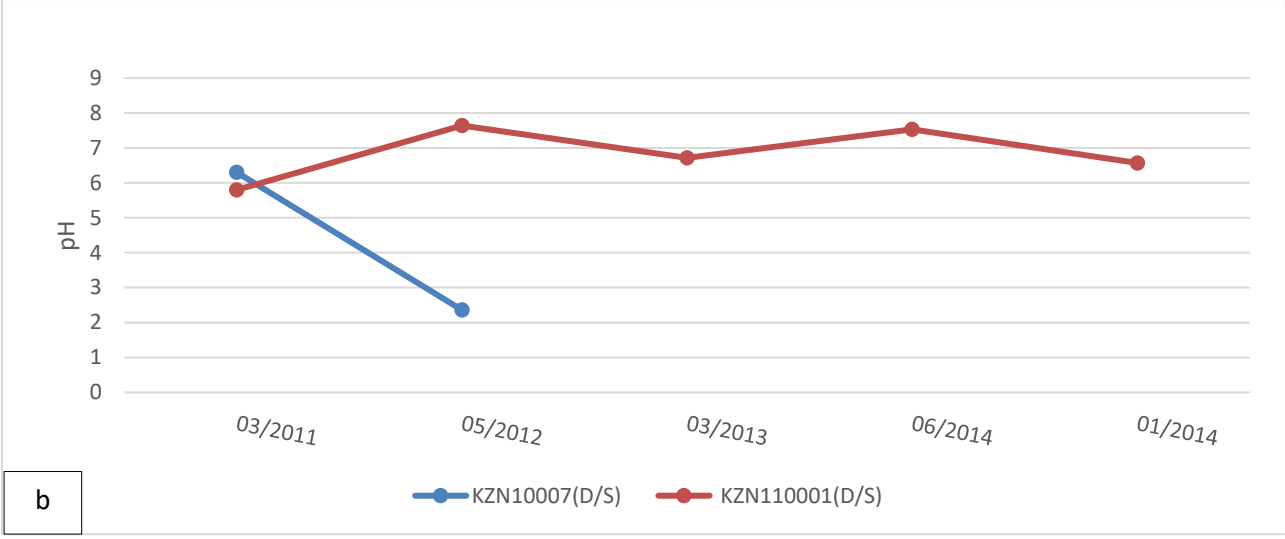

Figure 5. 4. (a) Circumneutral groundwater time series plot. (b) Acidic groundwater time series plot.

Talana mine has the highest pH recorded in March at 8.9 followed by St Georges (KZN100033) at 8.86. Most of the 2012 samples exhibit alkaline pH ranging from 7.6-8.9 with KZN10033 showing the highest pH of 8.9. The evolution of groundwater pH conditions in the study area remains circumneutral with the latest 2018 pH measurements ranging from 7.1 – 9.56. The mine water conditions can be said to be circumneutral to alkaline for boreholes throughout the monitoring period from 2010 to 2018.

5.3.2. EC and major ion Characteristics

The main threat posed by the coal mining industry is the generation of acid mine drainage at mines. Such pollution is characterised by high EC(>1500 µS/cm) and elevated Na^{2+} (> 300 mg/l) and SO_4^{2-}(> 1500 mg/l). The significance of EC in groundwater is important as it relates to the concentration of charged particles in the water. Average spatial variations in EC values around the study area is presented in Figure 5.5, which gives an overall general perspective of EC of groundwater in the region. EC values range from 250-1610 µS/cm for 2010, Dudley Willsand3(KZN100039) recorded the lowest EC value at 250 µS/cm. Gladstone2 mine (KZN070035) displayed an EC value of 1610 µS/cm for 2011 data, this mine displayed constant fluctuations in EC measurements for 2013 and 2014, eventually decreasing to 886 µS/cm in 2015. The EC for 2011 sampling ranged from 210 - 8420 µS/cm, with the lowest reading taken at Bannockburn (KZN100283) being 210 µS/cm and the highest recorded EC value at Indumeni (KZN110005) being 8420 µS/cm. This monitoring well still maintains these elevated EC readings where 2018 samples reveal an EC of 5954 µS/cm, the borehole was not

sealed, and the site is still being actively mined of anthracite. The 2018 field data measurements range between 166 – 5954 µS/cm. Groundwater EC appears to have a small fluctuation in 2018, where the average EC of the measurements was 939.6 µS/cm for all the mine sites which were sampled. The majority of the borehole sites which show signs of elevated EC levels (> 1500 µS/cm) are located downstream of the rehabilitated tailings and have pH > 7. It can be assumed that EC increases in the direction of preferential groundwater flow as most elevated EC levels are found in downstream wells.

Northfield (KZN110001) downstream borehole displays elevated EC, Mg^{2+} as well as Ca^{2+} measurements. The 2011-2013 groundwater samples appear to have elevated Na^{+} and Ca^{2+} levels which are evident in Northfield (KZN110001), where Na^{+} concentration levels reached 460 mg/l. The more apparent source of calcium in the system comes from the $CaCO_3$ which was applied to in the core of the discard dumps as part of the rehabilitation works. The 2018 EC measurements reveal similar elevated trends with Northfield (KZN110001) monitoring well reaching 2717 µS/cm. Gladstone (KZN070035) mine exhibits slightly elevated EC and sulphate levels of 1610 µS/cm and 1380 µS/cm for 2010 and 2011 groundwater samples with SO_4^{2-} concentrations being 589 mg/l and 447mg/l, respectively. Gladstone (KZN070035) mine site shows elevated EC and SO_4^{2-} levels for the years 2013-2018 with SO_4^{2-} > 300 mg/l & Ca^{2+} > 100 mg/l throughout the monitoring period.

Results of time series hydrochemical data analysis of groundwater samples show Ca^{2+} levels remain within SANS drinking water standards (Figure 5.6a). The aquifer system of the study area is characteristic of sandstone and shale of the Karoo sedimentary basin, with most of the intergranular cement material being calcite. Indumeni (KZN110004) & (KZN110005) downstream monitoring wells depict elevated Ca^{2+} concentrations for 2011. The 2018 field sampling data reveals measurements for KZN110005 being 156.5 mg/l which, according to (SANS, 2011) is slightly above aesthetic drinking water standard limits. KZN110004 calcium concentrations are below SANS (2011) drinking water limits. In 2013, Gladstone (KZN070035) had one of its highest calcium concentrations of 198.35 mg/l but concentrations have since declined with 2018 concentration being 34.3 mg/l. The remainder of the mine sites have had relatively low calcium concentration generally < 50mg/l since the beginning of the monitoring period.

Figure 5.6b displays how HCO_3^{-} dominates the anionic composition of average groundwater samples followed by SO_4^{2-}. The highest recorded HCO_3^{-} concentration was 1315 mg/l at Indumeni mine in 2011. The 2014 data displayed relatively high HCO_3^{-} levels for Malungisa

(KZN110009), Dudley Wallsend (KZN07002) and Avoca (KZN070027) mine sites, with bicarbonate concentrations ranging from 802 to 997 mg/l.

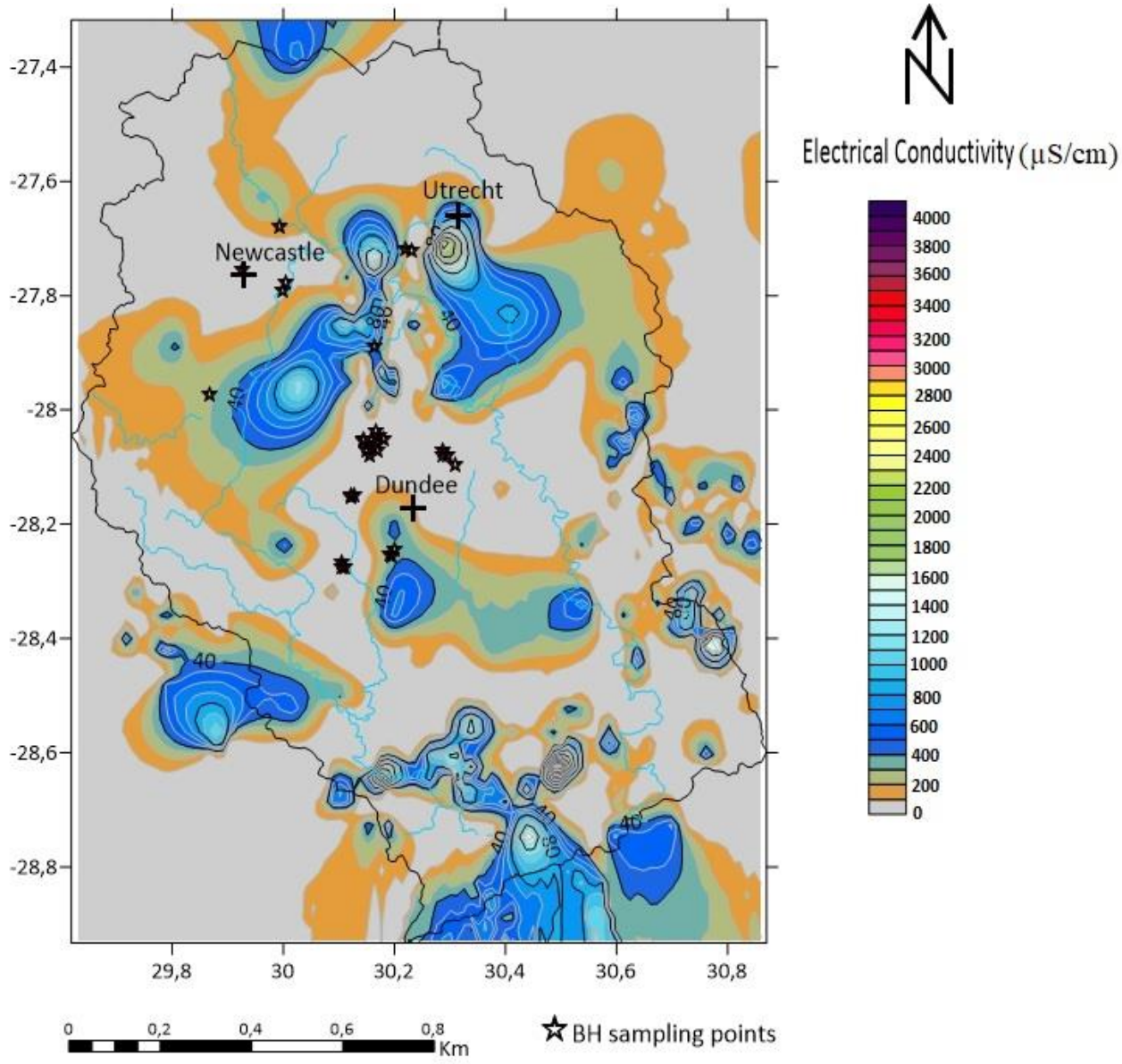

Figure 5. 5. Average EC map of the study area in northern KZN.

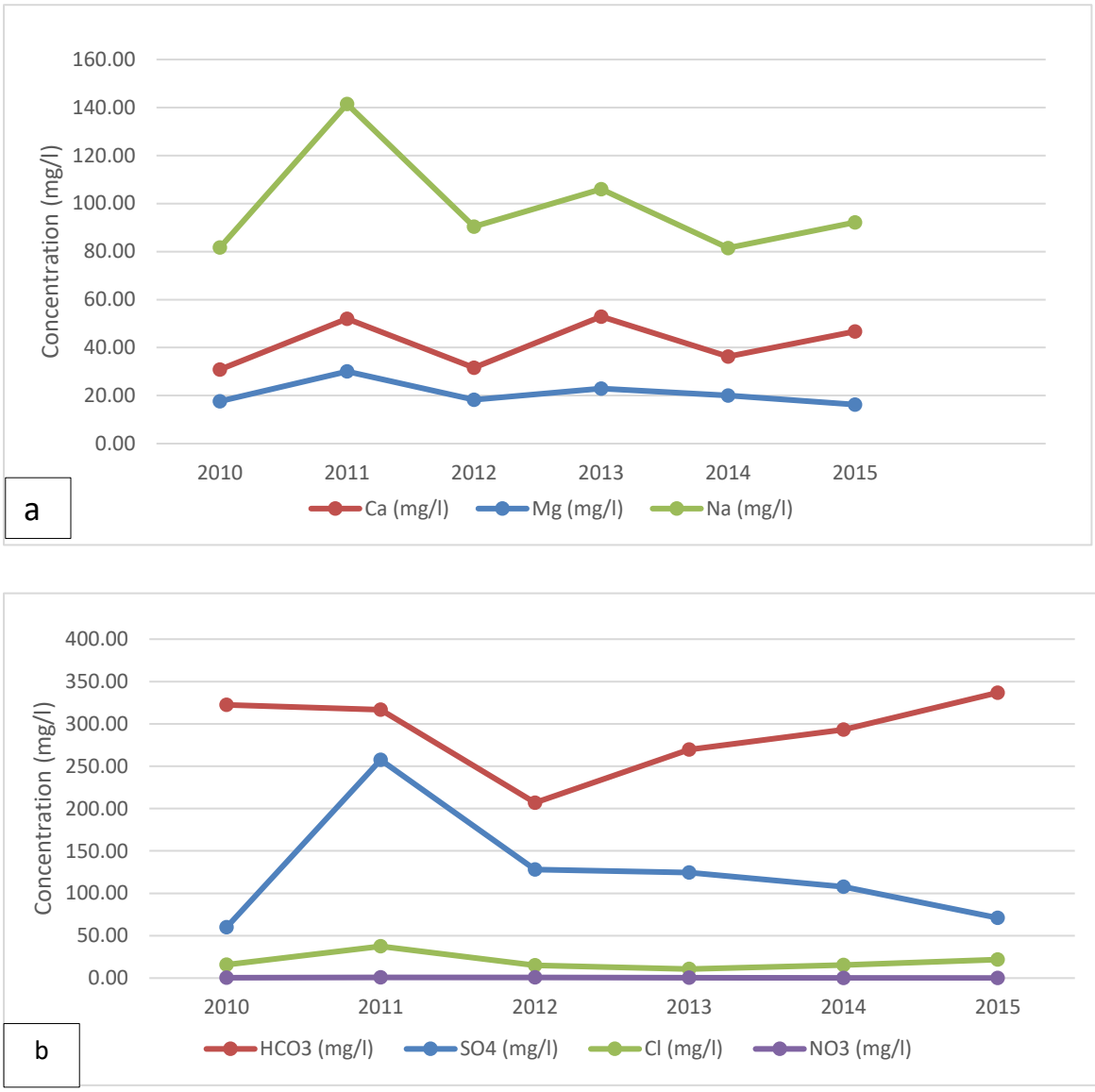

Figure 5. 6. (a) Series plot for major cations in groundwater. (b) Series plot for major anions in groundwater.

5.3.3. Variations of hydrochemical characteristics

Piper diagrams are widely used to represent and classify major ions into groundwater hydrochemical facies as well as summarizing the main variance in hydrochemical composition between different water sources. In the presence of disseminated clay minerals within aquifers, ion exchange causes Ca^{2+} to be replaced by Na^{+} in solution and the water evolves to a Na-HCO_3 water type (Majumder and Shimada, 2016).

Two main water types have been identified from the piper plots which classify the hydrochemical characteristics of the groundwater (Figure 5.7). Most groundwater samples were concentrated on the field of Na^{+}-HCO_3^{-} and few samples plotted Ca^{2+}-HCO_3^{-} for 2010 dataset. In most water samples, the anions are dominated by bicarbonate (HCO_3^{-}) with an abundance order of $HCO_3^{-} > SO_4^{2-} > Cl^{-}$, while the main cation is Sodium (Na^{+}) with an abundance order of $Na^{+} > K^{+} > Mg^{+} > Ca^{+}$. The concentrations of major ions and their

correlation give insight to the hydrochemical process triggered by water-rock interaction. Water containing HCO_3^- indicates the predominance of recently recharged water. CO_3^{2-} induced interactions with rocks and the balancing cations will indicate the types of rocks passed. Calcium concentration comes from the dissolution of carbonate minerals (calcite and dolomite). When calcite dissolves and complexes with hydrogen ion, it forms bicarbonate and carbonic acid which constitutes as the main source of bicarbonate in the system.

The 2011 groundwater hydrochemical facies (Figure 5.7), were concentrated in the Na^+ - HCO_3^- > Ca^{2+} - HCO_3^- field with a cation abundance order of $Na^+ > K^+ > Ca^{2+} > Mg^{2+}$ and an anion abundance order of $HCO_3^- > SO_4^{2-} > Cl^-$. There are some samples which tend towards mixed type waters including Ca^{2+}- Na^+ - HCO_3^- types. Elevated Ca, Mg, Na levels are evident in the Indumeni mine site borehole KZN110005 & KZN110004 both downstream, but due to a lack of comprehensive time series data for these monitoring wells, no conclusion can be made as to the nature of the hydrochemical evolution of groundwater at this site.

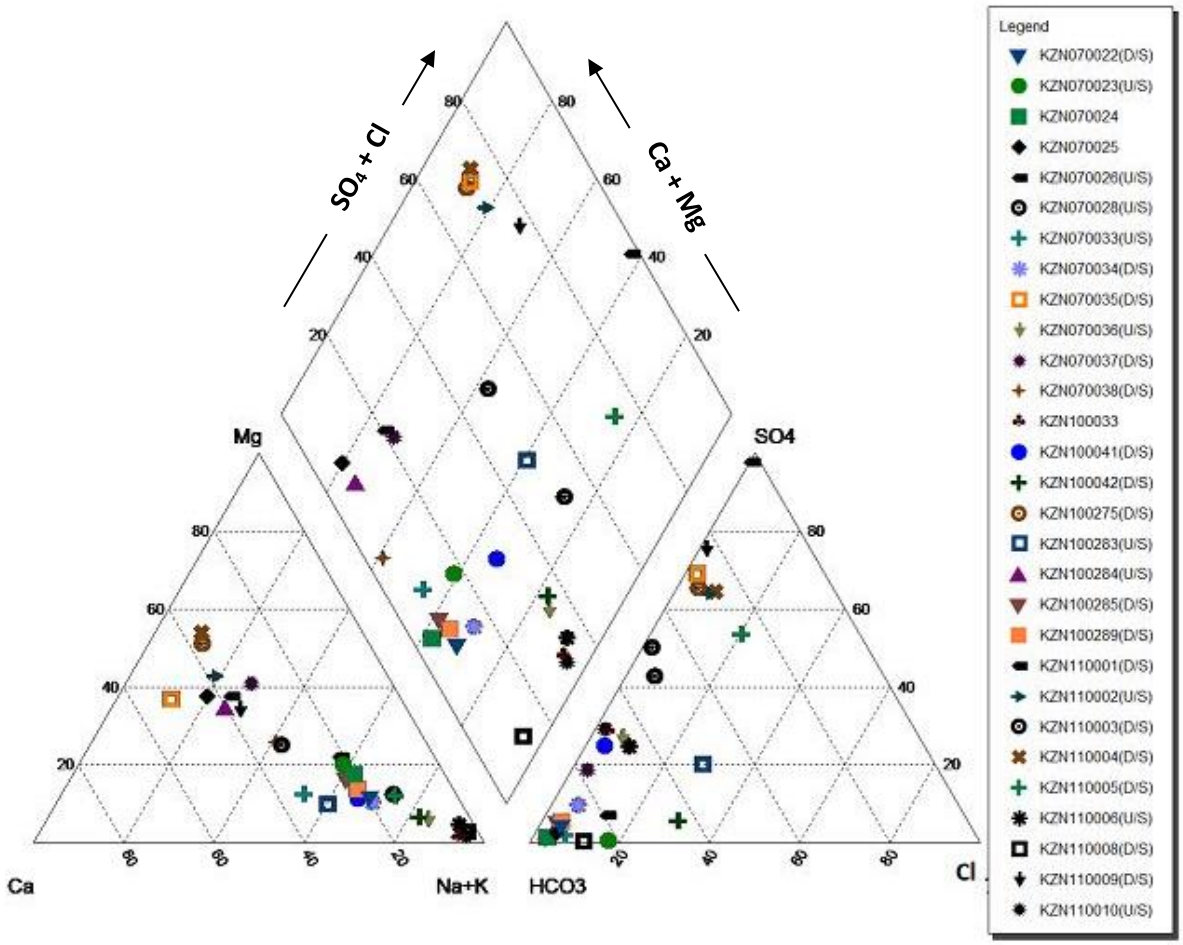

Figure 5. 7. Piper diagram illustrating 2011 hydrochemical facies distribution.

The piper plot for 2012 - 2018 groundwater samples (Appendix III), shows Na-HCO_3 type waters with cation abundance order of $Na^+ > K^+ > Ca^{2+} > Mg^{2+}$ and anion abundance order of $HCO_3^- > SO_4^{2-} > Cl^-$. The dominant cation being Na+K and dominant anion being HCO_3^-. There does not seem to have been any significant groundwater chemical evolution since the beginning of monitoring in 2010 until 2018, the hydrochemical facies remain Ca-Na-HCO_3 type (Appendix III).

Spatial distribution of major ions (Figure 5.8) shows bicarbonate dominated waters with the northern parts of Dundee revealing elevated sulphate concentrations and moving further north to Newcastle. The map of the study area (Figure 5.8) illustrates 2011 ion concentrations in the different monitoring wells, where waters in the eastern regions of Dundee were dominated by sulphate. Slight differences in water chemistry can be observed from 2013-2015 where groundwaters are of HCO_3^- type with the sulphate dominating western parts of the V32E quaternary catchment during the earlier stages of rehabilitation which could indicate seepage. Gladstone, Northfield and Corby Rock monitoring wells are of Ca-SO4 type waters.

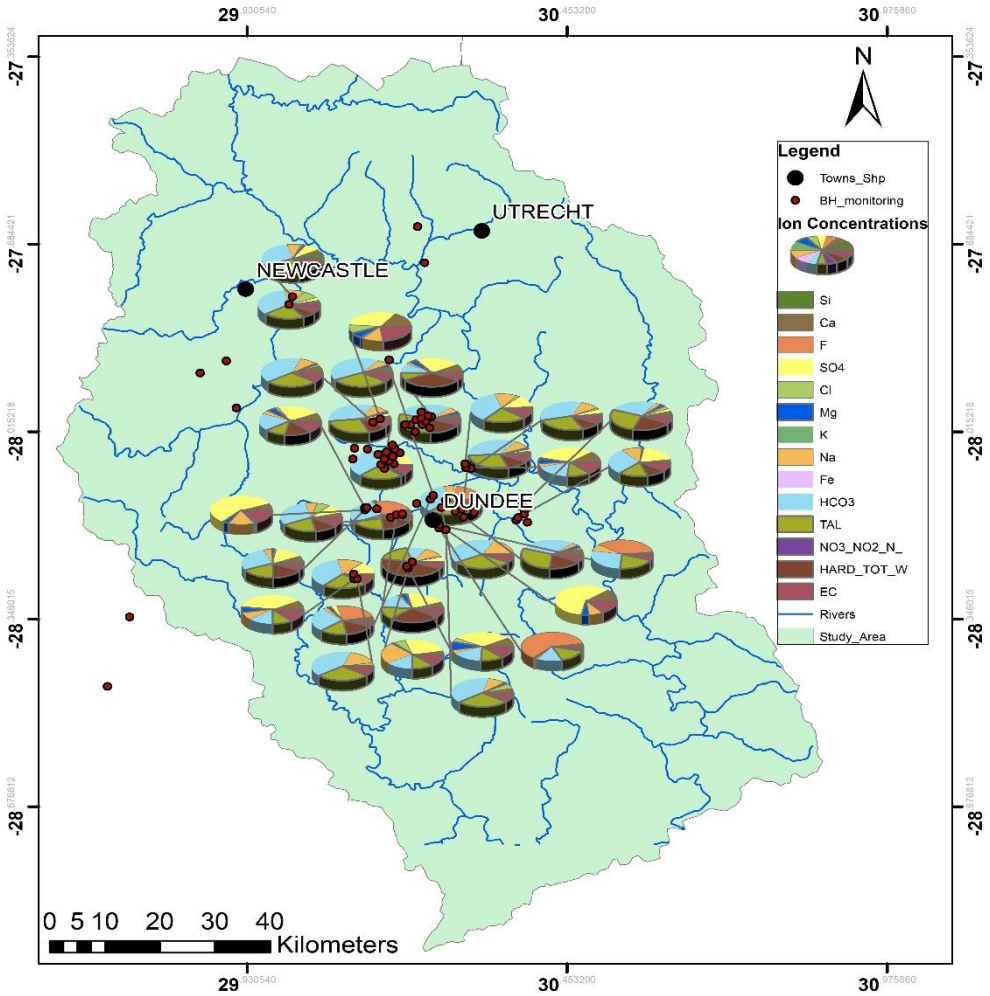

Figure 5. 8. Ionic concentration distributions for 2011 chemistry data.

5.4. Statistical analysis of hydrochemical parameters

5.4.1. Pearson Correlation

Pearson correlation coefficient is commonly used to measure and establish the strength of a linear relationship between two variables or two sets of data. It is a simplified statistical tool to show the degree of dependency of one variable to the other (Belkhiri et al., 2010). Positive correlations exist between Ca^{2+} and Mg^{2+}(r = 0.847) as well as $Ca^{2+}$and SO_4^{2-}(r = 0.743) for 2010 data (Appendix IV). The correlation between Ca^{2+} and Mg^{2+} in the groundwater could be related to the addition of lime as $CaCO_3$ during rehabilitation as well as the clastic sedimentary nature of the aquifer system in the study area, in which silicate hydrolysis may be considered. The process involves the weathering of groundwater silicate minerals, thereby depleting H^+ and produces clays, dissolved silica, metal ions (Ca^{2+}, Mg^{2+}, Na^+, K^+), as well as bicarbonate ions (Powell and Larson, 1985). While weathering of carbonate and silicates may contribute Ca^{2+} and Mg^{2+} in the groundwater, Ca^{2+}, Mg^{2+} and SO_4^{2-} are also AMD related parameters. Other weakly correlated ionic species in the 2010 data were between Na^+ and F^- (r = 0.573) as well as Mg and SO_4^{2-}(r = 0.543). Weak correlations exist between potassium and other major ion constituents, suggesting that potassium mostly originated from K-feldspar or K-bearing minerals.

The 2011 data (Table 5.2) displayed strong positive correlations between $Ca^{2+}$and Mg^{2+} (r = 0.949) as well as SO_4^{2-} and Ca^{2+} (r = 0.902). SO_4^{2-} is seen to have strong correlations with Mg^{2+} (r = 0.812). High positive correlations existed between K^+ and Na^+ (r = 0.898) for this dataset. The concentration range of potassium in groundwater samples was from 0.6 to 12 mg/l, strong correlations could suggest anthropogenic forces like potash fertilizer use in the agricultural lands.

The 2012 Linear Correlation plot (Appendix IV) depicts slightly different trends to the previous two years although similar strong positive correlations still exist between Ca^{2+}, Mg^{2+}& SO_4^{2-}. It is also to be noted the failure of HCO_3^- to correlate with any of the major ions. Strong positive correlations exist between SO_4^{2-} and NO_3 (r = 0.980) also between SO_4^{2-} and Na^+ (r =0.856). Na^+ ion had strong positive loading with most major ions. Average Na^+ concentrations in groundwater samples have ranged from 81.51 to 141.44mg/l with certain mines displaying sodium levels slightly above SANS (2011) drinking water standards. The relatively high Na^+ concentrations is indicative of groundwater moving slowly through a shallow aquifer and reacts with Na^+- rich minerals through dissolution. Correlation Trends for 2013 groundwater sampling (Appendix IV) show positive correlation trends between Cl^- and HCO_3^- (r = 0.899).

2016 and 2018 (Table 5.3) data display weak Ca^{2+} - SO_4^{2-} as well as Mg^{2+} - SO_4^{2-} correlations which differ from 2010 to 2015 data. It can therefore be established from the Pearson linear correlations that the groundwaters in northern KZN are characterized by hard water which is controlled by significant amounts of Ca^{2+}-Mg^{2+} correlation and some silicate clay minerals calcite, gypsum (Ca-SO_4) as well as traces of dolomite in some areas.

Table 5. 2.Linear correlation plot for the 2011 hydrochemical data.

Variable	Ca	Mg	Cl	HCO3	SO4	NO3	F	K	Na	Si
Ca	1									
Mg	**.949**	1								
Cl	.599	.481	1							
HCO3	.377	.299	**.775**	1						
SO4	**.902**	**.812**	.687	.465	1					
NO3	.315	.312	-.079	-.244	.498	1				
F	-.116	-.100	-.106	-.068	-.159	-.096	1			
K	.546	.414	**.772**	.651	**.778**	.289	-.217	1		
Na	.550	.414	**.883**	**.800**	**.788**	.211	-.140	**.898**	1	
Si	**.607**	.592	**.703**	-.245	-.580	-.953	-.458	-.441	-.354	1

Table 5. 3. Linear correlation plot for the 2018 hydrochemical data.

Variables	Na	Mg	Si	K	Ca	Fe	F-	Cl-	Br-	NO3-	SO4
Na	1										
Mg	.299	1									
Si	.112	.169	1								
K	.216	.457	-.052	1							
Ca	.312	**.955**	.227	.579	1						
Fe	-.155	-.203	-.171	.138	-.142	1					
F-	**.913**	.385	.105	.114	.383	-.129	1				
Cl-	.317	**.607**	.076	**.812**	**.706**	-.111	.299	1			
Br-	.584	.399	.499	.153	.409	-.180	.483	.276	1		
NO3-	-.050	.257	.156	-.028	.266	-.089	.030	-.027	-.018	1	
SO4	-.001	.550	.042	.148	.518	-.095	.144	.536	.165	.211	1

5.4.2. Hierarchical Cluster Analysis

Agglomerative hierarchical cluster analysis was undertaken by means of wards method using squared Euclidean distances as a measure of similarity (Michalik, 2008; Ukpatu et al., 2015). The dendrogram provides a visual summery of the clustering processes presenting a picture of the groups and their proximity with a distinct reduction in dimensionality of the original data.

The Euclidean distance usually gives the similarity between two samples and the distance can be presented by the difference in analytical values from the samples. The use of agglomerative hierarchical cluster analysis for studying the northern KZN groundwater quality in historic mining sites yielded a dendrogram (Figure 5.9), grouping 24 boreholes into two statistically significant clusters. Cluster 1-1 has 4 monitoring wells, cluster 1-2 grouping 11 monitoring wells with Malungisa1 well as an outlier, and cluster 1-3 groups three monitoring wells. The second major clustering group has two significant sub-clusters where cluster 2-1 groups 4 wells and cluster 2-2 groups only the Northfield1 monitoring well. The significance of these clustering groups can be said to be associated with the hydrochemical facies where cluster group 1-1 has Na-HCO_3-SO_4 type waters, cluster 1-2 has Na-Ca-Mg-HCO_3 water type and cluster 1-3 has a Na-HCO_3 water type. The second major cluster group has two sub clusters which have Ca-Mg-SO_4 and Na-Mg-Ca-SO_4 water types, respectively. EC for the two major cluster groups rages from 210-1060 µS/cm for the first major cluster and Malungisa1 monitoring well in sub cluster 1-2 being an outlier with an EC of 1860 µS/cm. Cluster 2 EC measurements range from 660-8420 µS/cm where Indumeni (downstream) borehole displays the highest EC value. Northfield1 downstream borehole clusters at the end because the borehole displays the lowest pH value of 5.8 - acidic water- for the 2011 dataset and an EC value of 660 µS/cm. In comparison to the entire dataset where pH ranges from 6.6 - 9.7, the Northfield1 downstream borehole may justifiably cluster at the end. It can also be recognised from the time series cluster analysis that the upstream Malungisa, Gladstone as well as Northfield boreholes cluster first according to similar water type followed by the clustering of the downstream boreholes also of similar water type. Malungisa and Gladstone monitoring wells seem to display similar behaviour and evidently cluster together for both downstream and upstream boreholes in Figure 5.9.

5.4.3. Principal Component Analysis

Principal Component Analysis (PCA) was undertaken using SPSS statistical analysis software for the 2010 and 2011 March sampling regimes. This method is used in order to identify closely related parameters as well as hydrogeochemical processes. The resultant principal components, communalities, percentage of variance as well as cumulative percent are presented in Table 5.4. Eleven chemical parameters pH, EC, Na^{2+}, K^{+}, Mg^{2+}, Ca^{2+}, Cl^{-}, SO_4^{2-}, HCO_3^{-}, NO_3^{+} and Fe^{2+} were used in the PCA.

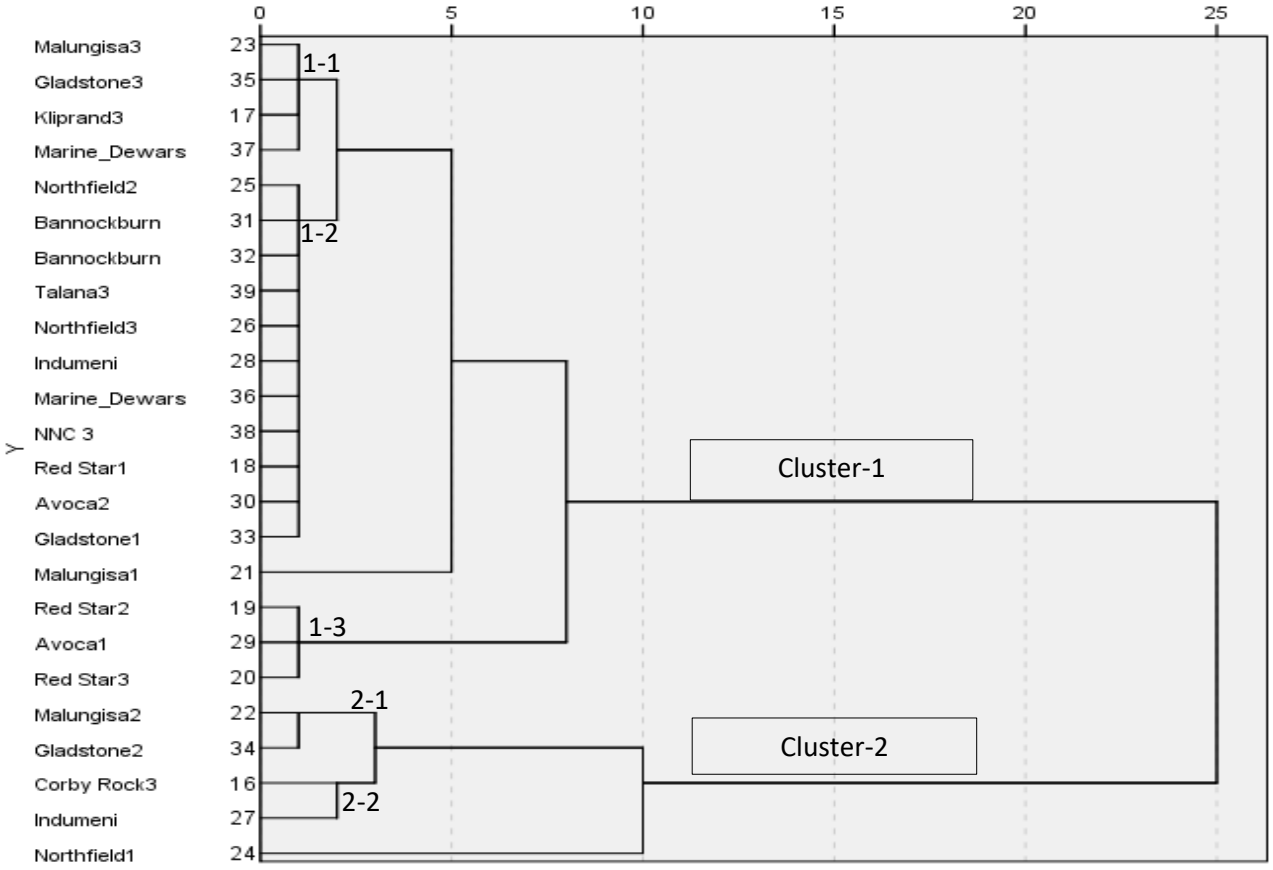

Figure 5. 9. 2011 Dendrogram of Similarity and Dissimilarity Clusters showing Similar Physiochemical Behaviour and the Amalgamation of Various Parameters into Domains.

High values of communality are represented by EC, Na^{2+}, Mg^{2+}, Ca^{2+}, K^{+}, NO_3^{+} and Fe^{2+}. The scree plot shows a distinct change in slope after the first two components. Component 1 has a total variance of 29.3% and a cumulative percent of 29.3. Component 2 has total variance of 17.5 and together the two components account for 46.8% of the total variance in the data set. High positive loadings exist for Mg^{2+}, Ca^{2+} and SO_4^{2-} (0.713 - 0.929) and a low positive loading for Cl^{-} (0.360). Negative loadings exist for pH, EC, Na^{2+}, K^{+}, HCO_3^{-}, NO_3^{+} and Fe^{2+} ranging from (-0.107 - -0.675). The positive PCA loading values are also evident in the correlation plot for 2011 samples where positive correlations were said to exist for Ca^{2+}- Mg^{2+}, Ca^{2+} - SO_4^{2-} and Si-SO_4^{2-}. In addition to this, component 2 shows high positive loading for EC and Fe^{2+} (0.849 - 0.710) and low positive loadings for pH, Mg^{2+}, Ca^{2+}, SO_4^{2-} and HCO_3^{-}.

The Principal component 1 versus Component 2 plot of the 2010 data (Figure 5.10) shows the relationship between the hydrochemical parameters. Hydrochemical parameters Mg^{2+}, Ca^{2+}

and SO_4^{2-} cluster positively in the first component, these AMD related chemical parameters cluster away from the other hydrochemical parameters.

Table 5. 4. Results of principle component factor analysis with direct oblimin rotation for March 2010.

	Communalities	Component 1	Component2
pH	.733	-.675	.396
EC	.842	-.248	**.849**
Na	.863	-.262	-.285
K	.785	-.492	-.266
Mg	.828	**.874**	.203
Ca	.941	**.929**	.235
Cl	.569	.360	-.332
SO4	.667	**.713**	.181
HCO3	.587	-.300	.189
NO3	.777	-.107	-.344
Fe	.709	-.159	**.710**
% of variance		29.275	17.528
Cumulative %		29.275	46.804

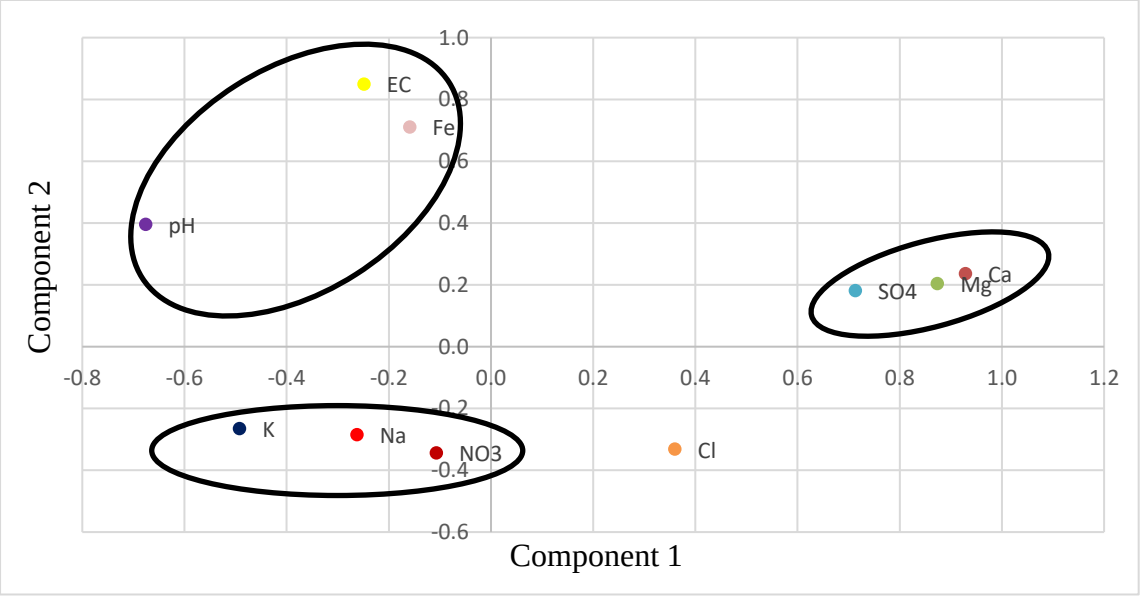

Figure 5. 10. PC scatter plot showing the distribution of hydrochemical parameters for March 2010 samples.

The 2011 data set PCA analysis is indicated in Table 5.5. The percentage variance for component 1 was 58.12 and component 2 being 18.64 with a cumulative percentage explained variance accounting for 78.8%. High positive loadings for EC, Na^+, K^+, Mg^{2+}, Ca^{2+} Cl^-, SO_4^{2-} as well as HCO_3^-. Ca^{2+}, Mg^{2+}, Na^+ and K^+ are displayed for component 1 and are related to salinization of groundwater and hence their contribution to EC. Sources of cations in groundwater is the weathering of the predominantly silicate and carbonate minerals in the aquifers host rock (Deutsch, 1997). Component two shows positive correlations for pH and HCO_3^- at (0.751 - 0.607), weak correlations exist with the remaining parameters ranging between (-0.733 - 0.062), indicating the carbonate buffering processes.

The principal components were plotted using the eigenvalues (Figure 5.11). Similar to the 2010 data set, the scatter plot displays positive correlations for Mg^{2+}, Ca^{2+} as well as SO_4^{2-} in component 1, these three parameters are clustering towards NO_3^+. Further cluster groups can be seen where pH and Fe^{2+} cluster in Component 1, indicating AMD generation and neutralization.

Table 5. 5. Results of principle component factor analysis with direct oblimin rotation for March 2011 samples.

	Communality	Component 1	Component2
pH	.748	-.353	**.751**
EC	.995	**.992**	.062
Na	.919	**.912**	.292
K	.824	**.879**	.216
Mg	.740	**.762**	-.383
Ca	.863	**.874**	-.303
Cl	.892	**.856**	.390
SO4	.979	**.956**	-.231
HCO3	.876	**.705**	**.607**
NO3	.651	.315	-.733
Fe	.968	-.313	.024
% of Variance		58.162	18.640
Cumulative %		58.162	76.802

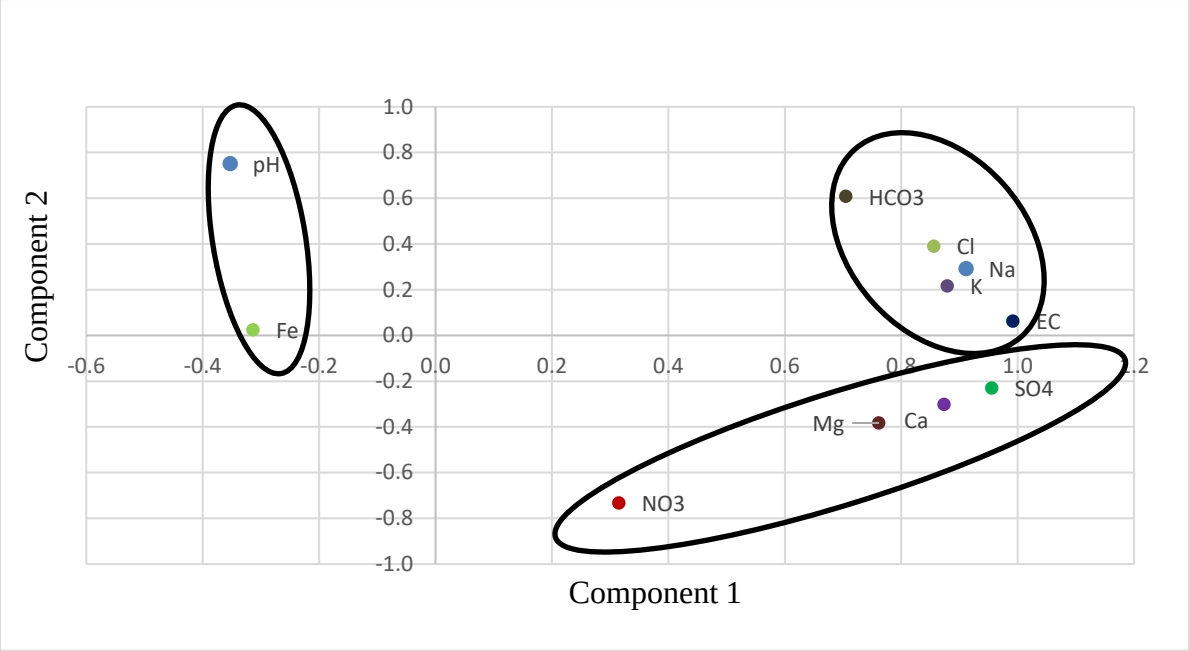

Figure 5. 11. PC scatter plot showing the distribution of hydrochemical parameters for March 2011 samples.

5.5. Surface water hydrochemical characteristics

The study area is characterised by two secondary drainage systems; namely, V6 and V3 which comprise several streams (Buffels, Sundays, Bloed rivers etc.) controlled by the local topography. The tributaries of the study area form part of the headwater region of the Tugela River. Physiochemical properties of surface waters were monitored in the vicinity of abandoned mines and surrounding areas to determine the impact of mine waters originating from these sites. Surface water quality was assessed by comparing mean river water pH and concentrations of Ca^{2+}, Na^{+}, K^{+}, Mg^{2+}, SO_4^{2-}, Cl^{-} as well as EC measurements for ten surface water monitoring points. The mean values for both wet (Table 5.6 in grey) and dry season do not differ to a great extent, while pH and EC remain within SANS drinking water standards. The Ncandu stream maintains the lowest EC measurements while Bannockburn downstream site has the highest EC measurement during wet season and Pietersdale downstream of NNC 2 & 3 presents high dry season EC measurements, most likely impact of AMD. Figures 5.12 and 5.13 shows a decrease in pH in 2005 and an increase in EC measurements during the same period which suggests that there could have been decanting from the abandoned mines. Mildly elevated EC, SO_4^{2-} and Na^{+} values are evident in downstream sampling points partially due to naturally occurring sulphide oxidation. Low EC ranging 68 - 688 µS/cm, circumneutral surface waters 6.64 - 9.33 and DO 1.42 – 4.66 are characteristic of the northern part of the study area's

surface water. Further south, around Dundee, the pH range remains invariable, but EC measurements increase to a maximum value of 1650 µS/cm at the Wasbank river sample, this river is situated downstream of Malungisa mine and is characterised by alkaline water pH 9.27. Similarly, elevated EC measurements were recorded for the three Malungisa monitoring wells (977- 1431 µS/cm) as well as Indumeni 3 downstream monitoring well (1235 µS/cm) following the groundwater flow direction (Figure 5.1).

These hydrochemical information highlights the interconnectivity of the surface water and groundwater systems in the area. It is therefore important that mine water problems must be analysed, not only within the sources (mining sites), but also in pollutants along different water pathways and environments (Younger and Wolkersdorfer, 2004 ; Atanackovic et al., 2013). Additional $\delta\,^{18}O$ and $\delta^{2}H$ isotopic evidence will also prove how surface water systems and groundwater systems are interconnected and influence one another.

5.6. Hydrochemical Processes

5.6.1. Identification of main processes

The previous discussions on the groundwater chemistry provided a picture of the hydrochemical characteristics of the study area. Groundwaters of northern KZN historic coal mining districts are characterised by circumneutral to basic pH conditions (pH 7-9) since the beginning of the monitoring in 2010. High correlation coefficients found in statistical analysis indicate Ca^{2+}, Mg^{2+} and SO_4^{2-} ions being released into the groundwater as a result of prevailing geochemical processes.

Bivariate statistical analysis including multivariate PCA tools were used in order to find the degree of association of ions or the strength of relationship between a dependant and an independent variable. Both these methods displayed strong positive correlation coefficients between Ca-Mg, Ca-SO_4 and SO_4 -Mg on the degree of association of ions. Therefore, it can be deduced that similar hydrogeochemical processes were taking place which caused them to strongly correlate and control the evolution of Ca^{2+}, Mg^{2+} and SO_4^{2-} ions in the groundwater system. Furthermore, results of PCA analyses when compared to linear correlation plots reveal similar trends with regards to Ca^{2+}, Mg^{2+} and SO_4^{2-} ion associations. All of these are indication of calcite-dolomite buffering in the area as a result of rehabilitation of the abandoned mine sites. Correlations between Ca^{2+}, Mg^{2+} and SO_4^{2-} persists throughout the monitoring period and as previously stated can be assumed to be the factors controlling the hydrogeochemical buffering processes in the groundwater system of the study area.

Table 5. 6. Mean seasonal physiochemical characteristics of surface water in the vicinity of abandoned mining sites. Concentrations are given in milligrams per litre except for pH (Wet season in grey and dry season in plain).

Sample	TYD.	SCH.	Ban. D/S	Ban. (U/S)	Glad. (U/S)	KLP.	P. (D/S)	S.V. (U/S)	S.V. (D/S)	Ncandu
pH	7.76	8.20	8.28	7.92	8.27	7.90	8.52	8.2	8.22	7.78
	7.94	7.92	8.51	7.76	8.09	7.56	8.33	8.1	8.08	7.51
EC (µS/cm)	453.3	220.7	1088.4	493.3	980.2	332.0	1180.7	686	1067.7	101.9
	540.0	170.5	1200.0	417.3	594.5	500.4	1106.0	762	792.5	88.5
Ca	24.64	12.90	32.05	39.44	64.51	28.97	31.63	28.0	35.10	6.26
	30.99	13.13	22.05	36.22	37.87	34.30	31.06	36.7	28.11	4.95
Cl	22.74	9.95	22.86	22.12	14.24	14.43	13.15	14.4	14.62	2.93
	24.68	6.35	21.71	18.24	40.56	9.15	13.91	11.7	16.52	3.24
K	5.15	2.46	4.38	3.92	2.32	2.86	3.46	3.0	3.59	1.92
	5.80	2.11	4.79	4.93	2.32	3.22	4.09	3.0	3.11	1.77
Mg	14.51	9.92	18.49	18.92	68.60	17.11	29.82	22.0	27.03	2.89
	16.41	9.24	8.07	12.82	31.93	27.96	29.38	25.4	23.47	1.58
SO4	76.49	11.63	227.59	89.39	335.40	68.79	156.41	73.9	140.36	3.96
	115.45	9.36	172.33	84.98	154.75	156.52	203.79	98.1	106.23	7.30
Na	37.04	10.80	193.59	33.42	79.17	20.04	197.94	90.4	167.77	5.52
	52.02	7.29	225.36	21.78	42.87	24.65	181.86	104.1	114.81	4.76

Legend

TAYSIDE ON BUFFELS RIVER	TYD.	KLIPRAND DAM ON TRIBUTARY OF MZINYASHANA	KLP.
SCHURVEPOORT ON BUFFELS RIVER	SCH.	PIETERSDALE D/S OF NNC2&NNC3	P. D/S
BANNOCKBURN D/S DECANT	Ban. D/S	SWISS VALLEY U/S OF NNC2 NNC3	S.V. U/S
BANNOCKBURN U/S DECANT	Ban. U/S	SWISS VALLEY D/S OF NNC2 U/S OF OLD BRIGDE ON NGOBIYA	S.V. D/S
GLADSTONE U/S OF GLADSTONE SEEPAGE	Glad. U/S	NCANDU RIVER AT RUST	Ncandu

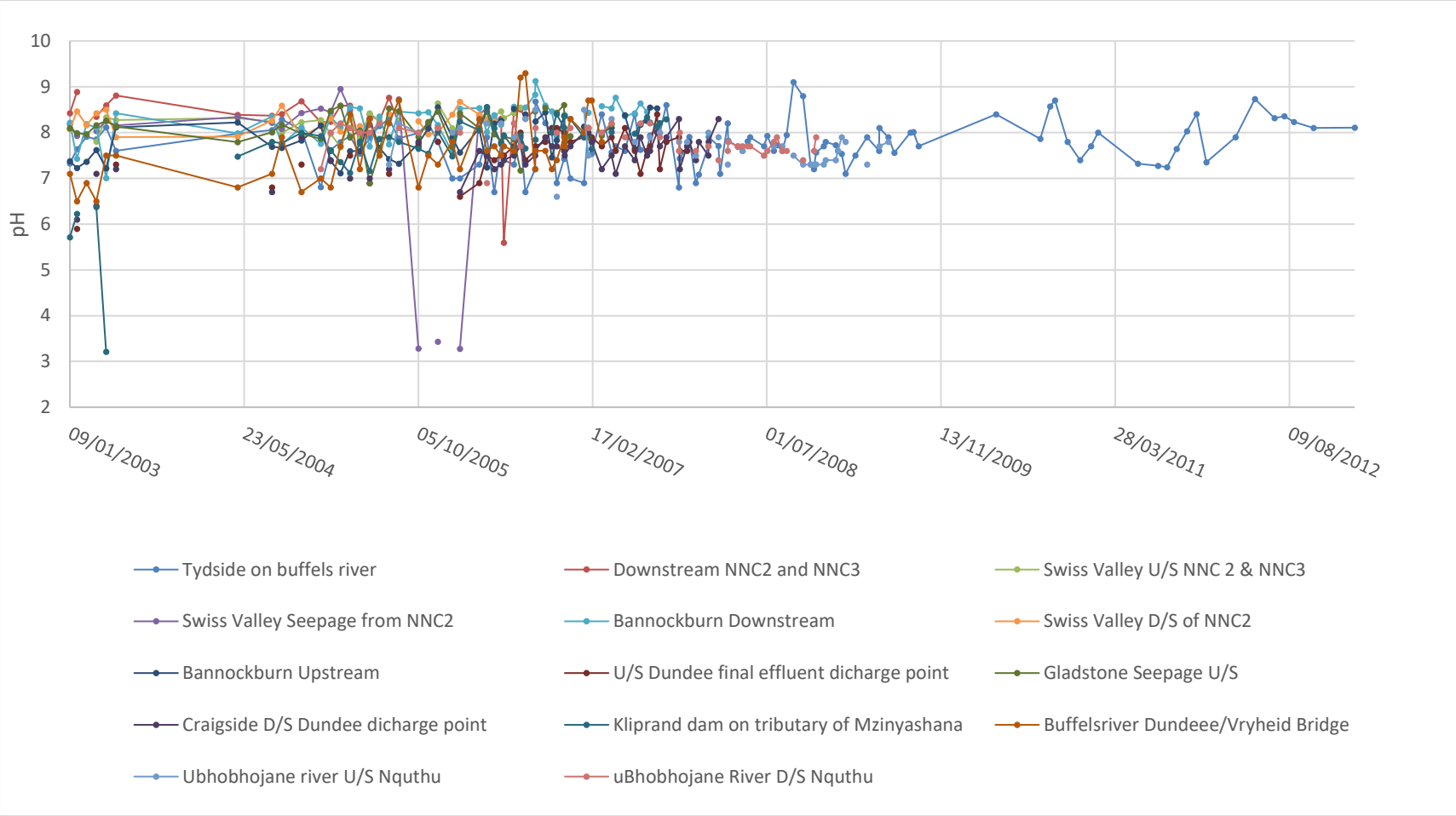

Figure 5. 12. Time series evolution of surface water pH changes.

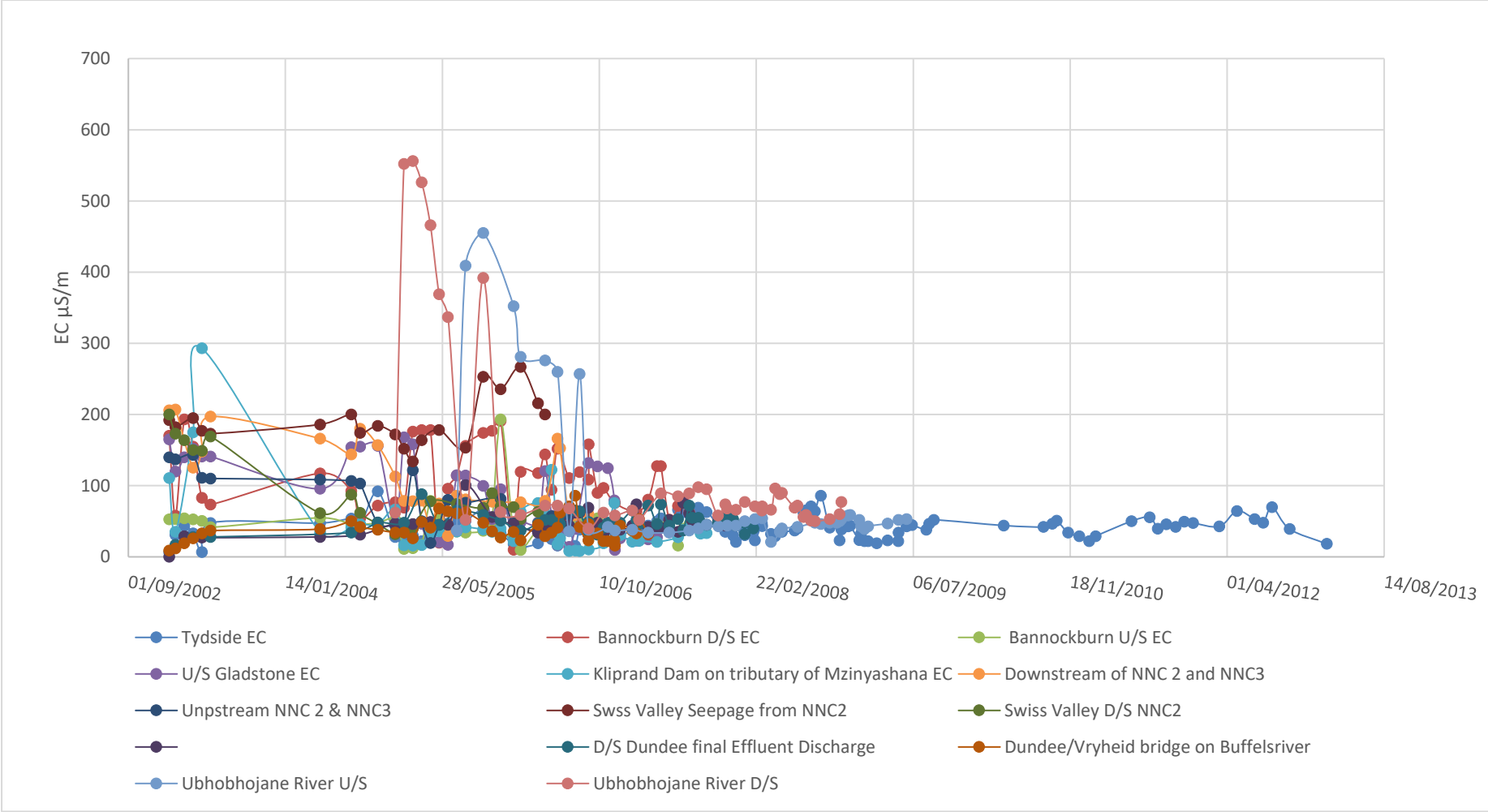

Figure 5. 13. EC time series of surface water monitoring sites.

5.6.2. AMD buffering hydrochemical process

Circumneutral waters in mining environments can occur as a result of different processes. Acidic waters can be neutralized through the processes of carbonate, feldspar, mafic-silicate and zeolite dissolution as well as through mixing with neutral or alkaline pH waters (Nordstrom, 2011). According to {Deutsch, 1997 #54}, the oxidation of pyrite and precipitation of ferrihydrite releases hydrogen to solution and increases the solution acidity unless hydrogen is neutralized by other water/rock interactions. The overall process of pyrite oxidation is described by the chemical reaction indicated in Equation 10. Based on the reaction stoichiometry, the overall pyrite oxidation reaction will produce 4 moles of H^+, 1 mole of $Fe(OH)_{3(s)}$ and 2 moles of SO_4^{2-} for each mole of pyrite oxidised {Gomo, 2018 #49}.

$$FeS_2 + 3.75O_{2(aq)} + 1.5H_2O_{(aq)} \longleftrightarrow Fe(OH)_{3(s)} + 2SO_4^{2-} + 4H^+ \quad \text{.....(10)}$$

In the presence of sufficient calcite and dolomite, the AMD is neutralized through the chemical reaction described in Equations 11 and 12 (Stumm and Morgan, 1981 in Gomo, 2018) as:

$$2CaCO_3 + 4H^+ \longleftrightarrow 2Ca^{2+} + 2H_2O + 2CO_2 \quad \text{..... (11)}$$

$$CaMg(CO_3)_2 + 4H^+ \longleftrightarrow Ca^{2+} + Mg^{2+} + 2H_2O + 2CO_2 \quad \text{.....(12)}$$

The chemical reaction in Equation. 11 indicates that 2 moles of calcite are required to neutralize 4 moles of acid generated. The dolomite-AMD buffering reaction Equation. 12 shows that 1 mole of dolomite is required to neutralize 4 moles of acid generated. Dolomite is thought to form when calcite ($CaCO_3$) in carbonate mud or limestone is modified by magnesium-rich groundwater. The magnesium will aid in the conversion of calcite into dolomite ($CaMg(CO_3)_2$). Assuming that aquifers are open groundwater systems, the majority of produced CO_2 would be released into the atmosphere and would be expected to have negligible effects on hydrogeochemical system (Gomo, 2018).

In practice, pyrite oxidation and neutralization occur simultaneously, therefore the reactions in Equations 10 and 11 can be combined thermodynamically into Equation 13. Equation 10 and 12 can also be combined into the reaction described by Equation 14. From the combined calcite-AMD neutralizing reaction of Equation 13, acid produced by 1 mole of FeS_2 is neutralized by 2 moles of $CaCO_3$. 1 mole of $CaMg(CO_3)_2$ is required to neutralize 1 mole of FeS_2 as indicated in Equation 14 (Gomo, 2018).

$$FeS_2 + 2CaCO_3 + 3.75O_2 + 1.5H_2O \longleftrightarrow Fe(OH)_3 + 2SO_4^{2-} + 2Ca^{2+} + 2CO_2 \quad \text{.....(13)}$$

$FeS_2 + CaMg(CO_3)_2 + 3.75O_2 + 1.5H_2O \leftrightarrow Fe(OH)_3 + 2SO_4^{2-} + Ca^{2+} + Mg^{2+} + 2CO_2$ ....(14)

In the AMD neutralization chemical reaction highlighted, for every mole of FeS_2 neutralized by a mole of $CaMg(CO_3)_2$, 2 mols of SO_4^{2-}, 1 mole of Ca^{2+} and 1mole of Mg^{2+} will be released into the solution (Equation 14). Based on the reaction stoichiometry for a hydrogeochemical system controlled by the reaction process presented in Equation 14, the molar ratio for SO_4^{2-}/Ca^{2+} and SO_4^{2-}/Mg^{2+} should be 2 and 1, respectively. This would suggest that the scatter plot between SO_4^{2-} against Ca^{2+} and SO_4^{2-} against Mg^{2+} in Meq/l should have a slope of 2 based on 2:1 molar ratio {Gomo, 2016 #43}.

5.6.3. Comparison of field data to AMD-dolomite buffering reaction stoichiometry

The agreement of field data to the modelled equation predicted by the AMD-dolomite buffering reaction stoichiometry in the previous section is assessed. Bivariate plots of (a) SO_4^{2-} against Ca^{2+}, (b) SO_4^{2-} against Mg^{2+}, (c) Mg^{2+} against Ca^{2+} measured concentrations for dolomite-AMD buffering reactions are shown in Figures 5.14, 5.15 and 5.16 and Table 5.7 for Avoca, Malungisa and Gladstone mine groundwater monitoring sites. Although the time series data for Avoca Mine displays slight deviation from theoretical stoichiometrically predicted trends as listed in Table 5.7, there is close agreement between theoretical and time series molar ratios for Mg^{2+} against Ca^{2+} plot (Figure 5.16). Avoca mine can be referred to in the hierarchical cluster analysis (Figure 5.9), under cluster 1 - 3 as having a Na-Mg-Ca-HCO_3 water signature. Malungisa molar ratio trends seem to be in exact agreement with the stoichiometrically predicted trends for Dolomite AMD buffering reactions and the same can be said for Gladstone molar ratios. Both these mine sites cluster in the first clustering group according to hierarchal cluster diagram (Figure 5.9). The clustering of these monitoring wells as well as chemical buffering reactions prove the calcite-dolomite buffering hydrogeochemical processes are taking place in the study area.

Table 5. 7. Predicted and actual molar ratios of SO_4^{2-}/Ca^{2+}, SO_4^{2-}/Mg^{2+} and Mg^{2+}/Ca^{2+} ,and correlation coefficients for dolomite - AMD buffering hydrogeochemical processes for selected groundwater monitoring boreholes.

Variables	Predicted Molar ratio	Molar ratio (Avoca)	Molar ratio (Malungisa)	Molar ratio (Gladstone)	Correlation Coefficient (R)
SO_4^{2-} Vs Ca^{2+}	2.00	1.12	1.96	1.52	0.90

SO_4^{2-} Vs Mg^{2+}	2.00	3.89	2.04	1.96	0.81
Mg^{2+} Vs Ca^{2+}	1.00	1.14	0.93	0.77	0.94

From Figure 5.16(c) the proportional mole concentration ratio for Mg^{2+} against Ca^{2+} in the groundwater system of Avoca, Malungisa and Gladstone mine sites all have a slope of 1, which translate to a 1:1 molar ratio of Mg^{2+}/Ca^{2+} as predicted by the dolomite AMD buffering stoichiometry of Equation 14. Strong linear correlations exist between the plots of SO_4^{2-} against Ca^{2+} and SO_4^{2-} against Mg^{2+} as indicated by correlation coefficients of 90% and 81% respectively (Table 5.7). If the molar ratios from the field data were to be rounded to the nearest integer, the molar ratios of SO_4^{2-}/Ca^{2+} and SO_4^{2-}/Mg^{2+} translate to 1 and 4, respectively for Avoca mine which means that dolomite AMD buffering reactions were not applicable for this particular mine site. Malungisa molar ratios for SO_4^{2-}/Ca^{2+} and SO_4^{2-}/Mg^{2+} translate to 2 and 2, respectively (Figures 5.14 & 5.15), which indicates a possibility of dolomite AMD buffering reactions taking place. Gladstone molar ratios for SO_4^{2-}/Ca^{2+} and SO_4^{2-}/Mg^{2+} also translate to 2 and 2 upon rounding up.

The dolomite and calcite AMD buffering hydrogeochemical processes depicted in Table 5.8 shows that the predicted molar ratio for SO_4^{2-}/Ca^{2+} and SO_4^{2-}/Mg^{2+} is 1.3 and 4, respectively which is in agreement with Avoca mine field data molar ratios with the exception of Mg^{2+}/Ca^{2+} molar ratio.

Table 5. 8. Correlation coefficients of predicted and measured data molar ratios for SO_4^{2-}/Ca^{2+}. SO_4^{2-}/Mg^{2+} and Mg^{2+}/Ca^{2+} for the dolomite and calcite AMD drainage buffering hydrogeochemical process.

Bivariate plot variables	Predicted molar ratio	Field data molar ratio (Avoca)	Correlation Coefficient (R)
SO_4^{2-} Vs Ca^{2+}	1.3	1.12	0.90
SO_4^{2-}Vs Mg^{2+}	4.0	3.89	0.81
Mg^{2+} Vs Ca^{2+}	3.0	1.14	0.94

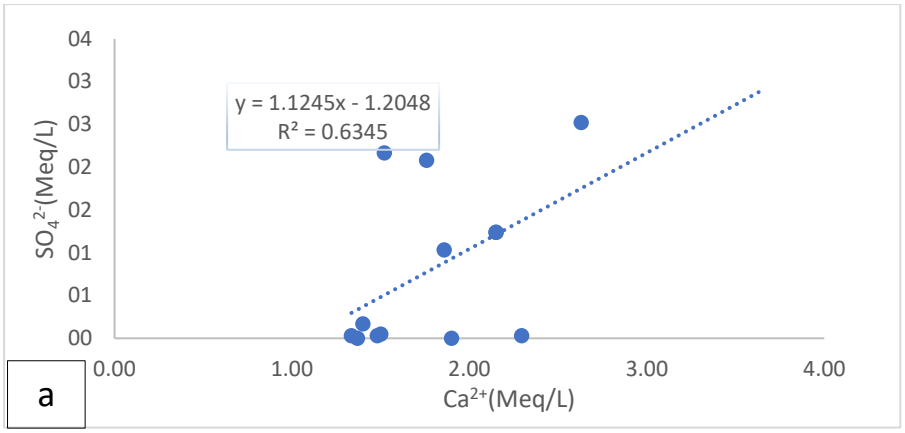

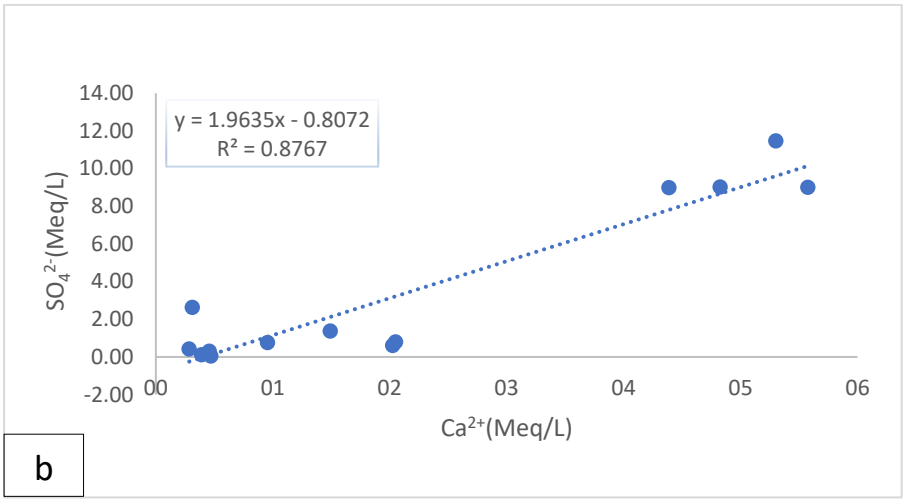

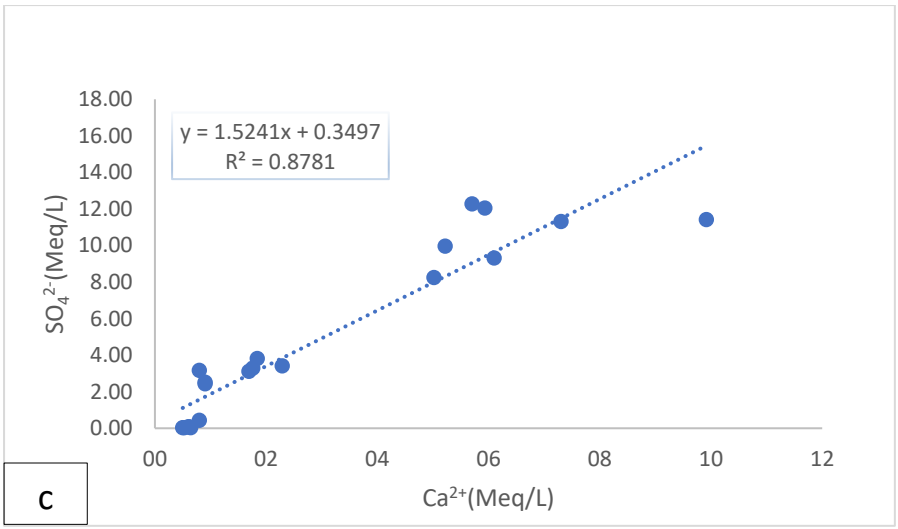

Figure 5. 14. Sulphate vs Calcium concentrations during monitoring period in (a) Avoca, (b) Malungisa and (c) Gladstone mine sites.

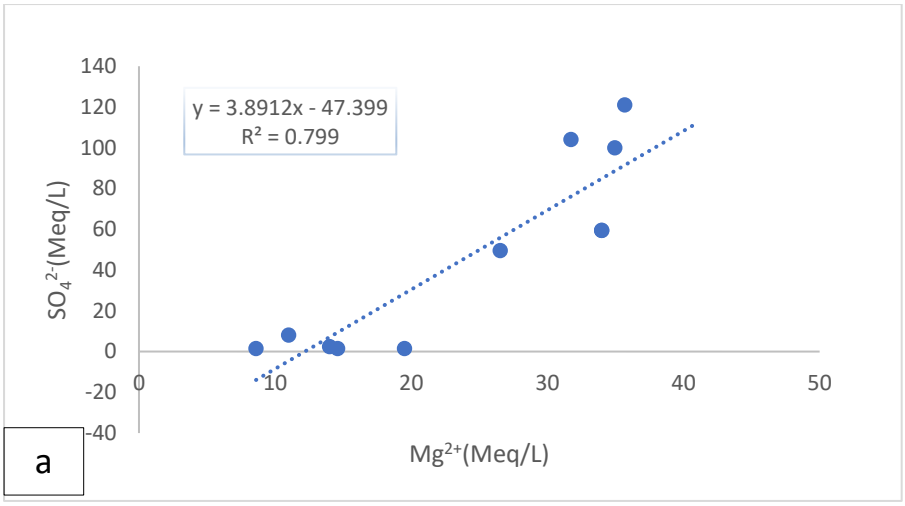

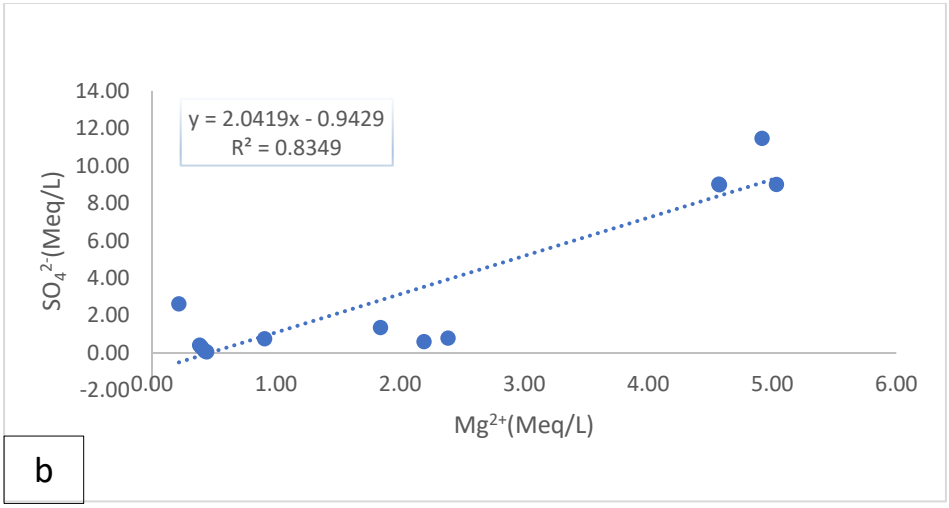

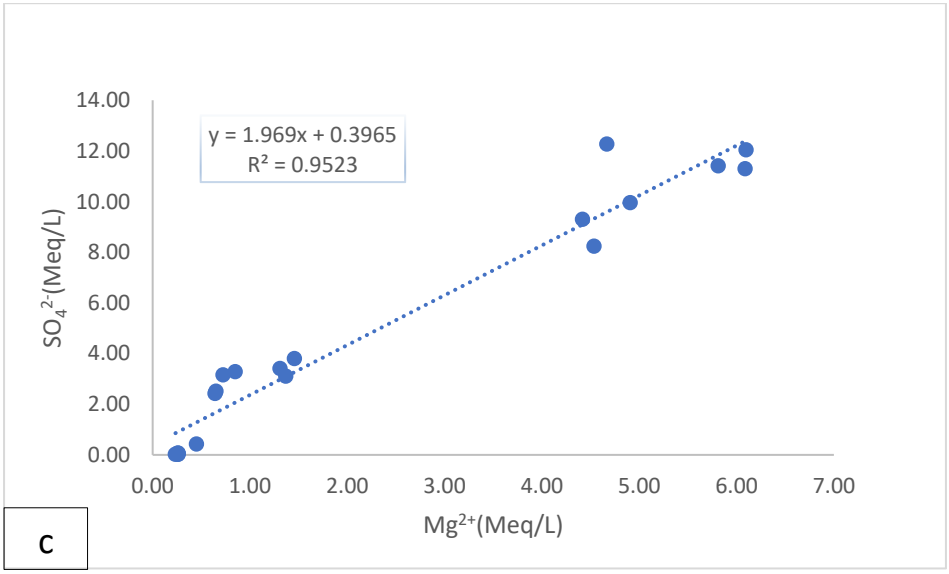

Figure 5. 15. Sulphate vs Magnesium concentrations during monitoring period in (a) Avoca, (b) Malungisa and (c) Gladstone mine sites.

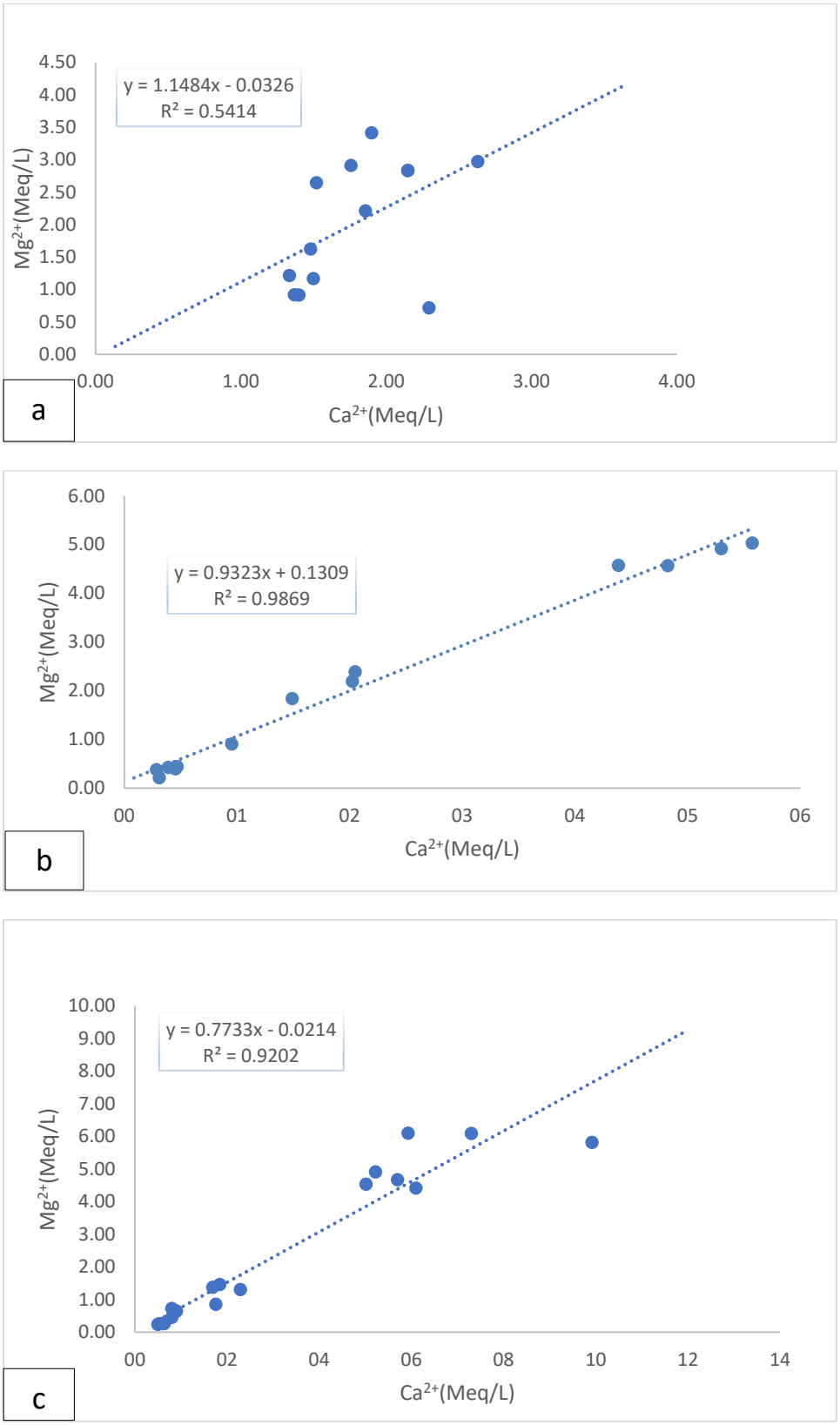

Figure 5. 16. Magnesium vs Calcite concentrations during monitoring period in (a) Avoca, (b) Malungisa and (c) Gladstone mine sites.

When both calcite and dolomite carbonate minerals are present in adequacy, they will together neutralize the AMD produced by pyrite as described by chemical reactions represented in Equations 13 and 14. These two chemical reactions occur simultaneously. As a result, their combined stoichiometry predicts that the SO_4^{2-} concentration in the groundwater should increase with both the concentration of Ca^{2+} and Mg^{2+} {Gomo, 2018 #49}. Based on chemical reaction stoichiometry, the combined overall effect of the two reactions of Equations 13 and 14 would effectively release 4 moles of SO_4^{2-}, 3 moles of Ca^{2+} and 1 mole Mg^{2+} in the hydrogeochemical system. This translates into molar ratio for SO_4^{2-}/Ca^{2+} and SO_4^{2-}/Mg^{2+} to be 1.33 and 4 respectively. The molar ration Ca^{2+}/Mg^{2+} would be 3 in a system where both dolomite and calcite AMD buffering are the dominant processes.

Although the field data deviates from the stoichiometrically predicted trends for SO_4^{2-} against Ca^{2+} for Avoca mine, Gomo (2018) suggested that in the calcite-AMD neutralization Equation 11, 2 moles of SO_4^{2-} and 2 moles of Ca^{2+} will be released into the solution for every 1 mole of FeS_2 neutralized by 2 mole of $CaCO_3$. Based on the reaction stoichiometry, Gomo (2018) further suggests that the molar ratio of SO_4^{2-}/Ca^{2+}should be 1:1. However, unlike the unique molar ratios predicted for calcite-dolomite and dolomite AMD neutralizing processes, calcite-AMD neutralisation ratios are not unique. This is because of the dissolution of gypsum through Equation 15 can also release SO_4^{2-} and Ca^{2+} in a 1:1 molar ratio just like the calcite-AMD buffering process. Based on the evidence presented by Gomo (2018), it is apparent that calcite-AMD buffering is taking place in Avoca mine as suggested by the 1:1 molar ratio of SO_4^{2-}/Ca^{2+}.

$$CaSO_4{\cdot}2H_2O \leftrightarrow Ca^{2+} + SO_4^{2-} + 2H_2O \quad \text{..... (15)}$$

5.6.4. Saturation state of the groundwater with respect to various minerals

The state of saturation of the groundwater system with respect to various minerals based on measured hydrochemical parameters is evaluated using calculated saturation indices. Saturation indices were calculated using the USGS hydrogeochemical software PHREEQC. Mineral equilibrium calculations for groundwater samples are useful in predicting the presence of reactive minerals such as calcite, ferrihydrite and barite which are commonly found in equilibrium with groundwater. If a groundwater sample is analysed and the saturation index is calculated to be near zero for one reactive mineral, then it is likely that the mineral occurs in the aquifer environment and is affecting solution composition. If saturation index for a mineral calculated to be less than zero, the water is said to be undersaturated with respect to that

mineral. This implies that the mineral cannot precipitate from solution and should dissolve into solution to reach equilibrium concentrations. Using similar reasoning for the case of oversaturation, if the saturation index of a mineral is greater than zero then the mineral is not reactive. If the mineral was reactive it would limit solution concentrations of its constituents to values that would produce a saturation index close to zero {Deutsch, 1997 #54}.

Mineral saturation indices have been calculated for (a) Northfield, (b) Gladstone and (c) Malungisa mine monitoring sites. Figure 5.17 below shows time series evolution of calcite, dolomite and gypsum saturation indices in the samples analysed. Throughout the monitoring period, groundwater has a temporal variation in calcite and dolomite alternating between oversaturation and undersaturation in the three monitored mine sites. Northfield 1&2 boreholes display undersaturation with respect to both calcite and dolomite in 2011 (Figure 5.17), with saturation values ranging from -2.25 to -0.91 for calcite and -4.38 to -1.35 for dolomite, while Northfield 3 monitoring borehole displays oversaturation for both calcite and dolomite in 2011. Saturation index values continue a cycle of over and undersaturation for this mine for the entire monitoring period. This could be explained by cation exchange processes taking place in the groundwater system where after AMD buffering process the system would favour oversaturation of minerals. Deuche (1997) explains that at low pH values (less than 6) hydrogen ions are strongly bonded to oxygen atoms at crystal edges and these sites are not available for cation exchange. This is the case for Northfield 1 & 2 monitoring wells, where 2011 & 2014 data displays pH values as low as 5.8 and 6.8, while the remaining years where saturation values are said to be positive, pH values were an average of 8.9 and 8.10, respectively. However, as the pH increases and aqueous hydrogen ion activity decreases, the bond with oxygen breaks releasing hydrogen into solution thereby creating new cation exchange sites. This explains the oversaturation with regards to calcite and dolomite for Northfield 3 mine with an average pH of 8.23 for the entire monitoring period. Gladstone mine site displays a similar trend to Northfield mine in 2011 but gradually tends towards the oversaturation of calcite and dolomite with time. The 2014 data displays saturation index close to zero which, according to Deuche (1997) entail reactivity of mineral calcite and dolomite in the groundwater system which is related to the calcite-dolomite AMD buffering reactions in the previous section. Malungisa mine displays oversaturation with regards to both calcite and dolomite throughout the monitoring period.

Gomo (2018) proposed an alternative explanation for the alternation between oversaturation and undersaturation of calcite and dolomite and is summarized as follows: 1) Dolomite is

dissolved in order to buffer the AMD imparting from oxidation of pyrite (Equation 14). 2) While preventing the pH from being acidic (Figure 5.4a), the hydrogeochemical process releases Ca^{2+}, Mg^{2+} and CO_2. The unconfined nature of the groundwater system in the spills generally allows for the interaction of gas phases with the atmosphere. The loss of carbon dioxide increases the alkalinity, pH and carbonate minerals saturation indices thereby effectively raising the precipitation potential of dolomite as well as calcite. These changes drive the groundwater solution towards over-saturation with respect to dolomite leading to their eventual precipitation, as depicted by equations 16 and 17.

$$CaCO_{3(s)} + CO_{2(aq)} + H_2O \leftrightarrow Ca^{2+} + 2HCO_3^- \quad \text{.....(16)}$$

$$CaMg(CO_3)_2 + CO_{2(aq)} + H_2O \leftrightarrow Ca^{2+} + Mg^{2+} + 2HCO_3^- \quad \text{.....(17)}$$

Saturation indices for gypsum have remained undersaturated throughout the monitoring period with Malungisa saturation index values gradually nearing zero which would mean in 2014 gypsum could affect mineral composition with SI value of (-0.94)but in small amounts.

The 2011 and 2014 Northfield monitoring borehole pH data show that the precipitation of calcite and dolomite result in lowering of alkalinity, therefore leading to the drop in pH and the solution becomes again under-saturated with respect to calcite and dolomite. This drop in pH effectively stimulates the dolomite-AMD neutralization reaction thus producing Ca^{2+}, Mg^{2+} and CO_2 to restart the process again. The process is likely to occur if there is enough dolomite/calcite carbonate to neutralize the produced AMD. It is therefore because of this process that both pH (Figure 5.18) and saturation indices (Figure 5.17) display up and down fluctuating trends.

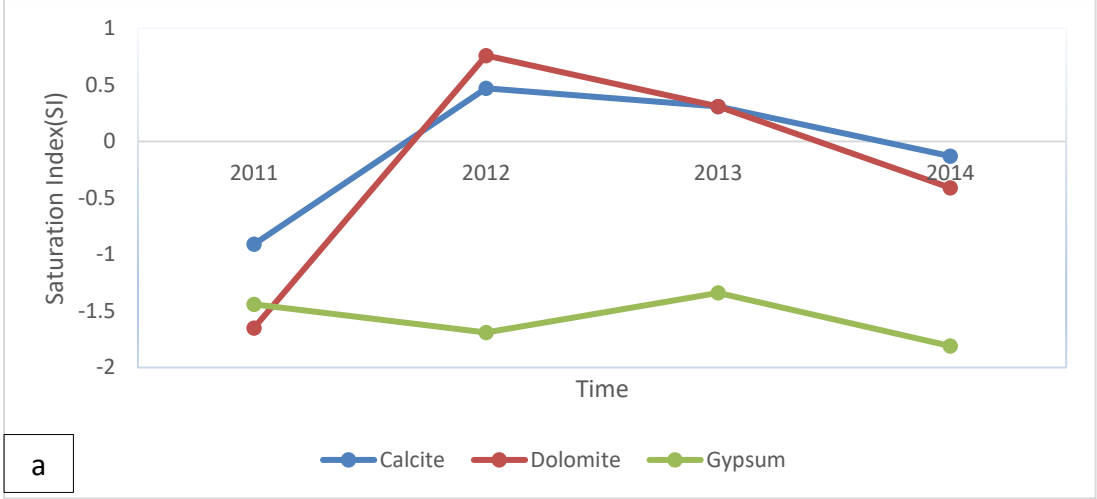

a

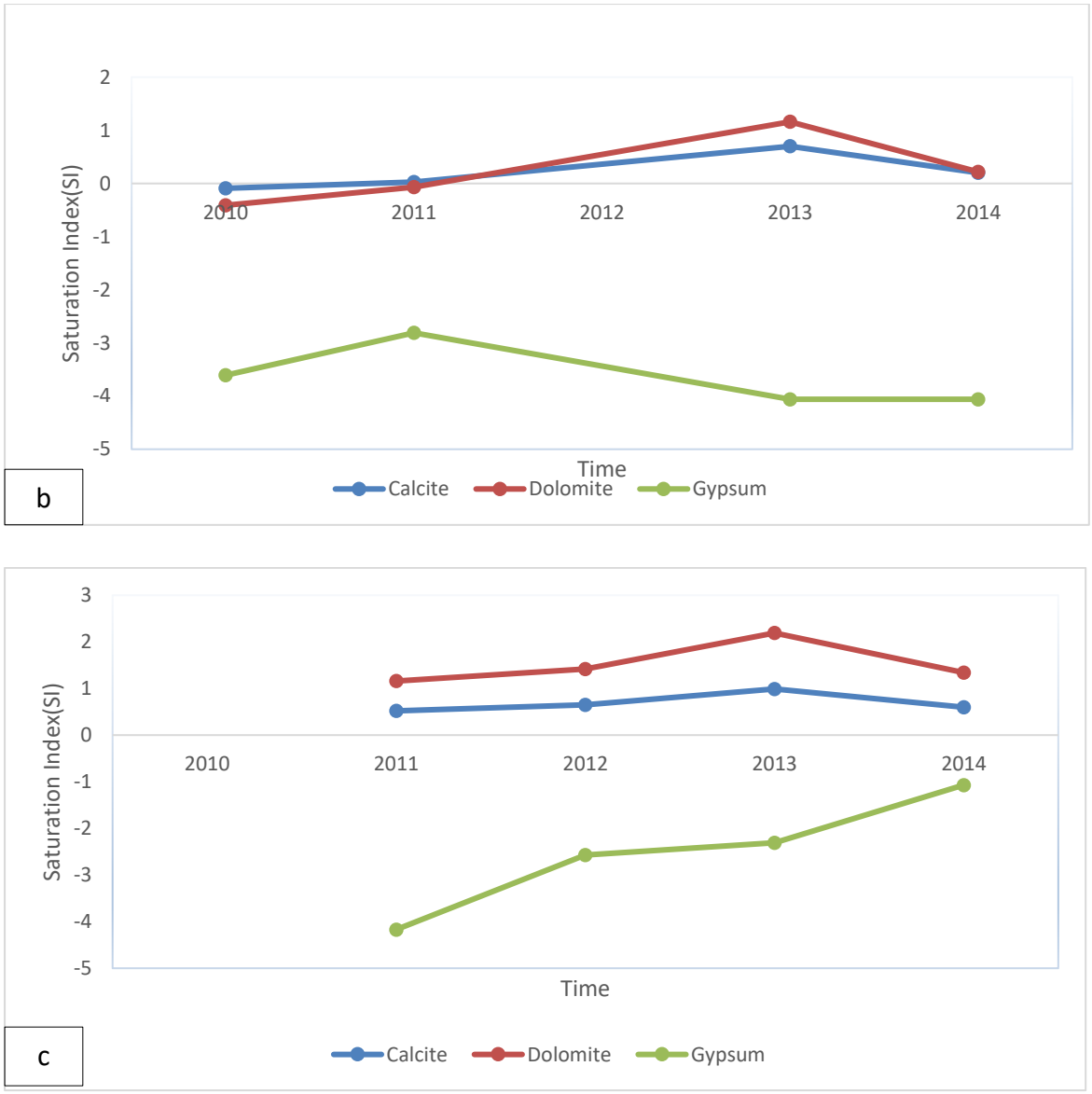

Figure 5. 17. Time series evolution of calcite, dolomite and gypsum saturation indices in groundwater samples collected from (a) Northfield, (b) Gladstone and (c) Malungisa mine sites

Figure 5.19 depicts some calcite and dolomite saturation indices which adhere to a positive linear trend characteristic of the correlation coefficients extensively discussed in section 5.4 from 2010 to 2018. High positive correlation indices indicate that the mineral phases are changing in a correlative and parallel trend which supports evidence that the reactions of calcite and dolomite are controlled by similar hydrogeological processes, i.e., calcite and dolomite buffering.

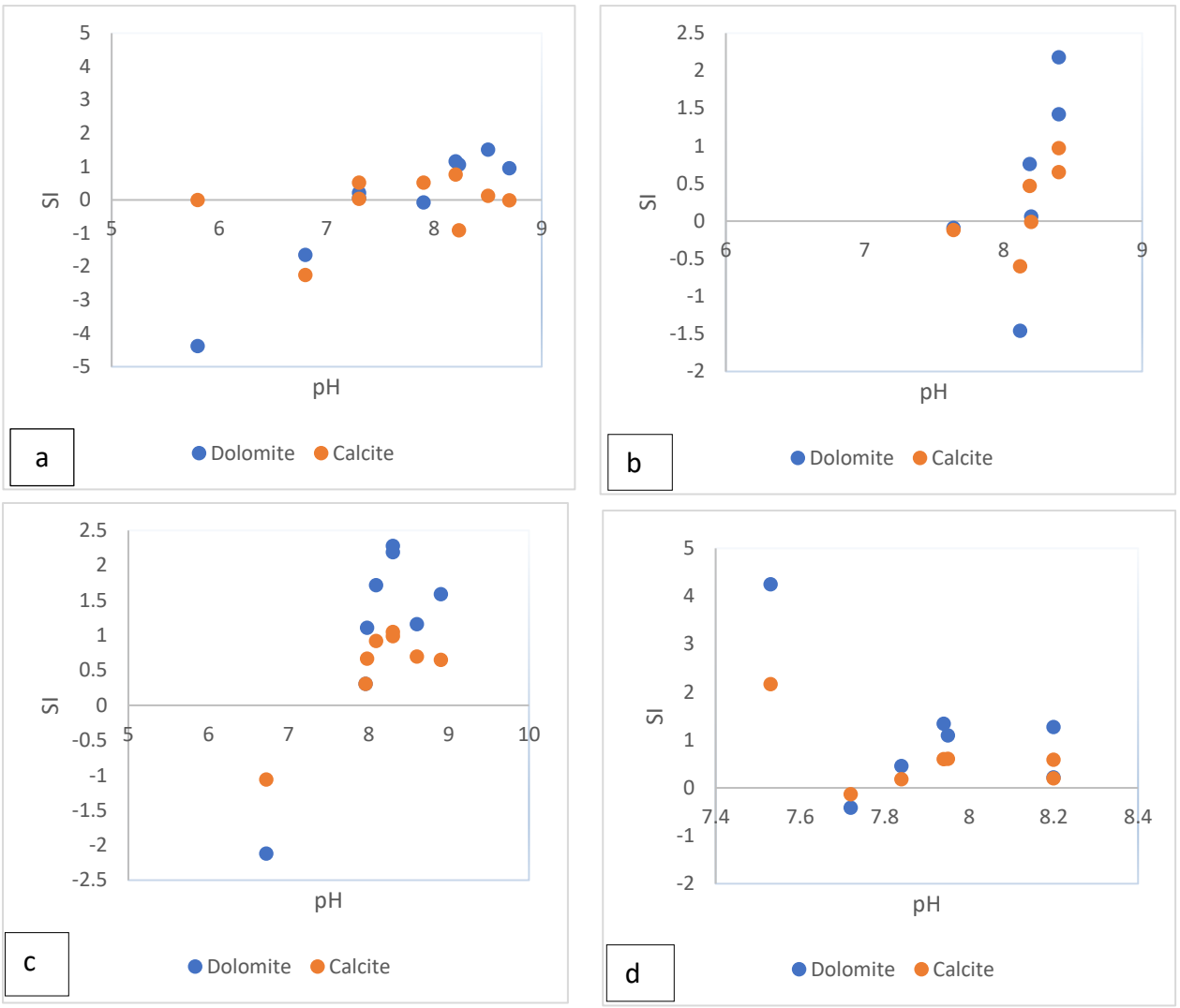

Figure 5. 18. Scatter plot of SI vs pH for (a) March 2011, (b) March 2012, (c) October 2013 and (d) April 2014 for Malungisa, Gladstone and Northfield mine sites.

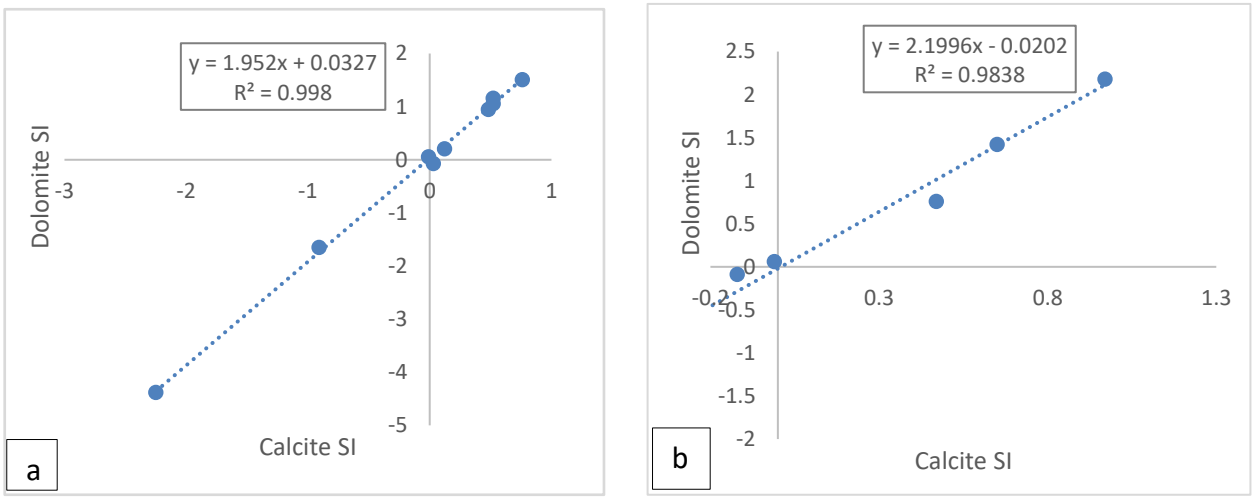

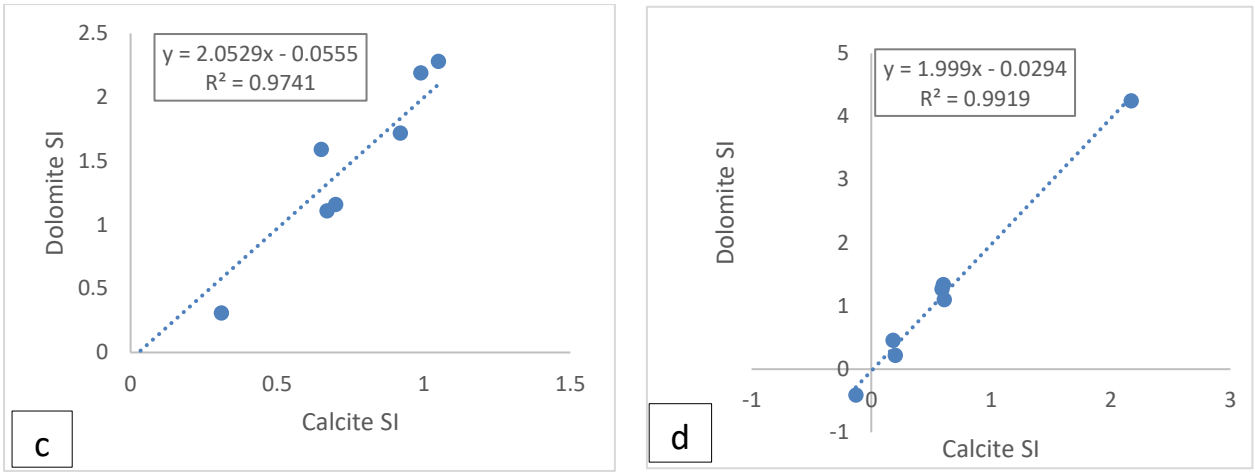

Figure 5. 19. Scatter plot of dolomite SI vs calcite SI for (a) March 2011 (b) March 2012 (c) October 2013 (d) April 2014 for Malungisa, Gladstone and Northfield mine sites.

5.7. Trace metals data analysis

One of the environmental problems of AMD in coal mining environments is the release and mobility of toxic trace metals and metalloids that pollute surface water and groundwater resources (Akcil and Koldas, 2006; Halim et al., 2013). In acid solutions, the presence of Al, As, Ca, Cd, Co, Cr, Cu, K, Mg, Mn, Na, Ni, Pb, and Zn results from leaching of minerals especially silicates, oxides and sulphides associated with coal layers and host rocks (sandstones, siltstones, shales, and limestones). In recent years, the mobility of trace metals in groundwater has received considerable attention. Trace metals in natural or contaminated groundwaters, apart from iron, typically occur at concentrations below 1 mg/l. Low concentrations are due to limitations imposed by solubility of minerals or amorphous substances and or hydrous oxides of iron and manganese or organic matter (Freeze and Cherry, 1979).

Trace metal analysis has been undertaken on various surface water and groundwater monitoring sites for the 2018 sampling campaign. Descriptive statistics of the trace metal data are presented in Table 5.9, which shows low levels of trace metals with the exception of Al and Mn for NC32 surface water sampling point located at the Mzinyashana/ Sterkstroom tributary with Mn concentrations exceeding SANS, 2006 drinking water standards, and NC37 surface water sampling point located downstream of the Sundays river showing Al concentration which exceed SANS, 2006 standards. Pearson correlation was done for trace metals in order to evaluate the associations among these metals in the surface water and groundwater samples (Table 5.10). Positive correlations exist for Zn and V (r = 0.806), Ni and Pb (r = 0.710), Ni and

Cr (r = 0.650). It must also be noted the failure of Fe and Mn to positively correlate with any of the metals.

Table 5. 9. Descriptive statistics of trace metals in surface water and groundwater samples collected in August 2018 against SANS (2006) drinking water guidelines.

Parameter	Minimum (µg/l)	Maximum (µg/l)	Mean (µg/l)	Standard Deviation (µg/l)	SANS (2006) (µg/l)
Li	3.55	284.79	56.34	70.56	b
B	1.01	118.83	27.14	28.94	b
Al	5.42	329.77	49	54.91	≤300
V	0.03	18.82	1.58	3.47	b
Cr	0.18	2.1	0.5	0.46	≤500
Mn	1.11	585.33	74.67	114.09	≤50
Fe	0.001	1.12	0.1	190.04	≤100
Co	0.02	1.41	0.26	0.33	≤1000
Ni	0.18	40.5	3.29	6.05	b
Cu	0.17	10.29	3.13	2.24	≤1000
Zn	0.77	5882.17	167.47	915.25	b
As	0.02	105.44	3.02	16.41	b
Se	0.01	0.97	0.42	0.37	≤20
Rb	0.41	26.13	4.78	5.45	b
Sr	34.78	5915.67	618.15	990.71	b
Mo	0.04	5.71	0.84	1.15	b
Sb	0.08	12.05	0.89	1.8	b
Ba	2.29	1353.55	198.28	347.72	b
Hg	0.02	0.88	0.08	0.132	b
Pb	0.03	0.73	0.23	0.13	≤10000
Th	1.32	1.32	1.32	-	b
U	0.3	6.55	1.27	1.82	

*b: no established guideline value

Table 5. 10. Pearson linear correlation matrix for trace metals in surface water and groundwater samples.

Variable	V	Cr	Mn	Fe	Ni	Cu	Zn	As	Se	Sr	Ba	Pb
V	1											
Cr	-.024	1										
Mn	-.095	.493	1									
Fe	.104	.174	.155	1								
Ni	-.015	**.650**	.019	.028	1							
Cu	.169	.357	.196	.041	.366	1						
Zn	**.806**	-.007	-.074	.160	.037	.306	1					
As	-.040	-.102	-.097	-.047	-.040	-.093	-.013	1				

Se	.049	.346	-.137	**-.578**	.411	-.126	-.215	.040	1			
Sr	-.141	.093	.138	-.145	.076	-.114	-.063	-.098	**.630**	1		
Ba	-.174	-.103	-.070	-.080	-.100	-.284	-.079	-.096	.001	.265	1	
Pb	.200	.389*	.065	.188	**.710**	**.508**	.264	.069	.294	.035	-.189	1

The hierarchical cluster analysis results of the trace metal dataset of surface water and groundwater samples is shown in figure 5.20. The variables are grouped into two major clusters and four sub-cluster groups, namely; (1-1) Cr, Pb, Co, Sb, Hg, As, Ni, Cu, Mo, pH, V and Rb; (1-2) Al, B, Li and Mn; (2-1) Ba, and Sr with (2-2) Zn being an outlier. Weak association of Fe with Pb, Cu, Cr, Mn, and As can be seen in cluster one. The Fe minerals play a significant role in controlling the mobility of these metals in water. The pH directly affects the metal contents of water samples and the coupling of pH with the trace metals could be an indication of pH control in the mobility of these metals and hence their low concentrations. Halim et al. (2013) reported that Cu and Zn are immobile under basic pH conditions, and Scokart et al. (1983) reported that a pH < 6 increases Cd mobility but Zn mobility increase only when pH < 5. Astrom (1998) found that due to a drop in pH, Mn and Ni would readily mobilized from sulphide bearing sediments, Cu was immobilized along with V which had limited mobility. The study area is characterised by circumneutral pH which ranges from 6.64 - 9.33 and this pH range minimizes the trace metal mobilization.

Additionally, PCA was undertaken on the trace metal data in order to identify closely related parameter and the hydrogeochemical processes responsible for their mobility. The resulting components, their communalities, percentage of explained variance as well as cumulative percent of variance are presented in Table 5.11. pH, V, Cr, Fe, Ni, Cu, Pb, Zn, As, Se, Sr and Ba show high values of communality and these metal group in cluster 1 of the hierarchical cluster dendrogram. High positive loadings exist for Cr, Mn, Ni, Cu and Pb in the first component. Component 3 has less positive loading representative of Se and Sr indicative of their similar geochemical behaviour.

The 3-component scatter plot of Figure 5.21 shows the relationship between the principal components (Component 1, Component 2 and Component 3). V, As, Zn and Fe cluster together in Component 2, subsequently, Cu, Mn, Pb, Ni and Cr cluster in Component 1 towards pH which can be deduced as pH being the limiting factor for the mobility of these metals. The pH of surface water and groundwater in the study area is neutral to alkaline, and consequently the

mobility of the metals is relatively low. The variables have high loadings (Table 5.11), further suggesting that these metals have similar geochemical behaviour.

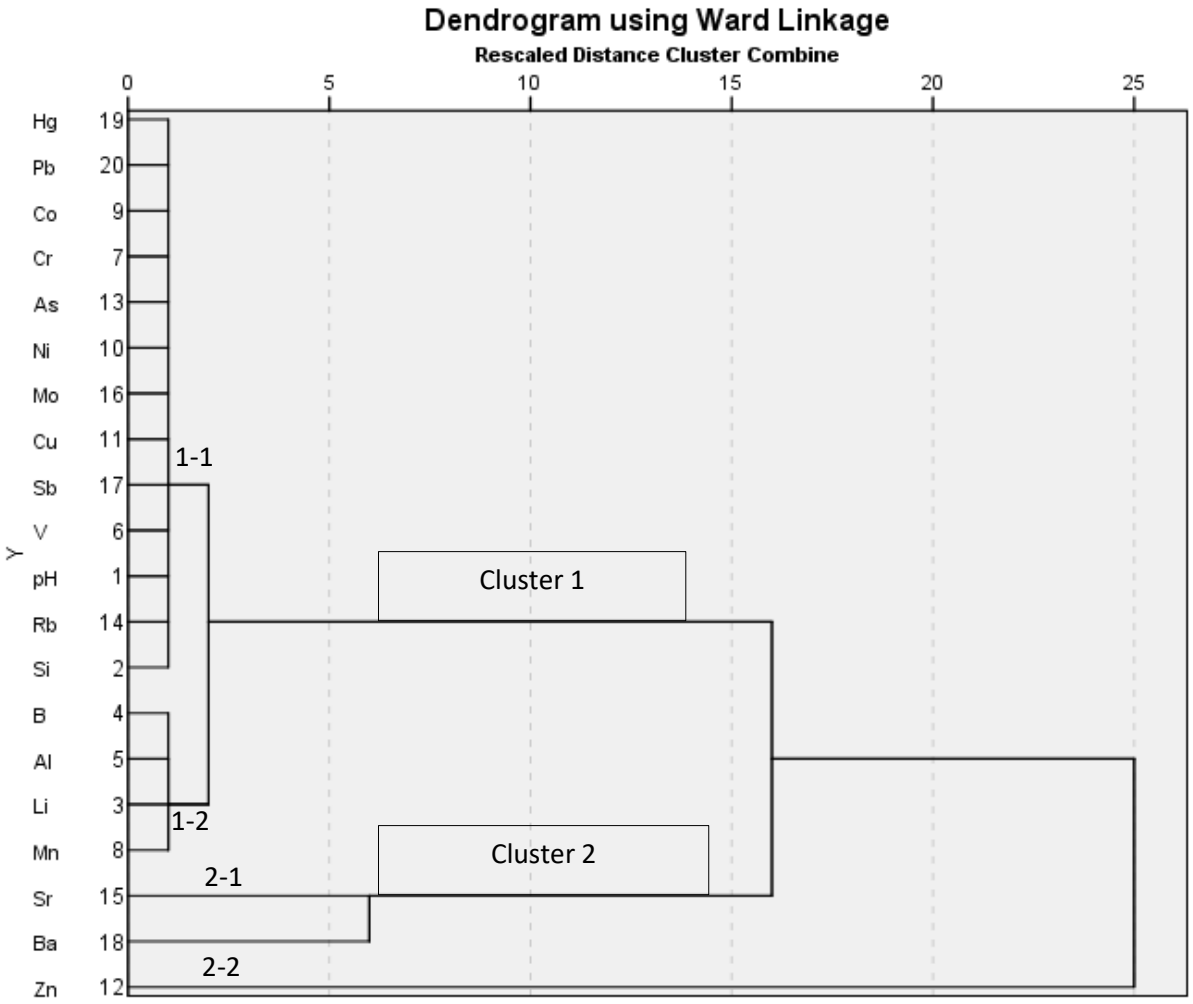

Figure 5. 20. Results of hierarchal cluster analysis of trace metals and associated parameters in surface water and groundwater samples. Cluster analysis was performed using Wards method.

Table 5. 11. Principal component analysis based on trace metals and pH in surface water and groundwater samples.

Parameter	Communality	Competent 1	Component 2	Component 3
pH	.788	-.437	-.069	**-.742**
V	.931	-.137	**.990**	.108
Cr	.904	**.801**	-.215	.359
Mn	.505	**.715**	-.121	-.142
Fe	.926	.250	**.842**	-.205
Ni	.894	**.782**	-.206	.384
Cu	.865	**.895**	.154	-.215

Zn	.941	.153	**.958**	.032
As	.925	-.187	**.966**	.040
Se	.793	-.136	.031	**.904**
Sr	.811	-.050	-.117	**.863**
Ba	.795	-.753	-.292	.338
Pb	.977	.877	.127	.372
Eigenvalue		4.8	4.4	1.8
% of Variance		37.8	33.8	14.1
Cumulative %		37.1	70.9	85.0

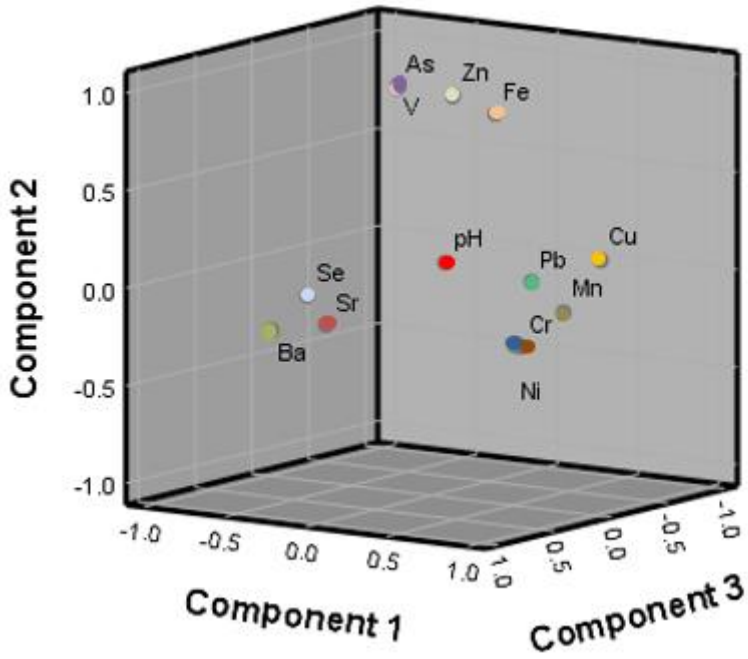

Figure 5. 21. PC Scatter plot showing distribution of trace metals for the August 2018 Samples.

5.8. Water resource quality in northern KZN historical mining districts

Surface water and groundwater quality vary across the study area due to various processes. Water quality is a result of natural, physical and chemical state of the water including the alterations that may have occurred due to anthropogenic activity including mining. Water quality in the study area are affected not only by coal mining but also other activities including industrial land uses, informal settlements, agricultural activities, as well as residential areas. The surface water and groundwater quality parameters analysed were compared with the South African National water quality standards (SANS, 2011). The water quality standard put a

maximum allowable concentration of a water quality parameter. Appendix II shows the South African National Standards as well as associated adverse risks when limits are exceeded.

The August 2018 hydrochemical data coupled with secondary data collected from DWS's monitoring program give a clear picture of the water quality in the area. The water quality predominantly adheres to fresh drinking water standards since the beginning of the mines monitoring. Indumeni and Northfield mines monitoring sites display elevated EC, Ca^{2+}, Mg^{2+} and SO_4^{2-} concentrations, where in 2013, the SO_4^{2-} concentration of Norethfield1 was 1623.70 mg/l which exceeds the water quality standards, in addition to 217.38 mg/l Ca^{2+} and 100.6 mg/l of Mg^{2+}. Time series groundwater quality data at the Northfield 1 mine site shows that it is being affected by mine water seepage from the mine spoils. However, due to limited time series data for the Indumeni monitoring well, the evolution of water quality at the site is not conclusive, nonetheless the 2011 and 2018 data shows poor water quality as a result of the active mining operations and in adequate historical mine rehabilitation (Figure 5.22).

Figure 5. 22. (a) Northfield and (b) Indumeni mine sites.

Apart from a few outliers groundwater as well as surface water, pH of the study area can be characterised as circumneutral from the beginning of monitoring, i.e from 2010-2018 for groundwater and from 1993-2018 for surface water samples. Since pH is a limiting factor in the trace metal mobility, the circumneutral pH conditions resulted in low levels of trace metals in the surface water and groundwater of the study area. Surface water quality does not appear to differ significantly from groundwater quality. Surface water major ions (Ca^{2+}, Mg^{2+}, NO_3 & K^{+}) remained below SANS (2011) water quality standards throughout the monitoring period.

5.9. Environmental isotope composition of ground water and surface water in in the study area

Combined hydrochemical and environmental isotope analysis is a powerful tool to understand the source, mixing process and recharge mechanism of surface water and groundwater systems (Clark and Fritz, 1997). Various water sources sampled within the study area were analysed for environmental isotopes (^{18}O, Deuterium and tritium) signatures. The results are plotted on $\delta D‰$ - $\delta^{18}O‰$ space along with the global meteoric line (GMWL) and local meteoric water line (LMWL) (Figure 5.20). The isotopic data reveals three distinct major cluster groups. These clustering of points is an indication of similar sources.

Isotopic data plotting below the LMWL is suggestive of secondary fractionation that has occurred or that the waters are ancient and were recharged in a different climatic regime

(Mazor, 1997). When water is subject to evaporation, the lighter isotopic species are preferentially removed, therefore, what remains in the reservoir will have a heavier isotopic signal. Isotope signatures groundwater samples collected in 2016 significantly differ from the 2018 groundwater isotope signatures. The data indicates that the 2016 groundwater samples have experienced evaporative loss as they were displaced further from the local meteoric water line (Figure 5.23). This is due to recharge from within the rehabilitated discard dumps where evaporation processes could have occurred. Surface water isotope signature indicate an obvious evaporative signal (Figure 5.23).

There were two outliers within the stable isotope dataset: Indumeni (KZN110005) monitoring borehole, which has been previously reported to having high EC measurement, displayed a highly depleted isotopic signal (-61.69 δD and -9.94 $\delta^{18}O$), most probably as a result of direct recharge from stormes as the borehole is not properly closed. The second outlier was a surface water point (NC 7) north of Newcastle displaying isotopically enriched signatures with 21.3 δD and 1.82 $\delta^{18}O$ respectively, which could be as a result of high evaporation. Comparing surface water and groundwater sample isotopic signatures, all plot along the meteoric water lines (Figure 5.23), indicating present day rainfall sources, with surface water subjected to some evaporation as expected.

The tritium activity of the groundwater samples ranges from 0.4 ±0.3 to 2.6 ±0.4 TU and based on the classification reported in Clark and Fritz (1997), the groundwater samples show a mixture between sub-modern to recent recharge. This detectable tritium activity in the groundwater means that the area is being actively recharged and hence vulnerable to AMD infiltration if generated.

Table 5. 12. Stable Isotope and trace element data for 2016 & 2018 surface water and groundwater samples.

Sample Identification	Date Sampled	Source	pH	EC (µS/m)	δ D (‰)	δ18O (‰)	Tritium (T.U.)	
NC1	08/08/2018	GW	7.26	688	-20.9	-4.51	0.8	±0.2
NC4	08/08/2018	GW	7.75	166	-22.67	-4.78	0.7	±0.2
NC5	09/08/2018	GW	7.6	453	-16.48	-3.93	0.9	±0.2
NC9	09/08/2018	GW	9.33	68	0	-0.81		
NC11	09/08/2018	GW	7.3	172	-19.15	-4.61	0.7	±0.2
NC13	10/08/2018	GW	7.1	581	-16.26	-4.07	1.5	±0.3

NC14	10/08/2018	GW	8.38	1629	-13.85	-3.36	1.1	±0.3
NC15	10/08/2018	GW	8.52	380	-15.55	-3.7	1.4	±0.3
NC16	10/08/2018	GW	7.66	2748	-20.56	-4.35	0.8	±0.2
NC17	10/08/2018	GW	8.32	198	-2.67	-1.13	2.1	±0.3
NC18	11/08/2018	GW	8.73	325	-11.4	-3.39	2.2	±0.3
NC19	11/08/2018	GW	8	166	-16.65	-4	0.7	±0.2
NC20	11/08/2018	GW	7.55	547	-12.79	-3.25	0.9	±0.2
NC21	11/08/2018	GW	8.78	1852	-26.87	-5.33	0.9	±0.2
NC22	11/08/2018	GW	8.02	189	-15.43	-3.62	0.4	±0.2
NC23	11/08/2018	GW	7.82	590	-19.05	-4.22	2.1	±0.3
NC24	11/08/2018	GW	8.08	594	-16.08	-3.7	1.1	±0.3
NC25	12/08/2018	GW	7.45	2717	-17.33	-4.14	1.5	±0.3
NC26	12/08/2018	GW	8.04	223	-14.35	-3.61	0.7	±0.2
NC27	12/08/2018	GW	7.75	445	-15.15	-3.58	0.5	±0.2
NC28	12/08/2018	GW	8.21	768	-17.33	-4.08	1.2	±0.3
NC29	12/08/2018	GW	9.29	808	-19.12	-4.37	0.5	±0.2
NC30	12/08/2018	GW	9.56	611	-16.45	-3.87	0.5	±0.2
NC31	12/08/2018	GW	8.6	155	-17.07	-4.15	2.6	±0.4
NC33	13/08/2018	GW	7.7	5954	-27.85	-5.32	1.2	±0.3
NC34	13/08/2018	GW	7.1	193	-61.7	-9.95	1.3	±0.3
NC35	13/08/2018	GW	7.7	1235	-21.64	-4.73	0.4	±0.2
NC39	14/08/2018	GW	7.85	977	-20.93	-4.65	1.4	±0.3
NC40	14/08/2018	GW	8.7	1431	-16.25	-3.82	0.9	±0.2
NC41	14/08/2018	GW	7.37	996	-13.6	-3.55	1.2	±0.3
SD-1	25/06/2016	GW	8.14	344	-16.46	-1.85	0.9	±0.3
SD-2	25/06/2016	GW	10.16	278	-18.87	-1.47	0	±0.2
SD-3	26/06/2016	GW	7.66	480	-16.77	-1.5	1.2	±0.3
SD-4	26/06/2016	GW	8.9	331	-23.64	-2.3	0.5	±0.2
SD-5	26/06/2016	GW	7.8	219	-17.67	-1.85	0.4	±0.2
SD-6	26/06/2016	GW	8	1069	-18.5	-1.62	0.3	±0.2
SD-7	26/06/2016	GW	9.3	579	-20.34	-1.91	0.1	±0.2
SD-8	26/06/2016	GW	9.6	468	-19.2	-1.73	1.2	±0.3
SD-9	27/06/2016	GW	7.4	615	-19.03	-1.41	0.5	±0.2
SD-10	27/06/2016	GW	8.3	550	-19.17	-1.58	0.1	±0.2
SD-11	27/06/2016	GW	7.04	1115	-17.28	-1.86	0.4	±0.2
SD-12	27/06/2016	GW	8	467	-18.68	-1.96	0.4	±0.2
NC2	08/08/2018	SW	6.64	203	-6.08	-1.95		
NC3	08/08/2018	SW	7.8	307	-3.13	-1.56		
NC6	09/08/2018	SW	8.43	306	-0.5	-0.87		
NC7	09/08/2018	SW	8.31	596	21.3	1.82		
NC8	09/08/2018	SW	7.92	390	-17.95	-3.8		

NC10	10/08/2018	SW	8.9	349	-3.5	-1.25		
NC12	10/08/2018	SW	7.76	86	-1.6	-1.05		
NC32	12/08/2018	SW	8.83	747	-2.42	-1.22		
NC36	13/08/2018	SW	9.27	1650	-5.27	-1.53		
NC37	13/08/2018	SW	8.23	269	-2.97	-1.26		
NC38	13/08/2018	SW	9.07	344	-2.5	-1.14		

*GW is Groundwater and SW is Surface water.

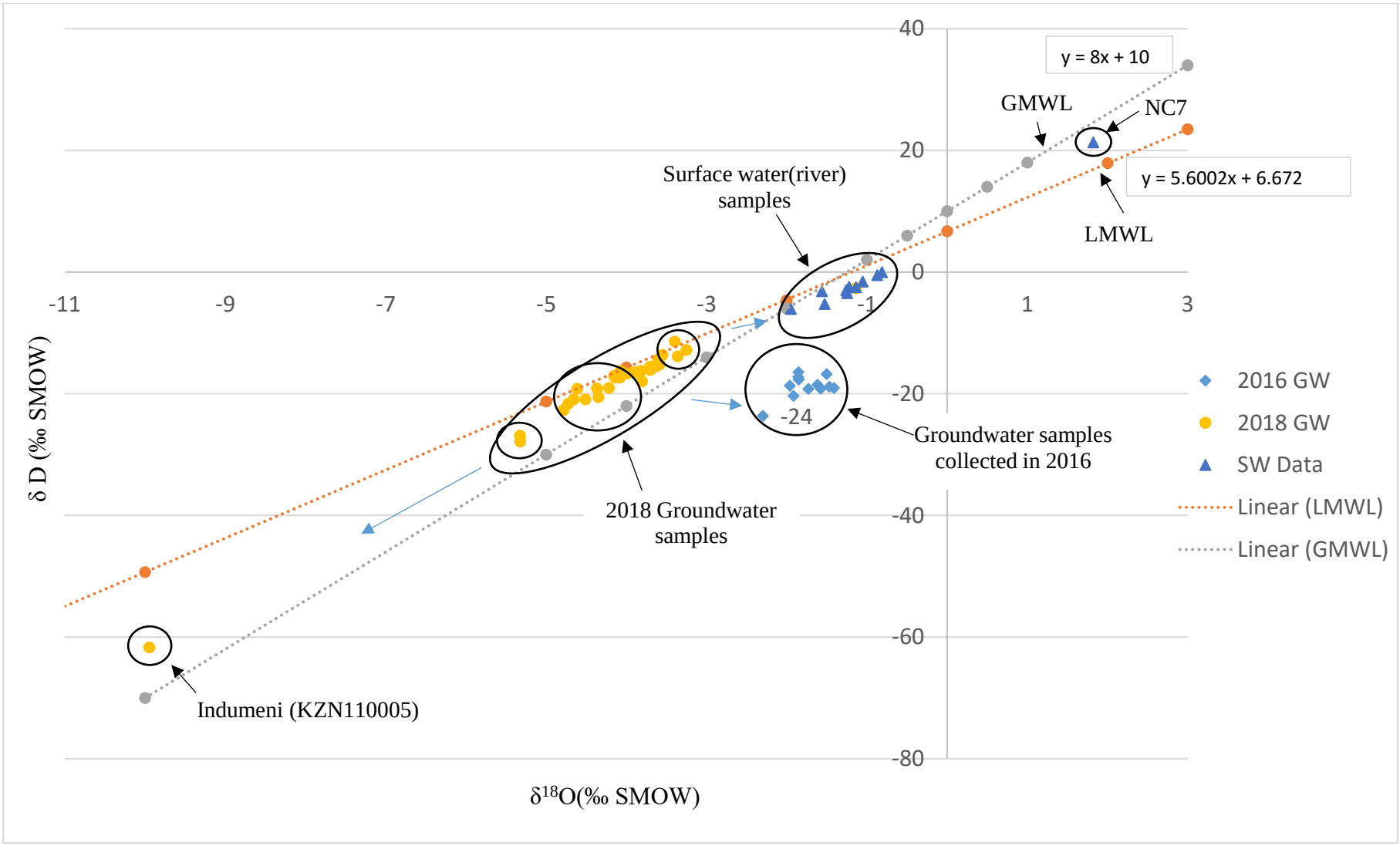

Figure 5. 23. Relationship between ^{18}O and deuterium from various water resources in relation to local and global meteoric lines.

5.10. Hydrogeological conceptualization of the study area

Based on the analysis of geological, hydrological, hydrochemical as well as environmental isotope data, a conceptual hydrogeological model for the study area has been proposed (Figure 5.24). The model is an attempt to summarize the hydrogeological information generated throughout the course of this study and systematically present it to describe the hydrology of the study area. The model is based on a W- E cross sectional line that cuts the main mining town of Dundee (Figure 4.2). Static water levels and thickness of lithological layers for five boreholes were used to define the aquifer unit (Volksrust and Vryheid Formations). It is difficult to tell where the Vryheid Formation starts and ends because of the similar stratigraphic characteristics (Intergranular fractured sandstone and weathered shale) of these two formations. The entire succession form alternating sandstone, shale and siltstone beds.

It is evident from the hydrochemical and isotopic data that there is a direct link between surface water and groundwater in the area. The hydrochemical evolution is of a fresh/ young water, sodium- magnesium- bicarbonate rich water with a depleted isotope signature, characteristic of areas located inland upland catchments. Shallow boreholes are typical of the area, with an average of 50 m depth. Most groundwaters are dominated by calcium and magnesium cations due to the calcite- dolomite AMD buffering in the system. Both Hydrochemical and environmental isotope data indicates active recharge taking place across the study area. The estimated amount of groundwater recharge is 4.1% of MAP or 29.3 mm/year.

A schematic conceptual hydrogeochemical model for the St Georges rehabilitated defunct mine and coal dump site is proposed in Figure 5.25 as an example of the hydrogeochemical processes taking place around the study region's rehabilitated abandoned mine sites. Coal mine tailings which were left scattered around the vicinity of abandoned mines were collected and rehabilitated including a grass soil cover. The rehabilitated coal mine tailings are characterized by FeS_2. Therefore, the rehabilitation processes involved the addition of powdered lime in different layers of the rehabilitated mine dump to neutralize the acid generated by the reaction of pyrite with oxygenated precipitation infiltrating into the pile.

$$FeS_2 + 3.75O_{2(aq)} + 1.5H_2O_{(aq)} + 2\ CaCO_3 + 4H^+ \rightarrow Fe(OH)_{3(s)} + 2SO_4^{2-} + 2Ca^{2+} + 2CO_{2(g)}$$

(carbon dioxide exsolves into the atmosphere)

For each mole of FeS_2 dissolved 2 moles of $CaCO_3$ is consumed to neutralize the acid generated and keep the pH circumneutral. Further neutralization reactions may occur once the leachate

reaches the groundwater, where solubility is higher than within the dump itself. The degassing of CO_2 produced during the neutralization process will further reduce acid from the system. Loss of carbon dioxide increases alkalinity, pH and carbonate minerals saturation indices thereby raising the precipitation potential of calcite (Nordstrom and McCleskey, 2006). Further dissociation of ions may occur thereby resulting in a final neutralization reaction of:

$$Fe\,(OH)_{3(s)} + 2SO_4^{2-} + 2Ca^{2+} + 2CO_{2(g)} \longleftrightarrow Fe^{2+}_{(aq)} + 3OH^-_{(aq)} + 2SO_4^{2-} + 2Ca^{2+} + 2CO_{2(g)}.$$

Calcium and magnesium carbonates which include minerals such as calcite and dolomite have been stated through literature as well as section 5.6.2 of this research, as being the better option for neutralization. These minerals are derived from secondary gypsum dissolution and weathering of calcite and pyrite (Nordstrom and McCleskey, 2006). The saturation index (SI) of gypsum is -1.60 and calcite being 0.61 which means the water remains undersaturated with regards to gypsum and oversaturated with calcite. Positive SI values indicate that a solution is supersaturated with respect to that mineral phase and precipitation of that mineral is possible.

$$CaCO_{3(s)} + CO_{2(aq)} + H_2O \longleftrightarrow Ca^{2+} + 2HCO_3^-$$

Given that gypsum is undersaturated, this suggests that gypsum dissolves in solution to its ionic components (Madzivire et al., 2011). As the pH increases due to AMD buffering reactions taking place, new cation exchange sites are created which explains supersaturation of calcite (Deuche, 1997).

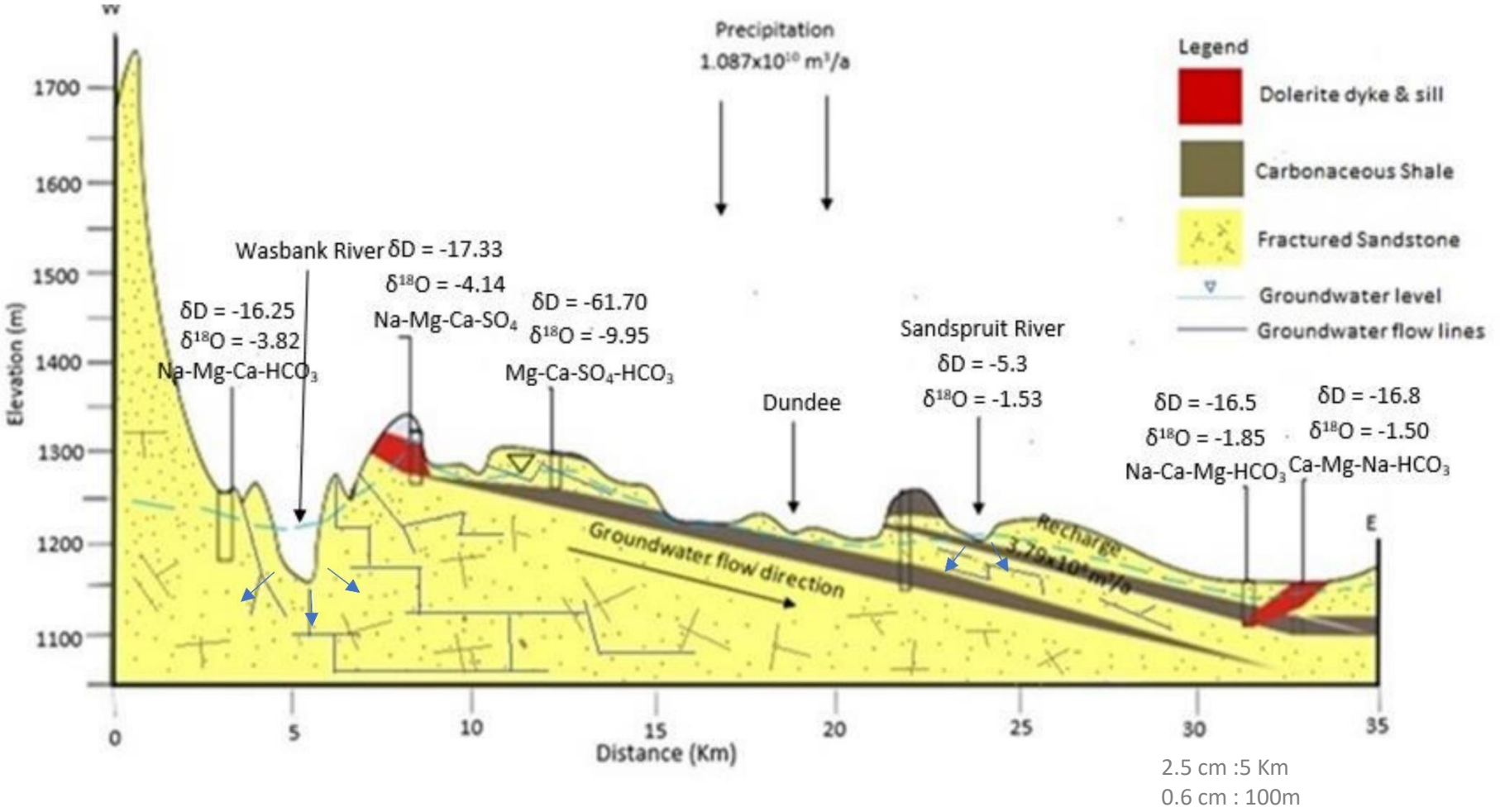

Figure 5. 24. Hydrochemical conceptual model of northern Kwazulu-Natal historic coal mining district.

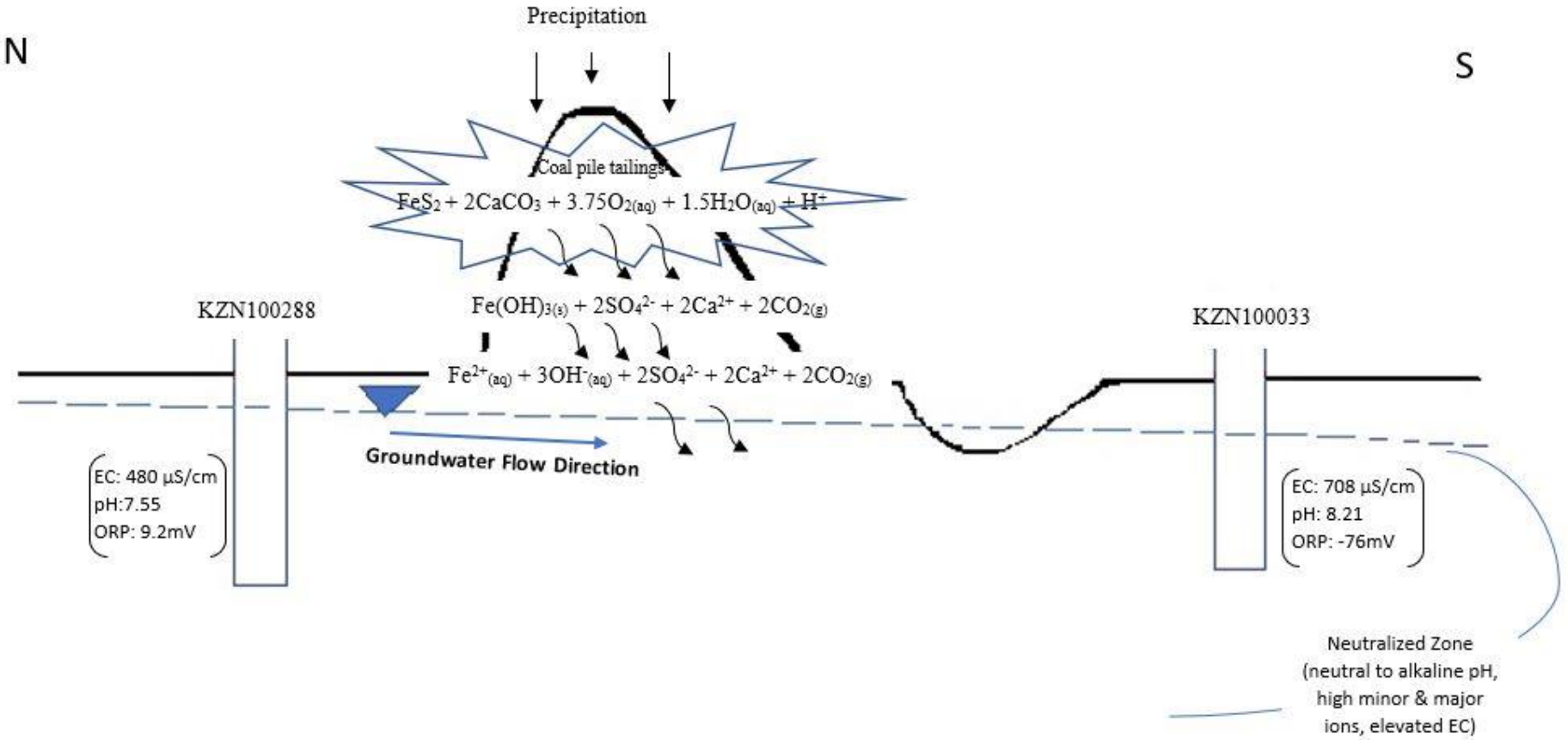

Figure 5. 25. Geochemical conceptual model of St Georges mine.

CHAPTER 6: CONCLUSION AND RECOMMENDATIONS

The historical coal mining districts located in northern KZN province of South Africa were investigated in order to understand the hydrogeochemical conditions of the region and assess the effectiveness of the defunct mine rehabilitation to improve the water resources quality. The investigation was undertaken by integrating monitored hydrochemical data with data from surface water and groundwater sampling points including environmental isotope data collected in the course of this research. The study area is characterised by alternating sandstone and shale beds of varying thickness. The hydrogeological properties are characteristic of the Volksrust and Vryheid Formations. Geological data, groundwater levels, hydrogeochemical as well as environmental isotopic signatures were used to identify and understand groundwater-surface water interactions and conceptualize the hydrogeology of the study area. In order to fully understand and conceptualise the surface water-groundwater interactions, geological, hydrological, hydrochemical and environmental isotope data were all integrated.

The general groundwater flow direction is from north-west to south-east, following the topography. The study area is characterised by circumneutral groundwaters in and around the rehabilitated mine sites which is indicative of adequate AMD acid neutralising capacity of the rehabilitated spoils. There appears to be sufficient carbonate present in the rehabilitated mines system to buffer acid generated through oxidation processes. The strong correlations among Mg^{2+}, Ca^{2+} and SO_4^{2-} were indicative of calcite and dolomite AMD buffering reactions being the main hydrogeochemical process influencing the groundwater chemistry around the abandoned mine sites. EC and TDS remain below aesthetic limits apart from a few outliers. There appears to be no signs of trace metal mobilisation in the area as trace metals remain below South African national drinking water standard values.

The hydrochemistry and environmental isotope signature of surface water and groundwater are similar indicating surface water - groundwater interconnections. The dominant hydrochemical facies in the study area is Ca-Na-HCO_3, which is characteristic of water-rock interactions of groundwater. The surface water and groundwater samples plot below and on the LMWL indicating their meteoric origin. The 2016 groundwater samples plot slightly further from the LMWL indicating evaporation prior to infiltration. The surface water samples are isotopically slightly enriched with the heavy isotopes of δD and $\delta^{18}O$ indicating moderate evaporations. The Ngangane River indicates strong evaporation (positive δD and $\delta^{18}O$ signals). The tritium

signature of groundwater samples indicates active and recent recharge from modern precipitation.

The following recommendations are emanated from the study:

- Continued seasonal sampling of the Northfield and Indumeni mines is important to see their continued response to rehabilitation as they have displayed signs of leaching;
- Surface water monitoring should be more widespread and not limited to V32 and V60 catchments in order to get an extensive view of the remediation effects on surface water;
- The location of some monitoring wells was not comprehensible for monitoring of contaminant transportations, as some were located much further from the discard dumps allowing for dilution. This could have been in part due to drillers being more concerned regarding the yield of the borehole, which was conflicting the main objective of governments monitoring strategy;
- Additional time series isotope analysis is needed to improve the temporal variation of environmental isotopic signals.

REFERENCES

Akcil, A., and Koldas, S. (2006). Acid Mine Drainage (AMD): causes, treatment and case studies. Journal of Cleaner Production, 14(12), 1139-1145.

Aken, M., Limpitlaw, D., Lodewijks, H., Viljoen, J. (2005). Post mining rehabilitation. land use and pollution at collieries in South Africa. Colloquium: Sustainable Development in the life of coal mining in South Africa, 13, 1-10.

Alhamed, M. (2015). Identification of geochemical processes controlling the neuralization of abandoned coal mine drainage using integration of geochemical modelling, geochemical analysis and batch test: An example from south of Bochum, Germany. Springer Berlin Heidelberg, 8(10), 8009-8025.

Alhamed, M. and Wisotzky, F. (2015). Investigate the generation of Acid Mine Drainage in the abandoned coal mine fields located south of Bochum. Germany. Research Gate, ,1-7.

Allison, G.B., Hughes, M.W., and Leaney, F.W.J. (1984). Effect of climate and vegetation on oxygen- 18 and deuterium profiles in soil. Isotope Hydrology. Proc. Symp. Vienna, IACA, p 105-123.

Arnesen, R.T., Banks, D., Banks, S.B., Iversen, E.R., and Younger, P.L. (1997). Mine water chemistry: The good. the bad and the ugly. Environmental Geology, 32(3).

Åström, M. (1998). Partitioning of transition metals in oxidised and reduced zones of sulphide-bearing fine-grained sediments. Applied Geochemistry, 13, 607-617.

Atanacković, N., Dragišić, V., Stojković, J., Papić, P. & Živanović, V. (2013). Hydrochemical characteristics of mine waters from abandoned mining sites in Serbia and their impact on surface water quality. Environmental Science and Pollution Research, 20, 7615-7626.

Bean, J.A. (2003). A critical review of recharge estimation methods used in South Africa. PhD dissertation. Bloemfontien: University of the Free State, Department of Geohydrology.

Banks, D., Younger, P. L., Arnesen, R.-T., Iversen, E. R. and Banks, S. B. (1997). Mine-water chemistry: the good, the bad and the ugly. Environmental Geology, 32**,** 157-174.

Belkhiri, L., Abderrahmane, B., and Mouni, L. (2010). A multivariate Statistical Analysis of Groundwater Chemistry Data. International Journal of Environmental Research, 5, 537-544.

Blodau, C. (2006). A review of acidity generation and consumption in acidic coal mine lakes And their watersheds. Science of the total environment, 369(1),307-332.

Cadle, A.B., Cairncross, B., Christie, A.M.D. and Roberts, D.L. (1990). The Permo-Triassic Coal bearing deposits of the Karoo Basin. Southern Africa. Economic Geology Research Unit Information Circular No.218. University of Witwatersrand. South Africa.

Cairncross, B. (2001). An overview of the Permian (Karoo) coal deposits of southern Africa Journal of African Earth Science, 33(3), 529-562.

Campaner, V. P., Luiz-Silva, W. & Machado, W. (2014). Geochemistry of acid mine drainage from a coal mining area and processes controlling metal attenuation in stream waters, southern Brazil. Anais da Academia Brasileira de Ciências, 86**,** 539-554.

Chevallier, L. P., Goedhart, M. L., & Woodford, A. C. (2001). Influence of Dolerite Sill and Ring Complexes on the occurrence of Groundwater in Karoo Fractured Aquifers: A Morphotectonic Approach: report to the Water Research Commission. Water Research Commission.

Chikte, U., Molefe, M., Rudolph, M. (1997). Dental Fluorosis with varying levels of fluoride in drinking water. University of Witwatersrand. Johannesburg.

Christie, A., Mason, T.R., Roberts, A., Smith, A., Smith, T.R., Spuy, A.D. (1988). Sedimentary Models for coal formation in the Vryheid Formation. Northern Natal. Department of

Mineral and Energy Affairs. Vryheid.

Clark, I.D., and Fritz, P. (1997). Environmental isotopes in hydrogeology. CRC press.

Colvin, C., Burns, A., Schachtschneider, K., Maherry, A., Charmier, J. & De Wit, M. (2011). Coal and water futures in South Africa: The case for protecting headwaters in the Enkangala grasslands. South Africa, World Wildlife Fund-South Africa (WWF-SA).

Connelly, R. and Taussig, D. (1994). Nitrite contamination of groundwater in the Kutama and Sinthumule districts of Venda. In: Seanego. G.K. (2014). Ecological status of the Sand river after the discharge of sewage effluent from Polokwane and Seshego wastewater treatment works. University of Limpopo.

Cravotta III, C. A. & Kirby, C. S. (2008). Acidity and alkalinity in mine drainage: Practical considerations. Proceedings of the National Meeting of the American Society of Mining and Reclamation and the 25th West Virginia Surface Mine Drainage Task Force, 2004. 334-365.

Dauda, M. and Habib, G.A. (2015). Graphical Techniques Presentation of Hydro-Chemical data. Journal of Environmental an Earth Science, 5(4), 65-75.

Demlie, M. (2015). Assessment and estimation of groundwater recharge for catchment located in highland tropical climate in central Etheopia using catchment soil-water balance (SWB) and chloride mass balance (CMB) techniques. J. Environmental Earth Sci, 74(2), 1137-1150.

Department of Mineral Recourses. (2014). South Africa's mineral industry. Final Report.

Department of Water Affairs and Forestry. (1994). Characterization and Mapping of the Groundwater Resources of Mapping Unit 1 of the KwaZulu-Natal Province (1st ed., Vol. 1). Johannesburg.

Department of Water Affairs and Forestry. (1995). Characterization and Mapping of the Groundwater Resources of Mapping Unit 5 of the KwaZulu-Natal Province. Johannesburg.

Department of Water Affairs and Forestry. (1995). Report on the groundwater resources and Hydrogeology of Unit 11 (1st ed., Vol. 1). Johannesburg.

Department of Water Affairs and Forestry. (1998). Water pollution control works in northern KwaZulu-Natal: Sandspruit catchment impact assessment, feasibility study, prioritization and preliminary design. Final Report.

Department of Water Affairs and Forestry. (2006). Annual State of the Water Report. Final Report.

Department of Water and Sanitation. (2014). Groundwater assessment at defunct rehabilitated mines in the Sandspruit catchment: Umzinyathi District Municipality northern KwaZulu-Natal. Water resources planning systems.

Deutsch, W. J. (1997). Groundwater Geochemistry. Fundamentals and Applications to Contamination (1st Ed). CRC Press LLC.: USA.

Egboka, B.C.E., Odoh, B.I., and Utom, A.U. (2013). Assessment of hydrogeochemical characteristics of groundwater quality in the vicinity of Okpara coal and Obwetti fireclay mines, near Enugu town, Nigeria. J. Appl Water Sci, 3, 271 – 283.

Equeenuddin, S.M., Tripathy, S., Sahoo, P. & Panigrahi, M. (2010). Hydrochemical characteristics of acid mine drainage and water pollution at Makum Coalfield, India. Journal of Geochemical Exploration, 105, 75-82.

Eriksson, E. and Khunakasem, V. (1969). Chloride concentration in groundwater, recharge rate of deposition of chloride in the Israel coastal plain. J.Hydrol.7, 178-197.

Freeze, R.A., and Cherry, J.A. (1979). Groundwater. Prentice-Hall, Inc.: New Jersy.

Gomo, M. & Vermeulen, D. (2014). Hydrogeochemical characteristics of a flooded Underground coal mine groundwater system. Journal of African Earth Sciences. 92. 10.1016/j.jafrearsci.2014.01.014.

Gomo, M. & Masemola, E. (2016). Groundwater hydrogeochemical characteristics in rehabilitated coalmine spoils. Journal of African Earth Sciences, 116, 114-126

Gomo, M. (2018). Conceptual hydrogeochemical characteristics of a calcite and dolomite acid mine drainage neutralised circumneutral groundwater system. Water Sci. https://dx.doi.org/10.1016/j.wsj.2018.05.004.

Gotz, A.E. and Hancox, P. (2014). South African Coalfields: A 2014 perspective. International Journal of Coal Geology, Issue 132, 170-254.

GRIP.(2010). Groundwater Resource Information Project [online], http://www.dwa.gov.za/Groundwater/GroundwaterOffices/KZN/GRIP_KwaZulu-Natal.pdf. Accessed June 2017.

Guest, B. 1988. Commercial Coal-mining in Natal: A Centennial Appraisal. Natalia, 18, 41-58.

Halim, M.A., Majumder, R.K., Zaman, M.N., Hossain, S., Rasul, M.G., and Sasaki, K. (2013). Mobility and impact of trace metals in Barapukuria coal mining area, Northwest Bangladesh. Arabian Journal of Geosciences, 6(12), 4593 -4605.

Hampson, G., Stollhofen, H., and Flint, S. (1999). A sequence stratigraphic model for the lower Coal Measures (Upper Carboniferous) of the Ruhr district, north-west Germany. Sedimentology. 46(6), 1199-1231.

Jeffrey, L. (2005). Characterization of the coal resources of South Africa. Journal of the Southern African Institute of Mining and Metal, 105(2), 95-102.

Kempster, P.L., Hattingh, W.H.J., Van Vliet. H.R. (1982). Department of Water Affairs. Forestry and Environmental Conservation: Summarized water quality criteria. Hydrological Research Institute. Pretoria.

Limpitlaw, D. (2004). Mine closure as a framework for sustainable development. Sustainable Development Practices on Mine Sites—Tools and Techniques, University of the Witwatersrand, Johannesburg, 8-10.

Mackay, C.A. (1988). Sedimentary Models for Coal Formation in the Klip River Coalfield: A thesis submitted in partial fulfilment of the requirements for the degree of Doctor of Philosophy. University of Natal. Durban.

Majumder, R.K., and Shimada, J. (2016). Hydrochemistry and Environmental Isotopes to Identify the Origin of Barapukuria Coal Mine Inflow Water, Northwestern Bangladesh.Austin Journal of Hydrology, 3(1), 1019.

Mazor, E. (2003). Chemical and isotopic groundwater hydrology (Vol. 98). CRC press.

Michalik, A. (2008). The Use of Chemical and Cluster Analysis for Studying Spring Water Quality in Świętokrzyski National Park. Polish Journal of Environmental Studies, 17.

MINTEK, (2007). Assessment of KwaZulu-Natal's coal mining and coal resources.

Munnik, V. (2010). The social and environmental consequences of coal mining in South Africa. A CASE STUDY. Environmental Monitoring Group.

Mutwiri, H.N. (2016). Corporate social responsibility and its role in the realization of the right to clean and healthy environment in the mining sector: A case study of coal mining in Kitui County-Mui Basin.

Nel, E.L., Hill, T.R., Aitchison, K.C. and Buthelezi, S. (2003). The closure of coal mines and local development responses in Coal-Rim Cluster, northern KwaZulu-Natal, South Africa. Development Southern Africa, 20, 369 – 385.

Nordstrom, D. K. (2011). Mine waters: acidic to circumneutral. Elements, 7, 393-398.

Nordstrom, D.K. and McCleskey, R.B. (2006). Mineral solubility and weathering rate constraints on metal concentrations in groundwaters of the mineralized areas near Questa. Lexington. American Society of Mining Reclamation (ASMR).

Okiongbo, K. & Douglas, R. (2015). Evaluation of major factors influencing the geochemistry of groundwater using graphical and multivariate statistical methods in Yenagoa city, Southern Nigeria. Applied Water Science, 5, 27-37.

Powell, J.D., and Larson, J.D. (1985). Relation between ground-water quality and mineralogy in the coal- producing Norton Formation of Buchanan County, Virginia. Department of the Interior. US Geological Survey.

Sherman, H.M. (1998). The assessment of groundwater quality in rural communities: Two Case studies from KwaZulu-Natal. University of Natal. Department of Geology and Applied Geology. Durban.

SAWS. (2017). South African Weather Service. Durban Weather Office Meteorological Data.

Scokart, P., Meeus-Verdinne, K. & De Borger, R. (1983). Mobility of heavy metals in polluted soils near zinc smelters. Water, Air, & Soil Pollution, 20, 451-463.

Suk, H., and Lee, K.K. (1999). Characterisation of a groundwater hydrochemical system through multivariate analysis: clustering into ground water zones. Groundwater, 37(3), 358-366.

Swart, E. (2003). The South African Legislative Framework for mine closure. Journal of the Southern African Institute of Mining and Metallurgy, 103(8), 489-492.

Townsend, A. R. (1983). The Impact of Recession on Industry, Employment, and the Regions, 1976-1981, Taylor & Francis.

Ukpatu, J., Udoinyang, E. & Udoh, J. P. (2015). The Use of Agglomerative Hierarchical Cluster Analysis for the Assessment of Mangrove Water Quality of Okoro River Estuary, Southeastern Nigeria. International Journal of Geology, Agriculture and Environmental Science, 3.

Utom, A. U., Odoh, B. I. & Okoro, A. U. (2012). Estimation of aquifer transmissivity using Dar Zarrouk parameters derived from surface resistivity measurements: A case history from parts of Enugu Town (Nigeria). Journal of Water Resource and Protection, 4, 993.

Van Wyk, W. (1963). Groundwater studies in Northern Natal. Zululand and surrounding areas Geological Survey Department of South Africa (Memoir 52).

Vermeulen, D. & Bester, M. (2009). Assessment of How Water Quality and Quantity will be affected by mining of the Waterberg Coal Reserves. International Mine Water Conference. Pretoria, South Africa.p 19-23.

Vorster, C.J. (2003). South African coal database [Online image]. Retrieved May 28, 2017 from:http://www.geoscience.org.za/index.php/component/content/article?id=107:databases-samindaba

Younger, P. L. and Wolkersdorfer, C. (2004). Mining impacts on the fresh water environment: technical and managerial guidelines for catchment scale management. Mine water and the environment, 23, s2-s80.

APPENDICES

Appendix I. Hydrochemical parameters and associated operational risks.

Hydrochemical Parameters

It has become evident that the absolute concentration of a particular element is perhaps not as significant as the chemical form in which the element exists and its interactions with other constituents. Further, while a large number of constituents are toxic at high concentrations, they may be essential to normal health in small amounts. Following is a brief discussion on some determinants as well as the Department of Water Affairs and Forestry water classification for the determinants discussed below:

Total Dissolved salts (TDS): This is the addition of individual anions and cations from a total macro analysis, or it could be calculated from electrical conductivity (EC). Total dissolved salts are closely related to total dissolved solids (may be referred to as TDS) and are used interchangeably. A discrepancy occurs when an unusually high concentration of a non-ionic substance, such as dissolved organic compounds, are present. The lower limit for DWAF Class 1 (1000mg/l) is primarily aesthetic, whereas the upper limit for Class 2 (2450 mg/l) is based on health considerations and may lead to salt overload in sensitive individuals (Hattingh et al., 1982).

pH= -log[H], or the negative logarithm of the hydrogen ion activity. The pH of water should be considered along with redox potential (Eh), temperature, electrical conductivity and major ions due to the corrosive potential of water. Metals tend to be more soluble in low pH (acidic) waters, increasing the risk of ingesting toxic corrosion products e.g. cadmium from galvanising. Alkaline (high pH) water, especially above a pH of 10, may lead to mucous membrane irritation (Hattingh et al., 1982).

Major ions

Sodium is an essential constituent in low concentration, but at higher concentrations (200-400 mg/l) it causes an unpleasant salty taste and may be unsuitable for individuals with salt restricted diets such as those with congestive heart failure, hypertension due to salt retention, or immature kidneys. Water sources that contain sodium concentrations above 400mg/l are generally considered unsuitable (Hattingh et al., 1982)

Potassium is an essential element for good health and is the seventh most common element in the earth's crust. Potassium is generally considered non-toxic, however, at very high doses it disturbs the electrolyte balance of the body (Hattingh et al., 1982).

Calcium standards for industry are low as this element causes scaling. For drinking purposes, the criterion is high as calcium is non-toxic and calcium phosphate is an integral constituent of bone. The body uses up to 2g/day. Calcium enriched water reduces the harmful effects of high fluoride concentrations though the precipitation of calcium fluoride (CaF_2) and reduces the harmful effects of heavy metals by hindering their adsorption. It has been noted that fish populations in calcium rich water experience reduced effects from lead and zinc. Therefore, in low calcium water stricter guidelines for heavy metals need to be adhered to than in high calcium water (Hattingh et al., 1982).

Magnesium is required by humans, animals and plants. When combined with calcium, magnesium is responsible for water hardness. At concentrations of 70mg/l a bitter taste becomes noticeable, and diarrhoea may occur in infants. Above 100mg/l the bitter taste is more pronounced, and diarrhoea is more common. Magnesium has also been linked to ischaemic heart disease (Arbuckle et al., 1997).

Chloride is associated with sodium and reflects the salinity of the water. Above concentrations of 200mg/l water will have a distinctive salty taste. Above 600 mg/l the water will not quench thirst. Because most plants do not have salt excreting mechanisms the criterion for irrigation water is only 100mg/l. Chloride is difficult to remove, requiring processes such as distillation, reverse osmosis or ion exchange (Arbuckle et al., 1997).

Sulphate is toxic to sensitive individuals at high concentrations due to its purgative effects. At concentrations between 200 to 400 mg/l diarrhoea may occur in non-adapted users. At concentrations between 400 to 600 mg/l an unpleasant taste may be noticed, and diarrhoea is common, though most users will adapt. However, at concentrations above 600mg/l water is not considered suitable for drinking purposes, particularly for infants for whom diarrhoea may be life threatening (Arbuckle et al., 1997).

Alkalinity is mainly due to bicarbonate species and reflects the acid neutralizing capacity of the water sample. Total alkalinity is referred to as TAL and is commonly measured in major ion analysis. Alkalinity effects the corrosive potential of water (Arbuckle et al., 1997).

Minor Ions

Fluoride is beneficial at low concentrations (= Ap1.0mg/l), at concentrations two or three times the beneficial level fluoride is responsible for teeth rotting and skeletal damage in people as well as livestock. High fluoride concentrations can occur naturally in groundwater or from waste water. The ideal concentration of fluoride is dependent on average daily intake. Average daily intake is dependent on the average maximum air temperature. In other words, people that live in warm climates drink more water than those that live in cold climates. Therefore, the ideal fluoride concentrations are dependent on air temperature. For an average maximum air temperature of 16^{o}C a fluoride concentration of 1mg/l is recommended, whereas for an average daily maximum of 30^{o}C only 0.7 mg/l is recommended (Chikte et al., 1997)

Nitrate and Nitrite are generally reported together as mg/l N. They result from the bacterial oxidation of organic nitrogen which comes from sewage effluent and fertilizer runoff from agricultural fields. Nitrite poisoning causes methaemoglobinaemia (blue baby) in infants and may be linked to stomach cancer in adults. Infants are especially at risk when they are bottle fed, have iron deficiency anaemia, insufficient vitamin C intake, or achlorhydria (high stomach pH) as well as elevated nitrate concentrations in their water sources. The Department of Water Affairs recommends a concentration below 10mg/l and considers 20mg/l unfit for infant consumption. The World Health Organisation lists 45mg/l as the maximum permissible level and other research suggests that up to 90mg/l is safe for adults. {Connelly, 1994, Nitrite contamination of groundwater in the Kutama and Sinthumule districts of Venda`, South Africa`, in Groundwater Quality}

Ammonium exists under acidic conditions and is converted to the more toxic ammonia under alkaline conditions through the reaction:

$$NH_4^+ \longrightarrow H^+ + NH_3$$

High ammonium concentrations indicate the presence of sewage effluent or nitrogen-based fertilizers{Connelly, 1994, Nitrite contamination of groundwater in the Kutama and Sinthumule districts of Venda`, South Africa`, in Groundwater Quality}.

Phosphate incorporates phosphorus, which is the eleventh most common element in the earth's crust and exists in the form of phosphate minerals. Phosphate is non-toxic and combined with calcium it is a necessary component of bones. Phosphates are an indication of pollution from

detergents, fertilizers and sewage and are therefore associated with more dangerous pollutants (Arbuckle et al., 1997).

Appendix II. Water Quality Classification (DWAF, 2012). Measurement units are in mg/l unless otherwise stated.

Constituent	Class 0 Ideal	Class 1 Potable	Class 2 Short Term	Class 3 Not Suitable
Total Dissolved Salts	0-450	450-1000	1000-2450	>2450
Electrical Conductivity(mS/m)	0-70	70-150	150-370	>20
Nitrate plus Nitrite as N	0-6	6-10	10-20	>20
Fluoride	0-1.0	1.0-1.5	1.5-3.5	>3.5
Sulphate	0-200	200-400	400-600	>600
Magnesium	0-30	30-70	70-100	>100
Sodium	0-100	100-200	200-400	>400
Chloride	0-100	100-200	200-600	>600
Ph (pH units)	6.0-9.0	5.0-9.5	4-5 or 9.5-10	<4 or >10
Iron	0-0.1	0.1-0.2	0.2-2.0	>2.0
Manganese	0-0.05	0.05-0.1	0.1-1.0	>1.0
Zinc	0-3.0	3.0-5.0	5.0-10.0	>10.0
Arsenic	0-0.010	0.010-0.050	0.050-0.2	>0.2
Cadmium	0-0.005	0.005-0.010	0.010-0.020	>0.02
Faecal coliforms (No/ 100ml)	0	0-1	1-10	>10

Appendix III. Piper Plots for time series groundwater chemistry data

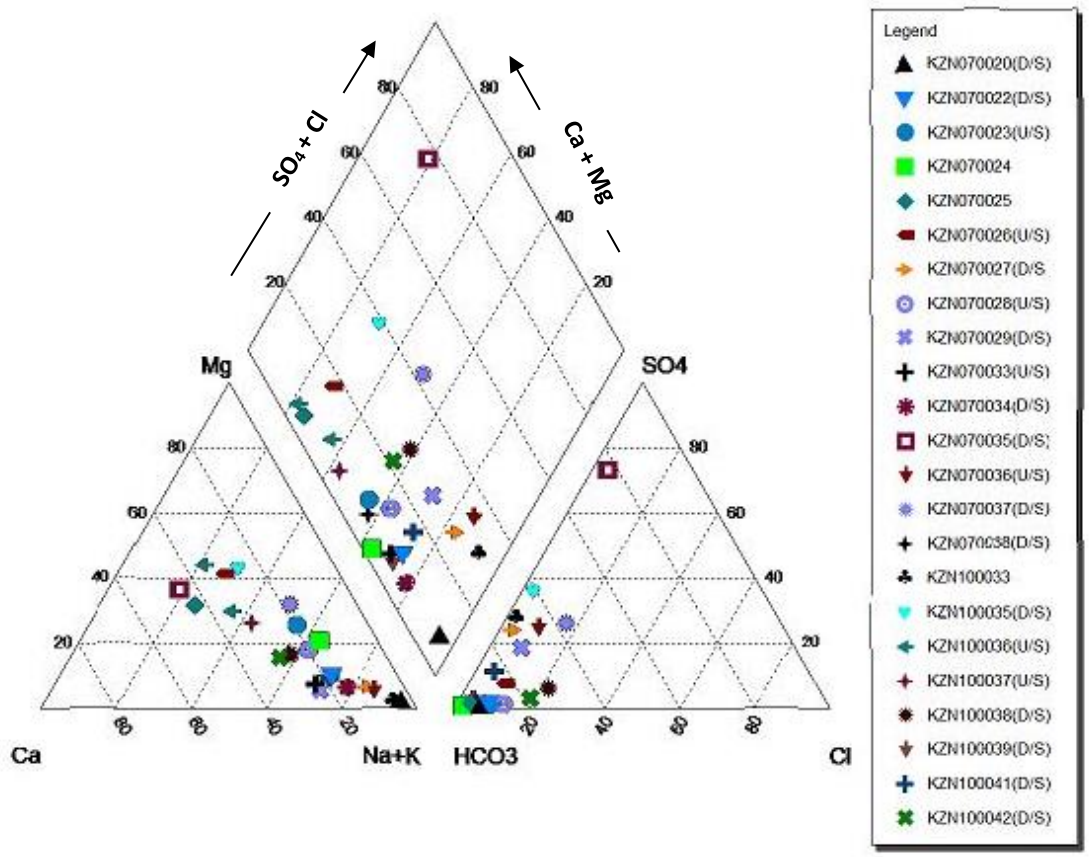

Piper plot of the 2010 hydrochemical data

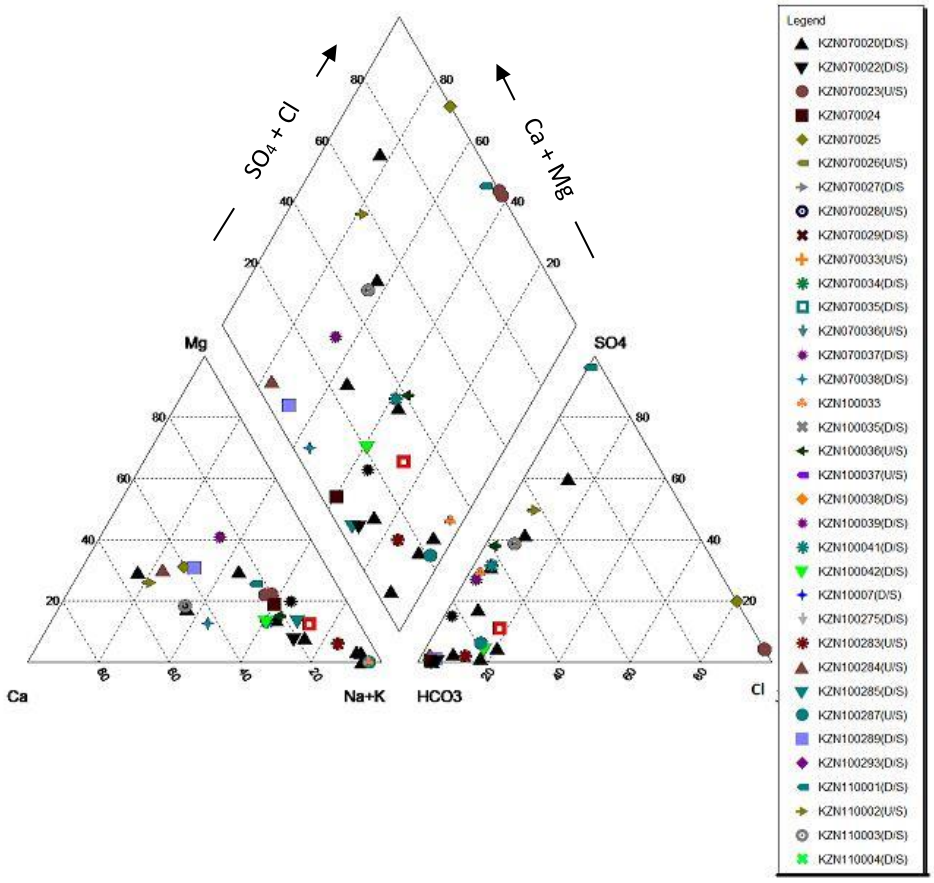

Piper plot of the 2012 hydrochemical data

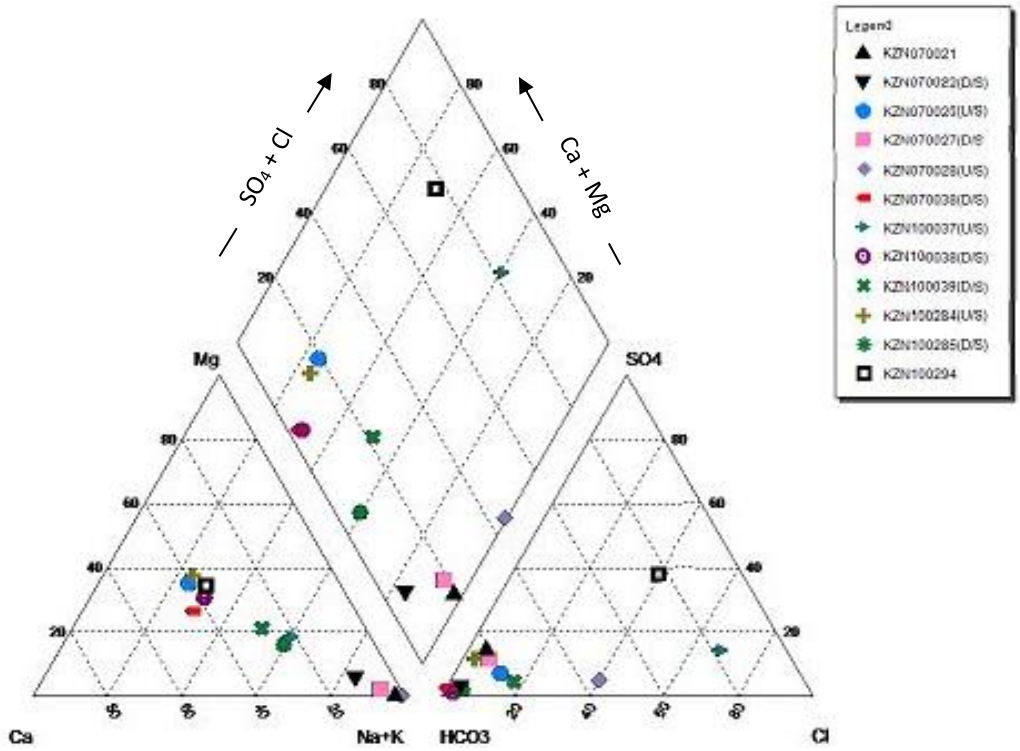

Piper plot of the 2016 hydrochemical data

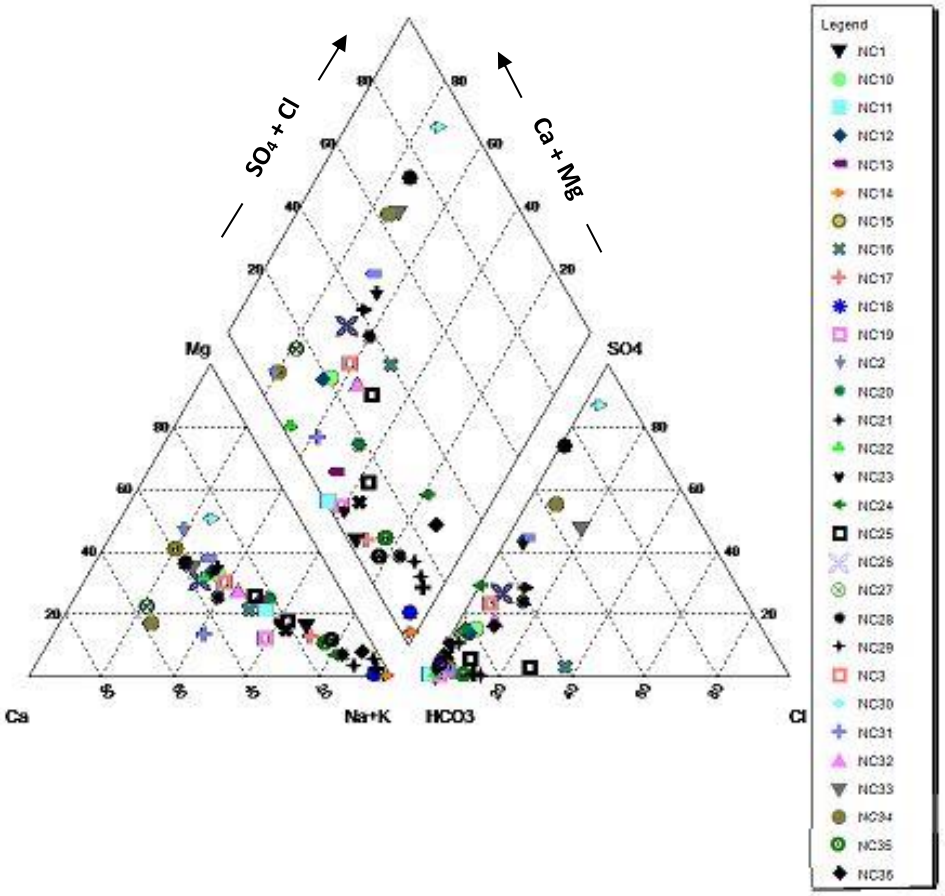

Piper plot of the 2018 hydrochemical data

Appendix IV: Time series linear correlation plots for 2011-2018 major and minor ions.

2010 Pearson Correlation Plot.

Variables	Ca	K	Na	Mg	NO3	Si	SO4	Cl	F	HCO3
Ca	1									
K	-.384	1								
Na	-.309	.113	1							
Mg	**.847**	-.453	-.287	1						
NO3	-.106	.487	-.128	-.075	1					
Si	.419	.249	-.288	.533	-.317	1				
SO4	**.743**	-.241	.122	**.543**	-.041	**.679**	1			
Cl	.239	.079	.395	.266	-.051	-.290	.211	1		
F	-.183	-.039	.573	-.173	-.075	.380	.142	-.088	1	
HCO3	-.166	.225	.429*	-.016	.003	**.624**	-.087	-.005	.265	1

2012 Pearson Correlation Plot

Variables	Ca	Mg	Cl	HCO3	SO4	NO3	F	K	Na	Si
Ca	1									
Mg	**.915**	1								
Cl	-.100	-.184	1							
HCO3	-.205	-.241	.215	1						
SO4	**.861**	**.948**	-.158	-.216	1					
NO3	**.760**	**.917**	-.188	-.221	**.980**	1				
F	-.202	-.089	.322	-.193	-.094	-.049	1			
K	.513	.547	-.184	-.001	.658	.671	.162	1		
Na	.428	.720	-.024	.079	**.856**	**.880**	.164	.717	1	
Si	-.040	-.047	-.271	-.187	-.161	-.160	-.250	-.249	-.408	1

2013 Pearson Correlation Plot

Variables	Ca	Mg	Cl	HCO3	SO4	NO3	F	K	Na	Si
Ca	1									
Mg	**.723**	1								
Cl	-.302	.117	1							
HCO3	-.330	-.315	**.899**	1						
SO4	.685	**.843**	.192	-.295	1					
NO3	.327	.567	-.140	-.230	**.802**	1				
F	-.330	-.315	.632	.655	-.231	-.123	1			
K	.526	.530	1.00	.182	**.735**	.687	.235	1		
Na	.277	.330	1.00	.356	.625	.550	.373	**.816**	1	
Si	**.814**	.602	-.409	-.704	.247	.003	-.916	-1.00	-1.00	1

2014 Pearson Correlation Plot

Variables	Ca	Mg	Cl	HCO3	SO4	NO3	F	Si
Ca	1							
Mg	**.954**	1						
Cl	-.111	-.123	1					
HCO3	-.360	-.362	**.722**	1				
SO4	**.782**	**.824**	-.102	-.269	1			
NO3	**.813**	**.835**	-.098	-.259	**.718**	1		
F	-.284	-.220	.532	.631	-.196	-.233	1	
Si	-.051	-.026	-.301	-.255	-.239	-.183	-.194	1

2015 Pearson Correlation Plot

Variables	Ca	Mg	Cl	HCO3	SO4	NO3	F	K	Na	Si
Ca	1									
Mg	**.845**	1								
Cl	-.399	-.374	1							
HCO3	-.546	-.647	**.906**	1						
SO4	.321	.611	**.954**	-.470	1					
NO3	-.025	.060	-.410	-.353	-.112	1				
F	-.599	-.651	**.947**	**.913**	-.243	-.356	1			
K	.015	.230	-.380	.048	-.112	.263	-.008	1		
Na	-.472	-.481	**.772**	**.723**	-.117	-.529	**.837**	-.248	1	
Si	**.902**	**.890**	-.755	-.962	-.526	**.907**	-.926	**.893**	-1.00	1

2016 Pearson Correlation Plot

Variables	Si	Ca	F	SO4	Cl	Mg	K	Na	Fe	HCO3	NO3
Si	1										
Ca	**.724**	1									
F	-.764	-.621	1								
SO4	-.259	-.233	.321	1							
Cl	-.006	.111	.291	.051	1						
Mg	**.784**	**.974**	-.617	-.207	.164	1					
K	-.164	.099	.129	.029	.270	-.053	1				
Na	-.805	-.670	**.918**	.506	.273	-.681	.108	1			
Fe	-.726	-.808	.616	.183	.025	-.808	-.202	**.750**	1		
HCO3	.114	.533	-.225	.112	-.104	.423	.190	-.086	-.168	1	
NO3	.212	.147	-.200	-.121	.371	.087	**.732**	-.137	-.251	.126	1

Appendix V. Hierarchical Cluster Analysis Dendrogram of Similarity and Dissimilarity Clusters showing Similar Physiochemical Behaviour and the Amalgamation of Various Parameters into Domains for 2011-2016 Groundwater Data.

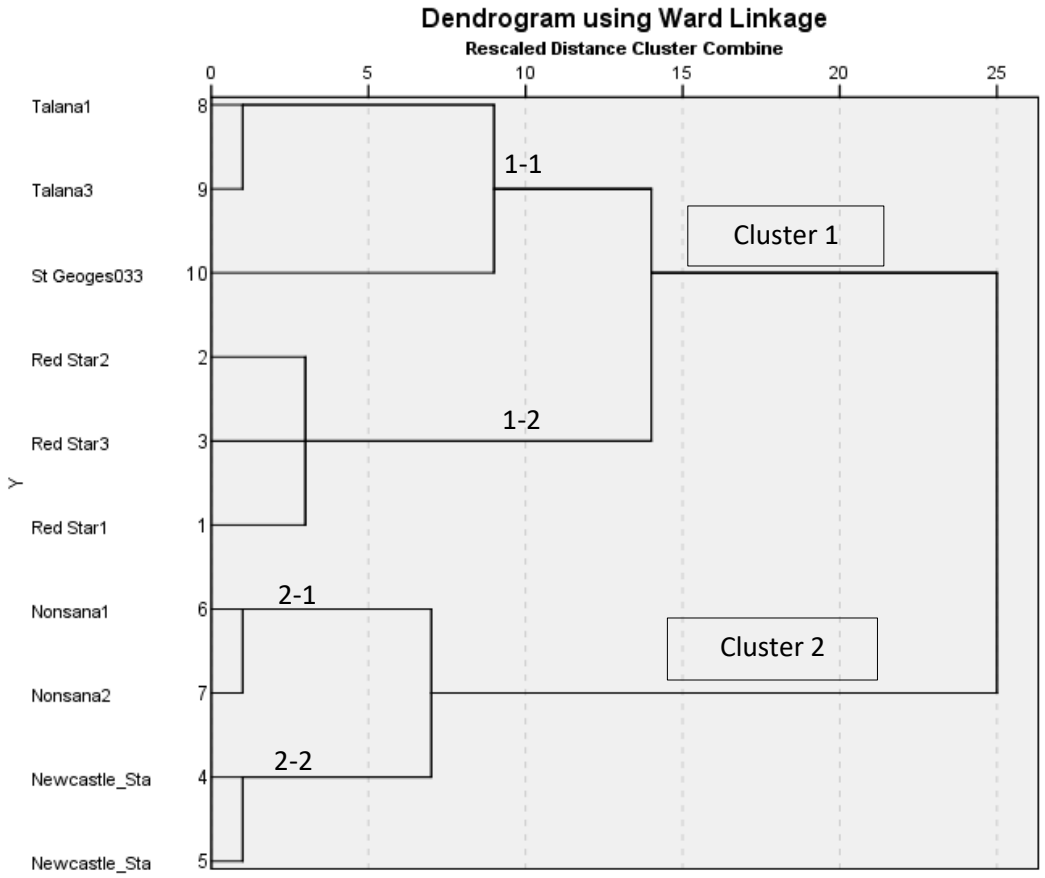

2010 Hydrochemical data Dendrogram using Wards linkage reduction technique.

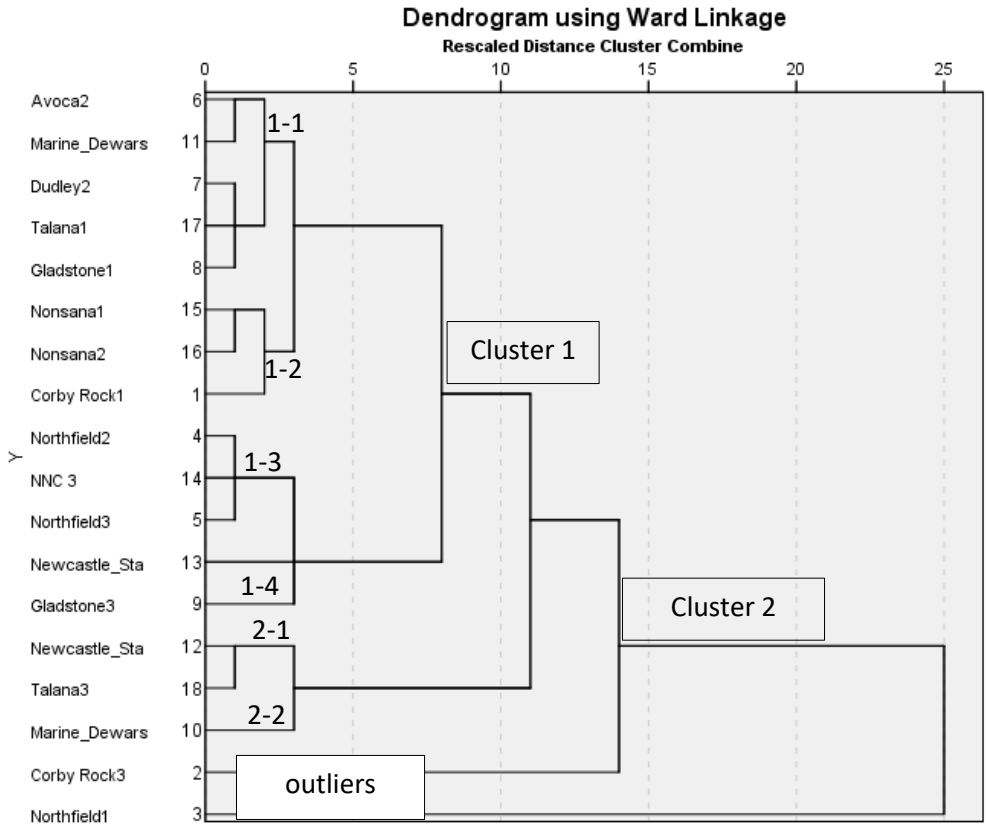

2012 Hydrochemical data Dendrogram using Wards Linkage reduction technique.

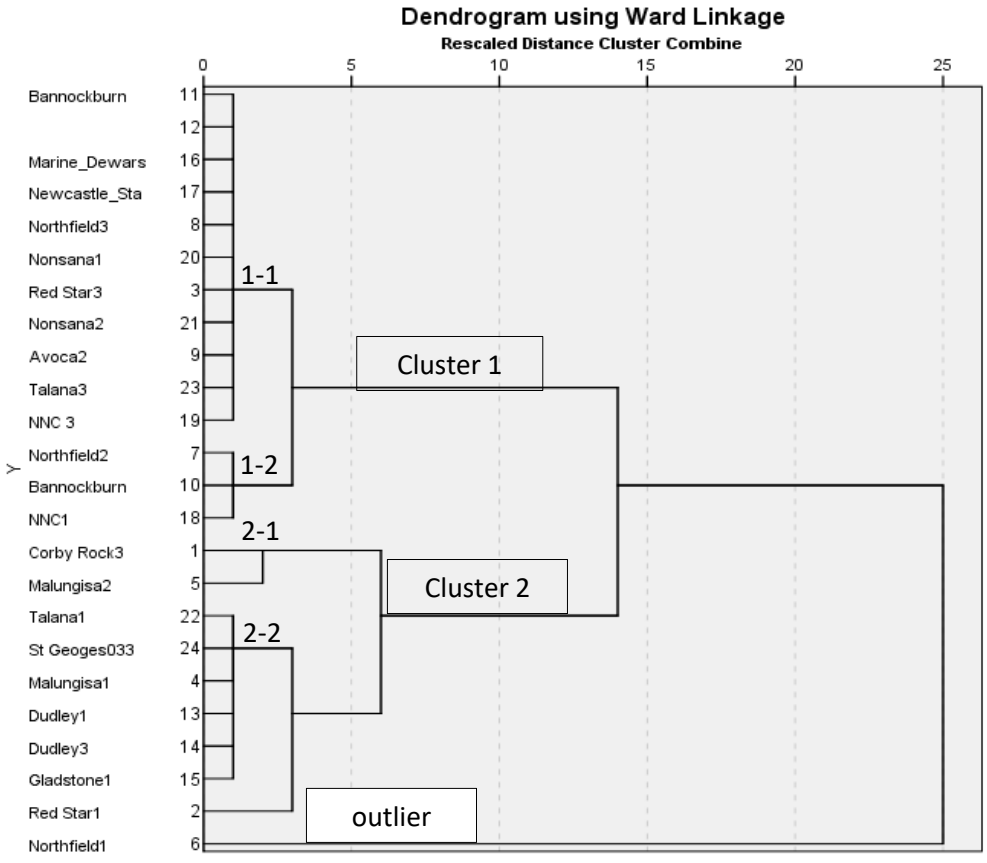

2013 Hydrochemical data Dendrogram using Wards Linkage reduction technique.

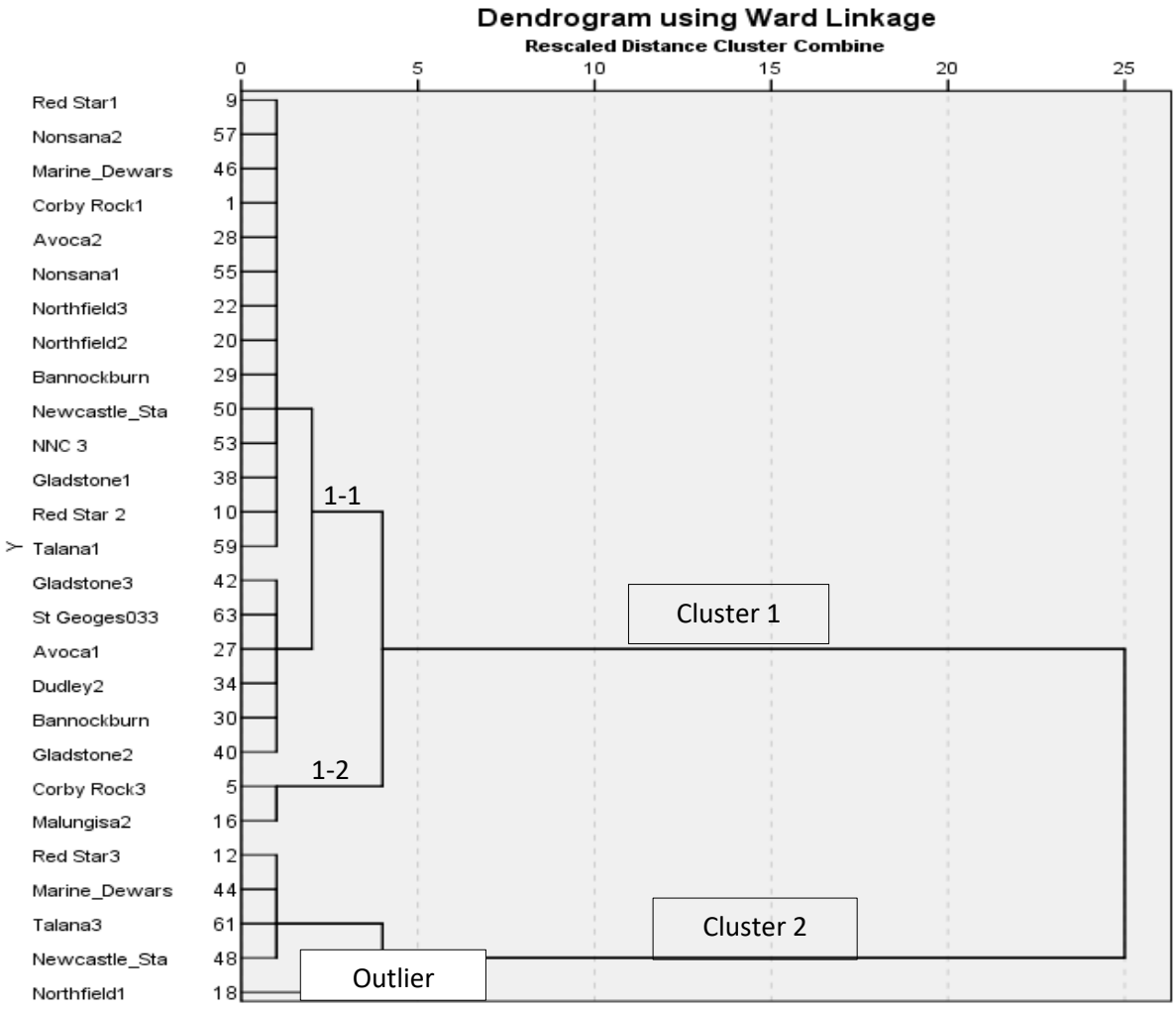

2014 Hydrochemical data Dendrogram using Wards Linkage reduction technique.

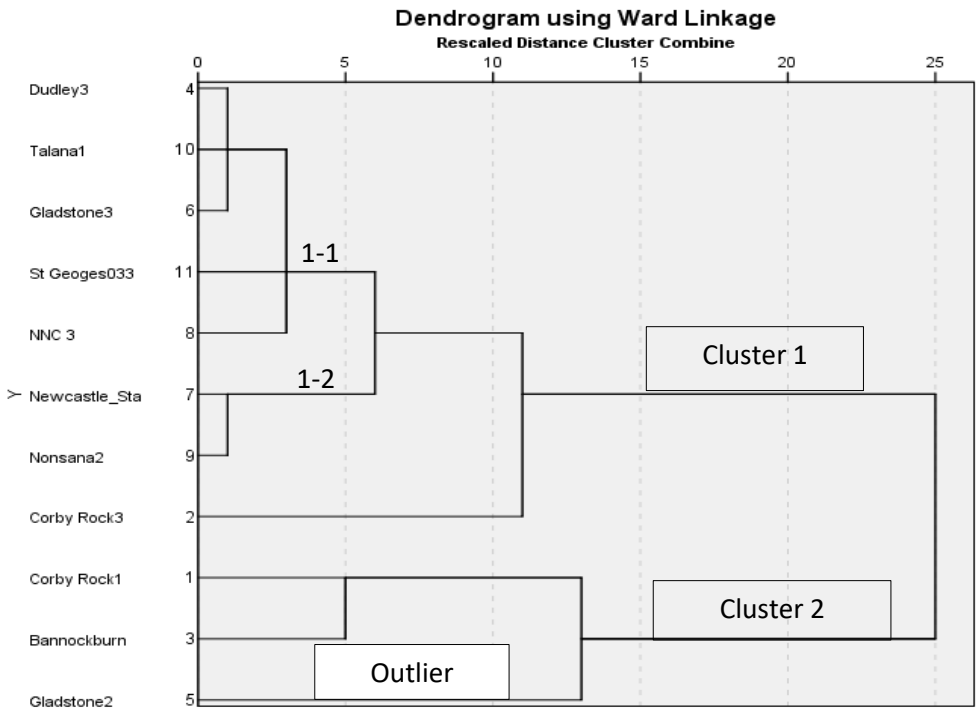

2015 Hydrochemical data Dendrogram using Ward Linkage reduction technique.

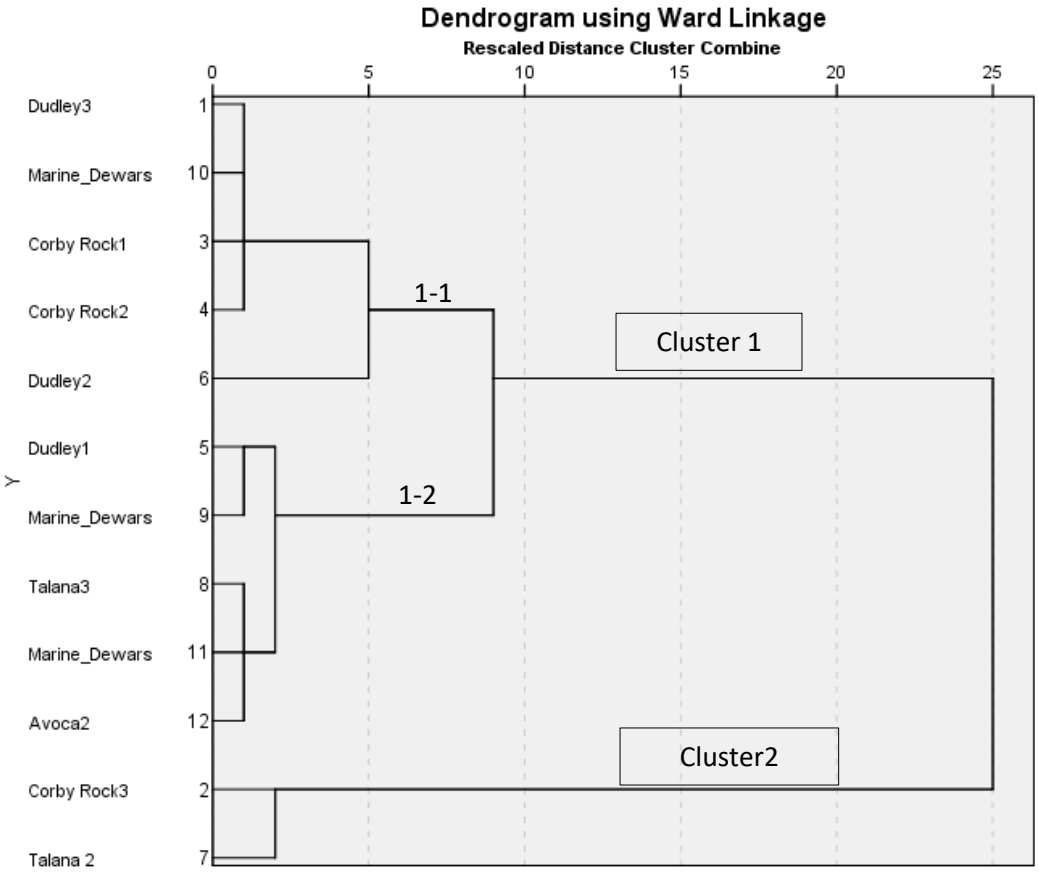

2016 Hydrochemical data Dendrogram using Ward Linkage reduction technique.

Appendix VI. PCA and Scree Plots for 2012-2015 Hydrochemical data using Direct Oblimin rotation method.

2012 Hydrochemical data Principal Component Analysis (PCA)

pH	Communality	Component 1	Component2
EC	.536	-.540	.494
Na	.988	**.959**	.263
K	.929	**.815**	.515
Mg	.695	**.828**	.098
Ca	.913	**.949**	-.114
Cl	.819	**.881**	-.206
SO4	.240	-.126	.474
HCO3	.970	.985	-.004
NO3	.756	-.157	**.855**
Fe	.947	**.973**	.002
% of Variance		61.949	15.991
Cumulative %		61.949	77.940

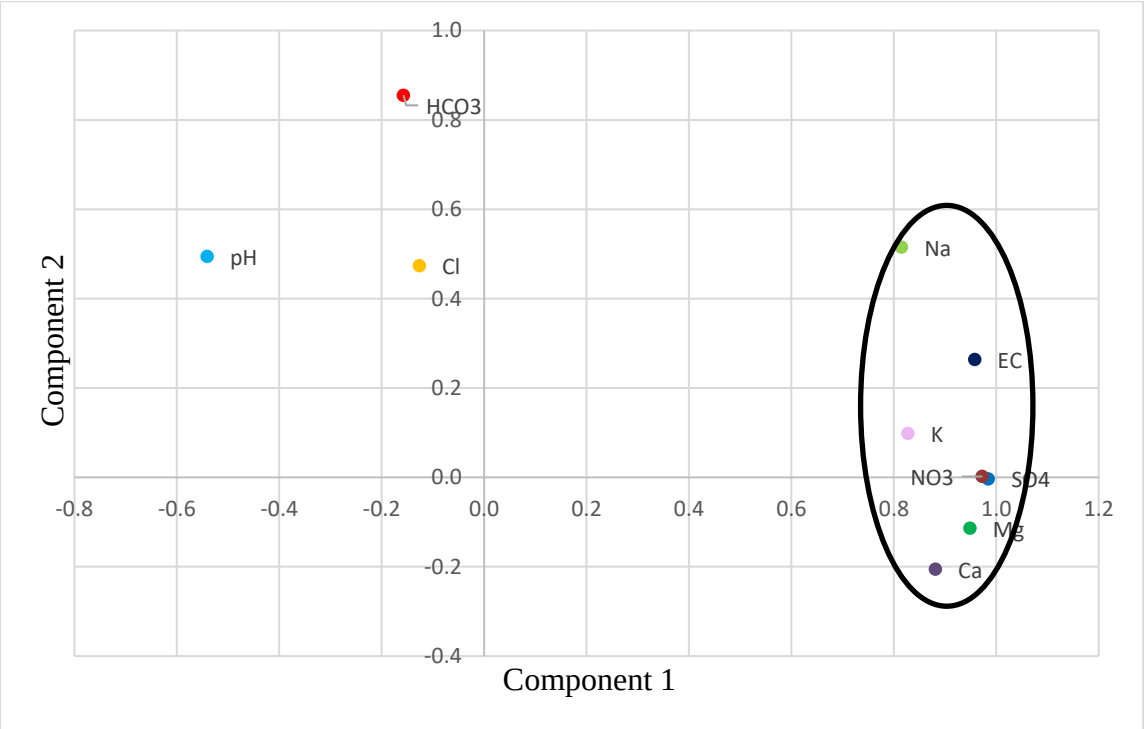

2012 Hydrochemical data PCA Scatter Plot

2013 Hydrochemical data Principal Component Analysis (PCA)

	Communality	Component1	Component2
pH	.761	-.748	.449
EC	.968	**.885**	.431
Na	.928	**.640**	**.720**
K	.868	**.784**	.504
Mg	.820	**.876**	-.229
Ca	.903	**.884**	-.350
SO4	.979	**.989**	-.023
HCO3	.876	-.325	**.878**
NO3	.887	**.938**	-.088
% of variance		65.308	23.471
Cumulative %		65.308	88.779

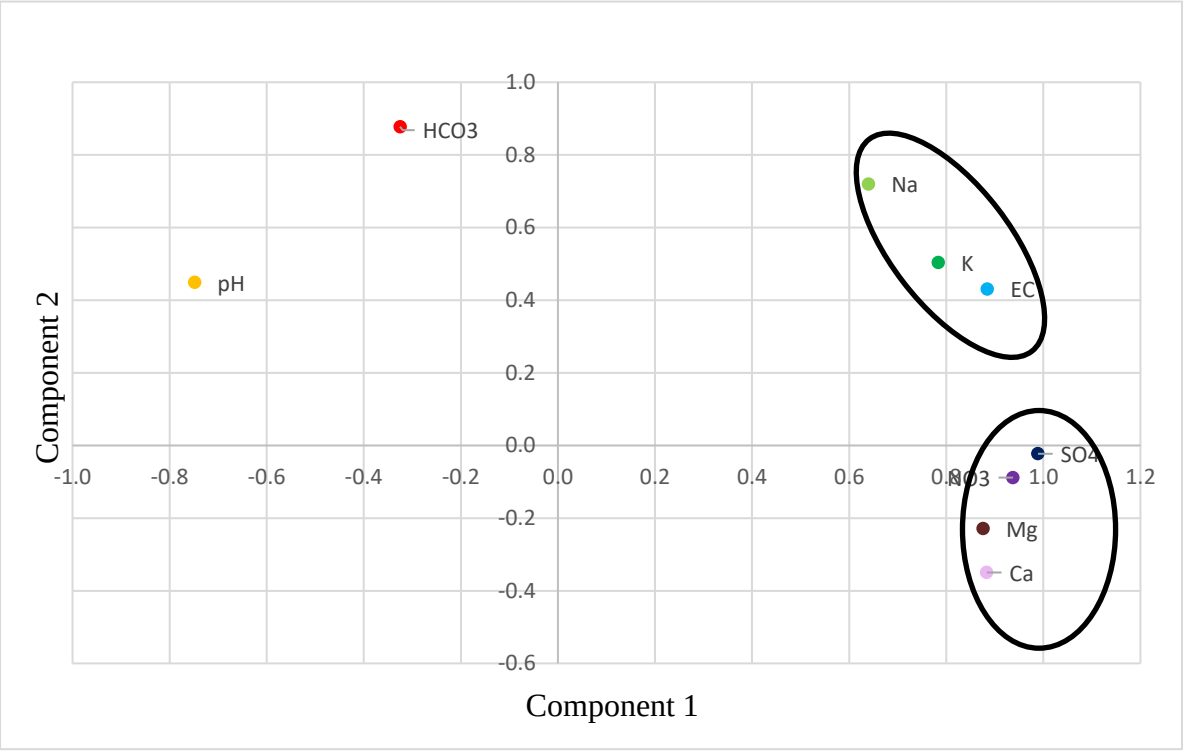

2013 Hydrochemical data PCA Scatter Plot

2014 Hydrochemical data Principal Component Analysis (PCA)

	Communality	Component 1	Component2
pH	.262	-.427	.283
EC	.208	.438	.129
Ca	.908	**.945**	.119
SO4	.970	**.969**	.177
Cl	.785	-.222	**.858**
Mg	.909	**.939**	.162
HCO3	.902	-.386	**.868**
NO3	.958	**.966**	.157
% of variance		52.740	21.02
Cumulative %		52.740	73.761

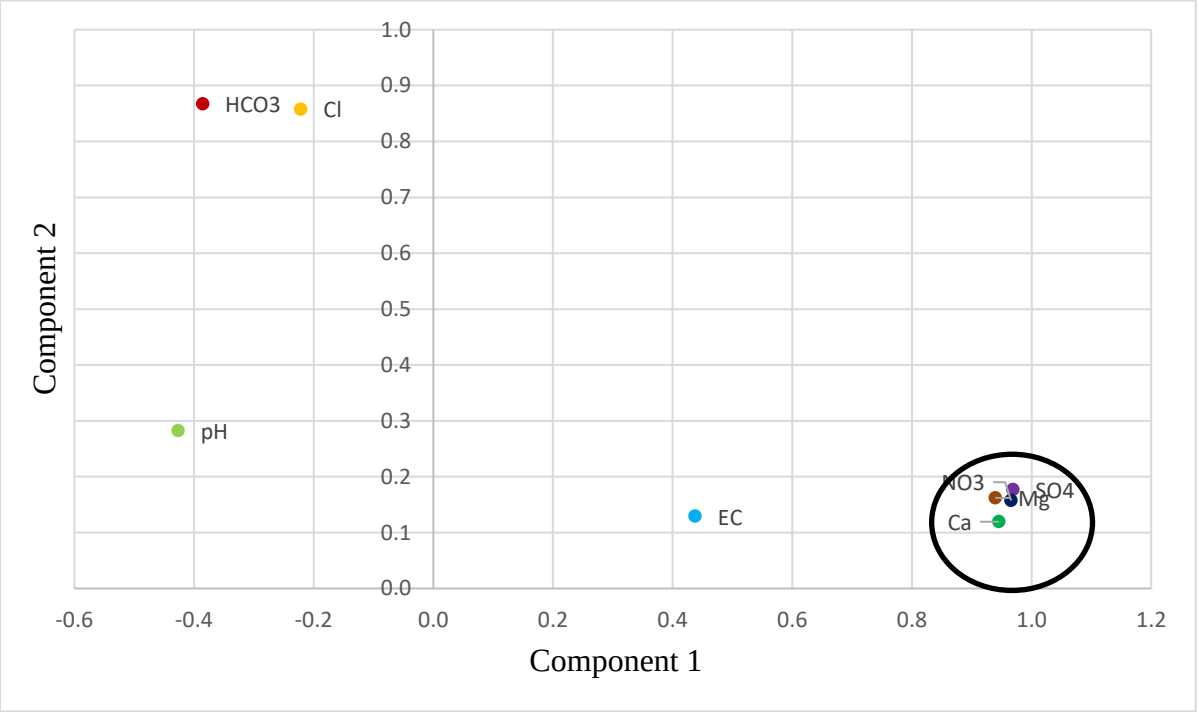

2014 Hydrochemical data PCA Scatter Plot

2015 Hydrochemical data Principal Component Analysis (PCA)

	Communality	Component 1	Component2
pH	.826	**.849**	-.099
EC	.867	.452	**.760**
Ca	.697	-.742	.380
SO4	.765	-.503	**.707**
Mg	.956	-.873	.420
K	.927	-.287	-.269
HCO3	.937	**.878**	.090
NO3	.621	-.423	-.657
Na	.762	**.759**	.408
% of variance		45.540	23.175
Cumulative %		45.540	68.715

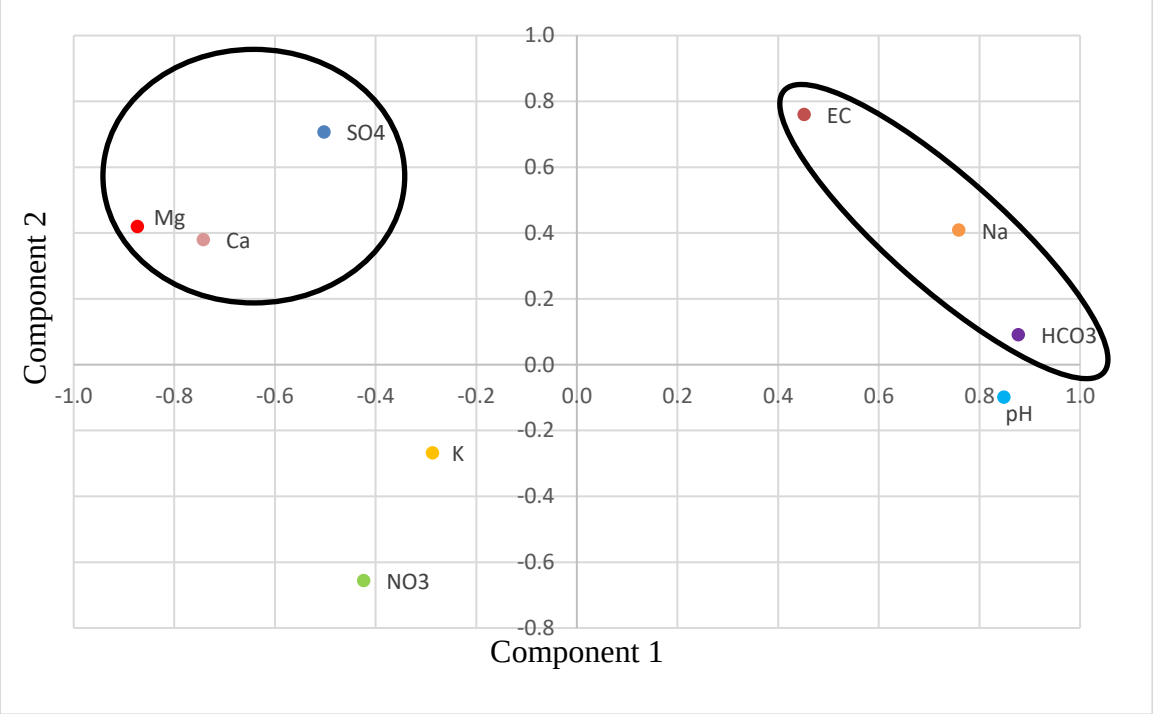

2015 Hydrochemical data PCA Scatter Plot

Appendix VII. Groundwater and surface water major ion hydrochemical laboratory and field measured data collected from 8-14 August 2018.

Sample ID	Source	pH	EC µS/cm	DO	Eh	Temp(°C)	Na^{2+} mg/l	Mg^{2+} mg/l	Si^{+} mg/l	K^{+} mg/l	Ca^{2+} mg/l	Fe^{2+} mg/l	F^{-}mg/l	Cl^{-} mg/l	Br^{-} mg/l	NO_3^{-} mg/l	SO_4^{2-} mg/l	PO_4^{3-} mg/l
NC1	BH	7.26	688	1.42	-17.8	18.1	122.1	15.5	19	2.4	23.5	0.23	1.89	17.97	1.22	0.83	1.026	
NC2	SW	6.64	203	3.07	-6.7	15.35	10.4	14.9	5.7	1.8	17.6	0.06	0.69	7.52	0.83	1.9	10.268	
NC3	SW	7.8	307	3.12	-60	14.21	26.2	11.6	6	3.9	20.1	0.03	0.75	12.17	0.7	4.29	67.576	1.167
NC4	BH	7.75	166	3.06	-48.7	18.73	28.1	3.6	16.4	2.4	8.9	0.03	1.2	3.45	0.65	1.27	16.904	
NC5	BH	7.6	453	2.9	-36.5	18.21	70.7	10.5	18.3	1.5	19.9	0.02	1.66	35.93	1.61	3.2	29.74	
NC6	SW	8.43	306	4.1	-75.6	11.48	25.4	14.1	5.3	2.6	20.8	0.04	0.77	9.13	0.51	1.28	104.02	
NC7	SW	8.31	596	4.61	-72	9.7	46.8	18.5	4	13.3	42.5	0.13	1.61	39.41	0.57	106.72	88.41	
NC8	BH	7.92	390	2.48	-18.8	9.7	50.93	11.52	12.43	12.62	22.23	0.5	2.09	26.37	0.89	0.64		
NC10	SW	8.9	349	4.8	-84.4	11.5	29.1	15.3	3.46	3.93	24.15	0.02	0.82	15.77	0.78	8.96	52.6	0.944
NC11	BH	7.3	172	3.6	-25.3	18.8	28.46	6.02	14.93	1.35	11	0.03	1.61	1.32	0.84		1.28	
NC12	SW	7.76	86	5.6	-44.1	11.05	7.98	4.93	5.42	2.37	7.96	0.19	0.74	4.23	0.44	1.28	15.34	
NC13	BH	7.1	581	3.6	-27.6	19.9	107.27	26.75	16.64	1.28	42.83	0.03	2.93	11.1	2.58	1.61	71.36	
NC14	BH	8.38	1629	3.2	-81.5	19.54	416.66	0.76	8.15	2.38	4.13	0.02	13.09	17.66	5.26	2.62	2.41	3.815
NC15	BH	8.52	380	3.35	-105	17.95	20.44	22.81	21.71	1.59	35.97	0.02	1.04	18.43	0.89	0.8	16.37	
NC16	BH	7.66	2748	3.81	-50.5	19.83	288.41	71.48	11.55	46.3	157	0.01	5.38	717.64	3.93	29.55	80.94	
NC17	BH	8.32	198	3.8	-92	19.8	38.41	3.71	2.96	1.54	7.51	0.02	1.76	11.1	0.41	0.64	0.89	
NC18	BH	8.73	325	3.5	-99	20.3	83.46	0.22	12.72	0.99	3.53	0.03	0.95	9.78	0.9	1.17	11.83	0.92
NC19	BH	8	166	3.69	-64	20.04	26.45	3.01	8.12	3.11	12.12	0.19	0.58	6.39	0.45	0.71	0.76	
NC20	BH	7.55	547	4.4	-49	18.5	73.85	19.14	16.5	8.19	26.88	0.04	2.47	14.63	1.58	1.82	100.23	
NC21	BH	8.78	1852	4.17	-111	16.99	404.43	7.71	14.59	2.89	34.53	0.17	16.67	129.65	1.58	3.26	2.85	
NC22	BH	8.02	189	4	-82	17.43	17.38	9.29	27.35	1.36	17.52	0.06	0.71	4.48	0.68	0.92	1.84	

NC23	BH	7.82	590	4.3	-56	18.48	95.5	14.63	13.08	3.46	30.95	0.04	2.08	12.67	2.23	1.53	17.82	
NC24	BH	8.08	594	3.5	-61.1	14.5	137.27	6.11	8.62	4.58	18.02	0.06		3.39		5.09	440.43	2.054
NC25	BH	7.45	2717	4.2	-86	19.93	387.38	105.9	15.24	6.49	171.97	0.02	13.14	42.22	6.91	6.57	5.98	
NC26	BH	8.04	223	4.2	-90	19.83	16.04	9.17	16.7	3.09	18.11	0.02	0.41	9.3	0.44	10.38	46.84	1.029
NC27	BH	7.75	445	2.8	-61	20.19	25.17	14.23	15.89	1.58	59.04	0.02	0.86	13.53	1.06	1.51	76.94	
NC28	BH	8.21	768	3.7	-76	20.76	169.01	7.52	12.23	1.5	17.92	0.28	2.48	8.01	1.82	2.76	110.82	
NC29	BH	9.29	808	3.6	-145	18.54	193.22	6.23	1.96	3.2	3.99	0.01	3.45	23.2	1.24	1.92	99.74	
NC30	BH	9.56	611	3.9	-153	18.09	39.67	43.17	0.28	1.72	34.28	0.03		12.22	0.48	1.37	336.86	
NC31	BH	8.6	155	3.83	-105	19.7	22.54	4.02	1.06	2.63	22.54	0.02	0.65	4.6	0.61	0.7	1.23	
NC32	SW	8.83	747	6.5	-127	11.88	75.73	26.51	5.37	8.64	45.55	0.11	1.44	55.9	1.03	13.26	131.26	3.412
NC33	BH	7.7	5954	4.2	-442	21.78	127.9	90.27	15.18	11.52	156.53	0	6.95	552.29	5.36	8.38	1888.29	
NC34	BH	7.1	193	4.1	-30	23	4.69	3.83	2.32	10.68	21.92	1.12	0.54	5.85	0.65	0.79	54.11	1.11
NC35	BH	7.7	1235	4.35	-580	22.11	266.05	19.78	33.07	4.24	40.07	0	5.44	59.22	15.56	4.35	5.84	3.893
NC36	SW	9.27	1650	7.3	-140	16	392.39	18.62	1.03	4.5	15.76	0.03	8.47	61.94	2.8	3.28	130.61	
NC37	SW	8.23	269	6.4	-70	15.9	21.52	14.94	4.74	2.17	20.85	0.06	0.78	5.38	0.67	0.76	63.02	
NC38	SW	9.07	344	6.08	-114.8	15.46	30.75	17.05	1.6	4.04	27.65	0.05	0.89	17.32		6.55	50.09	
NC39	BH	7.85	977	4.3	-69	20.8	194.87	15.47	14.85	3.14	23.73	0.06	2.84	7.62	3.31		22.67	
NC40	BH	8.7	1431	3.66	-100.5	21.01	224.3	3.07	6.49	1.57	5.59	0.02	6.82	75.61	2.48		5.33	
NC41	BH	7.37	996	2.34	-25.7	22.06	70.25	53.77	19.1	1.23	95.34	0	3.85	5.8		770.49	522.97	

Appendix VIII. Trace element data generated for surface water and groundwater sampled from 8-14 August 2018.

Sample ID	NC1	NC2	NC3	NC4	NC5	NC6	NC7	NC8	NC10	NC11	NC12	NC13	NC14	NC15	NC16	NC17
Description	148750	SW	SW	KZN100041	KZN100042	SW	SW	N/A	SW	V3N0017	SW	KZN100282	KZN100282	KZN100279	V3N0016	KZN100287
Li (µg/l)	22.26	<3	<3	6.92	6.08	3.55	22.05	12.34	<3	25.02	<3	33.19	171.24	9.17	56.86	<3
B (µg/l)	47.82	4.08	24.23	48.99	20.01	10.6	26.8	6.23	16.35	22.7	6.54	19.93	118.83	5.04	21.8	17.57
Al (µg/l)	69.41	27.13	29.81	23.51	23.19	48.27	38.17	23.09	15.76	26.58	159.45	14.79	24.12	24.41	28.51	47.4
V (µg/l)	0.07	0.88	1.26	0.36	0.43	0.39	0.42	0.05	2.26	0.59	0.8	0.23	0.08	9.43	1.84	0.1
Cr (µg/l)	1.56	0.58	0.31	0.36	0.34	0.47	0.39	<0.2	<0.2	0.49	0.46	0.34	0.23	0.31	0.33	0.22
Mn (µg/l)	26.56	37.68	237.61	2.08	1.63	132.04	92.33	44.38	43.05	4.86	6.57	78.04	17.36	4.77	7.73	10.79
Co (µg/l)	0.05	0.19	0.36	<0.05	0.05	0.41	1.09	0.09	0.27	<0.05	0.09	0.47	0.04	0.05	0.09	0.05
Ni (µg/l)	2.52	1.94	2.56	2.25	1.95	3.16	4.87	2.12	2.56	1.88	4.5	1.52	1.75	2.28	2.6	2.07
Cu (µg/l)	2.9	1.86	1.66	4.33	2.15	2.53	6.29	1.58	1.45	2.16	2.49	1.83	1.27	1.56	2.28	2.5
Zn (µg/l)	17.65	26.37	19.06	78.09	19.51	16.38	26.19	27.23	11.15	17.98	19.72	14.76	19.89	19.06	25.25	25.58
As (µg/l)	0.03	0.23	0.46	0.11	0.19	0.28	0.82	0.08	0.45	0.3	0.42	1.08	0.02	0.94	0.64	0.74
Se (µg/l)	<0.06	<0.06	<0.06	<0.06	<0.06	<0.06	0.23	0.01	<0.06	<0.06	<0.06	<0.06	<0.06	0.97	0.85	<0.06
Rb (µg/l)	5.1	0.96	3.61	2.99	2	1.17	25.47	3.37	3.6	0.94	0.94	2.48	6.02	1.43	10.27	1.57
Sr (µg/l)	585.23	83.09	158.84	114.14	259.34	198.87	261.58	326.07	153.49	277.28	71.68	307.07	381.27	268.32	1900.03	61.68
Mo (µg/l)	0.04	<0.12	0.18	0.14	0.14	0.14	0.45	0.31	0.22	1.56	0.1	0.22	<0.12	0.32	1.11	3.11
Cd (µg/l)	<0.1	<0.1	<0.1	<0.1	<0.1	<0.1	<0.1	<0.1	<0.1	<0.1	<0.1	<0.1	<0.1	<0.1	<0.1	<0.1
Sb (µg/l)	12.05	0.42	0.6	0.45	0.56	0.98	0.71	0.43	0.55	0.46	0.67	0.25	0.75	0.78	0.77	0.48
Ba (µg/l)	541.01	37.66	46.86	106.84	129.17	51.79	79.45	153.75	65.36	49.33	36.1	67.23	329.3	80.44	179.1	10.83
Hg (µg/l)	0.05	0.03	0.06	0.04	0.04	0.04	0.04	0.04	0.05	0.03	0.04	0.1	0.04	0.03	0.88	0.11
Pb (µg/l)	0.05	0.1	0.16	0.29	0.16	0.23	0.35	0.31	0.1	0.36	0.25	0.05	0.09	0.25	0.21	0.3
Th (µg/l)	<0.7	<0.7	<0.7	<0.7	<0.7	<0.7	<0.7	<0.7	<0.7	<0.7	<0.7	<0.7	<0.7	<0.7	<0.7	<0.7
U (µg/l)	<0.3	<0.3	<0.3	<0.3	<0.3	<0.3	<0.3	<0.3	<0.3	<0.3	<0.3	0.53	<0.3	0.35	6.55	<0.3

Sample ID	NC18	NC19	NC20	NC21	NC22	NC23	NC24	NC25	NC26	NC27	NC28	NC29	NC30
Description	KZN100290		KZN100288	KZN100034	KZN100289	KZN100281	140063	KZN110001	KZN110002	KZN110003	KZN100033	KZN070036	KZN070035
Li (µg/l)	<3	<3	39.62	60.58	<3	55.64	74.33	71.91	12.26	28.59	5.87	80.62	5.17
B (µg/l)	11.18	3.84	11.89	29.84	2.15	34.27	71.68	1.85	1.01	2.79	32.27	55.48	2.17
Al (µg/l)	86.77	22.83	38.64	155.88	35.21	25.54	33.08	50.31	38.86	39.21	36.72	36.7	36.11
V (µg/l)	0.41	0.07	0.55	2.39	9.14	0.06	0.04	0.29	0.25	0.07	18.82	0.09	0.03
Cr (µg/l)	0.22	0.18	0.41	0.51	0.45	0.25	0.24	2.09	0.53	0.27	0.46	0.33	0.32
Mn (µg/l)	1.29	62.54	4	71.91	2.82	117.82	54.89	60.11	2.86	286.14	24.18	11.62	32
Co (µg/l)	0.05	<0.05	0.06	0.28	<0.05	0.09	<0.05	0.98	0.06	0.05	0.19	0.02	<0.05

Ni (µg/l)	1.79	1.55	2.95	1.62	2.23	2.36	1.58	40.5	2.52	2.1	4.15	1.43	1.8
Cu (µg/l)	1.79	1.02	2.35	1.57	2.85	1.18	1.23	7.33	6.43	10.29	7.32	4.06	4.01
Zn (µg/l)	14.75	24.9	23.72	17.34	15.34	14.68	15.76	98.72	23.51	18.68	5882.17	8.62	12.48
As (µg/l)	105.44	0.3	0.11	0.38	0.18	0.14	0.14	0.15	0.09	0.08	1.79	0.15	0.04
Se (µg/l)	<0.06	<0.06	<0.06	<0.06	<0.06	<0.06	<0.06	0.83	0.21	<0.06	0.21	<0.06	<0.06
Rb (µg/l)	1.64	2	6.65	6.82	0.62	7.19	9.51	5.93	4.43	1.55	1.73	4.7	1.2
Sr (µg/l)	34.78	68.15	364.04	342.94	84.51	1904.05	2028.65	1388.34	199.73	633.63	237.94	600.21	154.04
Mo (µg/l)	0.47	0.2	0.54	0.85	0.14	0.17	<0.12	<0.12	<0.12	0.38	5.71	2.22	0.34
Cd (µg/l)	<0.1	<0.1	<0.1	<0.1	<0.1	<0.1	<0.1	<0.1	<0.1	<0.1	<0.1	<0.1	<0.1
Sb µg/l)	0.72	0.6	0.91	0.51	0.56	0.59	0.57	0.48	0.69	0.63	0.51	0.5	0.65
Ba (µg/l)	3.63	2.29	66.39	105.68	20.24	1116.03	1290.93	36.5	84.05	126.75	30.42	9.81	8.56
Hg (µg/l)	0.06	0.05	0.13	0.07	0.05	0.05	0.03	0.07	0.06	0.06	0.04	0.03	0.18
Pb (µg/l)	0.28	0.22	0.17	0.1	0.27	0.12	0.14	0.73	0.32	0.3	0.42	0.12	0.17
Th (µg/l)	<0.7	<0.7	<0.7	<0.7	<0.7	<0.7	<0.7	<0.7	<0.7	<0.7	<0.7	<0.7	<0.7
U (µg/l)	<0.3	<0.3	<0.3	0.3	<0.3	<0.3	<0.3	<0.3	<0.3	<0.3	1.82	<0.3	<0.3

Sample ID	NC31	NC32	NC33	NC34	NC35	NC36	NC37	NC38	NC39	NC40	NC41
Description	KZN070034	SW	KZN110005	KZN110004	KZN110006	SW	SW	SW	KZN110010	KZN110008	KZN110009
Li (µg/l)	4.76	<3	249.42	13.06	16.85	124.41	<3	<3	121.44	284.79	15.95
B (µg/l)	7.46	17.68	77.76	12.84	97.49	48.17	6.65	11.72	26.2	96.61	5.1
Al (µg/l)	38.89	48.87	15.93	48.6	5.42	46.58	329.77	35.14	46.65	35.55	<2.5
V (µg/l)	0.03	1.97	0.2	1.09	0.34	2.87	0.78	2.49	0.49	0.08	<0.04
Cr (µg/l)	0.37	2.1	<0.2	0.76	<0.2	0.28	0.43	0.21	0.41	0.26	<0.2
Mn (µg/l)	17.91	585.33	166.87	216.34	126.32	2.6	1.11	2.81	73.61	3.8	310.46
Co (µg/l)	<0.05	1.41	0.12	0.3	0.07	0.26	0.09	0.42	0.2	<0.05	<0.05
Ni (µg/l)	1.65	4.71	1.05	5.17	0.78	1.52	2.51	2.92	3.01	1.1	0.18
Cu (µg/l)	7.49	6.25	1.74	3.61	1.79	2.61	5.26	2.9	2.38	0.71	0.17
Zn (µg/l)	18.29	14.97	1.33	27.48	0.85	0.77	18.73	20.3	30.66	9.87	0.94
As (µg/l)	0.05	1.03	0.15	0.87	0.62	0.54	0.27	0.37	0.34	0.02	0.57
Se (µg/l)	<0.06	<0.06	<0.06	<0.06	<0.06	0.06	<0.06	<0.06	<0.06	<0.06	<0.06
Rb (µg/l)	2.88	6.38	26.13	2.75	8.59	1.06	0.41	2.74	5.57	5.56	3.07
Sr (µg/l)	689.87	252.08	5915.67	238.5	892.44	346.78	154.93	164.38	1212.61	644.82	764.77
Mo (µg/l)	0.54	0.36	2.51	<0.12	0.82	0.97	<0.12	0.38	1.62	<0.12	0.58
Cd (µg/l)	<0.1	<0.1	<0.1	<0.1	<0.1	<0.1	<0.1	<0.1	<0.1	<0.1	<0.1
Sb (µg/l)	0.7	0.82	0.68	0.66	0.38	0.46	0.61	0.73	0.83	0.9	0.08

Ba (µg/l)	47.33	49.3	21.57	32.7	246.87	93.21	79.35	87.67	1007.21	1353.55	46.96
Hg (µg/l)	0.04	0.11	0.05	0.06	0.04	0.03	0.05	0.05	0.02	0.04	0.03
Pb (µg/l)	0.18	0.25	<0.1	0.34	<0.1	0.03	0.26	0.28	0.26	0.23	<0.1
Th (µg/l)	<0.7	<0.7	1.32	<0.7	<0.7	<0.7	<0.7	<0.7	<0.7	<0.7	<0.7
U (µg/l)	<0.3	0.68	1.2	<0.3	<0.3	0.6	<0.3	0.41	0.31	<0.3	<0.3

*SW stands for Surface water